

RPSEA

Final Report

07123-03.FINAL

***Near Miscible CO₂ Application to
Improve Oil Recovery for Small
Producers***

07123-03

October 29, 2010

Jyun-Syung Tsau
Associate Scientist
TORP, University of Kansas
The University of Kansas Center for Research, Inc.
2385 Irving Hill Road, Lawrence, KS 66045-7563

LEGAL NOTICE

This report was prepared by *University of Kansas Center for Research, Inc.* as an account of work sponsored by the Research Partnership to Secure Energy for America, RPSEA. Neither RPSEA members of RPSEA, the National Energy Technology Laboratory, the U.S. Department of Energy, nor any person acting on behalf of any of the entities:

- a. **MAKES ANY WARRANTY OR REPRESENTATION, EXPRESS OR IMPLIED WITH RESPECT TO ACCURACY, COMPLETENESS, OR USEFULNESS OF THE INFORMATION CONTAINED IN THIS DOCUMENT, OR THAT THE USE OF ANY INFORMATION, APPARATUS, METHOD, OR PROCESS DISCLOSED IN THIS DOCUMENT MAY NOT INFRINGE PRIVATELY OWNED RIGHTS, OR**

- b. **ASSUMES ANY LIABILITY WITH RESPECT TO THE USE OF, OR FOR ANY AND ALL DAMAGES RESULTING FROM THE USE OF, ANY INFORMATION, APPARATUS, METHOD, OR PROCESS DISCLOSED IN THIS DOCUMENT.**

THIS IS A FINAL REPORT. THE DATA, CALCULATIONS, INFORMATION, CONCLUSIONS, AND/OR RECOMMENDATIONS REPORTED HEREIN ARE THE PROPERTY OF THE U.S. DEPARTMENT OF ENERGY.

REFERENCE TO TRADE NAMES OR SPECIFIC COMMERCIAL PRODUCTS, COMMODITIES, OR SERVICES IN THIS REPORT DOES NOT REPRESENT OR CONSTITUTE AND ENDORSEMENT, RECOMMENDATION, OR FAVORING BY RPSEA OR ITS CONTRACTORS OF THE SPECIFIC COMMERCIAL PRODUCT, COMMODITY, OR SERVICE.

ABSTRACT

This final report presents the research results in investigation of the feasibility of near miscible CO₂ flooding for improved oil recovery in an Arbuckle reservoir in Kansas. The experimental and computational studies were carried out to characterize the phase behavior, the displacement process, the oil recovery and CO₂ sequestration under near miscible condition.

In the experimental studies, phase behavior tests between CO₂ and Arbuckle crude oil were carried out to define near miscible condition at reservoir temperature. The results of swelling/extraction tests combined with slim-tube experiments were interpreted to identify the mass transfer mechanisms at near miscible condition. A phase behavior model was developed to match PVT data and MMP in the slim-tube experiment. Good agreement was obtained between simulated and observed data from slim-tube experiments. Core flooding tests were conducted to evaluate oil recovery at near miscible condition at which pressure varies from 1350 psi (MMP) to 1150 psi. Recovery of over 50% of the waterflood residual oil saturation was observed when CO₂ was used to displace Arbuckle oil from Berea, Baker dolomite and Arbuckle dolomite cores.

At near miscible conditions, extraction appears to be the primary mechanism for mass transfer between hydrocarbon components and CO₂. However, the reduction of oil viscosity by a factor of five occurred when CO₂ dissolved in the oil. This suggests that some of the additional oil recovery may be attributed to reduction of the mobility ratio between CO₂ and resident oil.

In the computational studies, a 47 acre lease containing four wells was extensively examined for the effect of CO₂ injection pressure, rate and pattern on the oil recovery efficiency. The average reservoir pressure was maintained at the near miscible condition during the CO₂ injection as the pressure was supported by the underling aquifer. In general, the simulation results show that improvement of oil recovery at near miscible condition is achievable under current reservoir operation pressure. The incremental oil recovery was increased with the injection pressure. The oil recovery efficiency was increased by 1.3 to 4.8% as a result of the injection of CO₂. This improved recovery efficiency is likely resulting from the improvement of relative mobility ratio of the CO₂ and oil and the efficacy of CO₂ extraction. However, the recovery efficiency is affected by the reservoir heterogeneity as it was shown in the pattern design where the recovery results depend on the placement of the injectors. The theoretical storage capacity of CO₂ in this 47 acre lease was estimated to be 1.58 BSCF. With 1.45 BSCF of CO₂ injected in 10 years, the effective storage capacity of CO₂ varied from 39 to 63%.

THIS PAGE INTENTIONALLY LEFT BLANK

TABLE OF CONTENTS

	<u>Page</u>
TABLE OF CONTENTS	i
LIST OF TABLES	ii
LIST OF FIGURES	iii
1. INTRODUCTION	1
Background Information	2
2. EXPERIMENTAL STUDY	2
2.1 Slim-tube Experiments	3
2.2 Swelling/Extraction Tests	8
2.3 Viscosity Measurements	18
2.4 Estimation of MMP	21
2.5 Phase Behavior Model	23
2.6 Core Flow Test	29
3. COMPUTATIONAL STUDY	37
3.1 Geological Model	37
3.2 Reservoir Model and Simulation	48
3.2.1 History Match of Primary Production	50
3.2.2 Simulation of Carbon Dioxide Injection	58
4. SUMMARY AND CONCLUSIONS	75
ACKNOWLEDGEMENT	77
REFERENCES	78

LIST OF TABLES

		<u>Page</u>
Table 1	Physical property of Ogallah crude oil	4
Table 2	Slim-tube characteristics	6
Table 3	Phase equilibrium data of CO ₂ /n-decane at 71.1°C	13
Table 4	Adjustments of EOS parameters	26
Table 5	Maximum percentage errors between simulated and experimental data	26
Table 6	Slim- tube model properties	28
Table 7	Core plug properties	31
Table 8	Tertiary CO ₂ flood results of Berea sandstone	36
Table 9	Tertiary CO ₂ flood results of Arbuckle dolomite	36
Table 10	Tertiary CO ₂ flood results of Baker dolomite	36
Table 11	Type of well logs available at Ogallah unit	38
Table 12	Visual indication of rock type: shale, dolomite, sandstone, and granite-wash	38
Table 13	Ogallah wells with lithology information available	39
Table 14	PVT data used in simulator	51
Table 15	Well block properties at well locations	58
Table 16	Comparison of incremental oil and water production in 10 years of CO ₂ injection (CO ₂ injected at well 3-3)	60
Table 17	Comparison of incremental oil and water production in 10 years of CO ₂ injection (CO ₂ injected at well 3-2)	60
Table 18	Result of case study with CO ₂ injection at BHP of 1300 psi	70
Table 19	Result of case study with CO ₂ injection at BHP of 1200 psi	71
Table 20	Result of case study CO ₂ injection at 200 MSCF/day/well	72

LIST OF FIGURES

		<u>Page</u>
Figure 1	Ogallah unit, Trego County, Kansas	3
Figure 2	GC compositional analysis result of Ogallah crude oil	4
Figure 3	Schematic of slim- tube setup	5
Figure 4	Minimum miscibility pressure determinations at 110°F and 125°F.....	7
Figure 5	Density profile of the effluent at 110°F	8
Figure 6	Schematic of swelling/extraction test apparatus setup	9
Figure 7	Image of the swelling/extraction experimental setup	10
Figure 8	Comparison of liquid phase compositions for CO ₂ + n-decane system at 71.10°C	14
Figure 9	Change of initial oil volume with pressure	15
Figure 10	Effect of pressure on CO ₂ solubility and swelling factor at 110°F	16
Figure 11	Effect of temperature on CO ₂ solubility	17
Figure 12	Effect of temperature on Swelling/ Extraction curves	17
Figure 13	Schematic of high-pressure viscosity measurement setup	19
Figure 14	Image of the high-pressure viscosity measurement setup	20
Figure 15	Effect of pressure on Ogallah oil viscosity at 110°F	20
Figure 16	Viscosity of crude oil saturated with CO ₂ at 110°F	21
Figure 17	Estimation of MMP from extraction test of Ogallah crude oil	22
Figure 18	Comparison of viscosity/density experimental data and simulated data	27
Figure 19	Comparison of saturation pressure/swelling factor experimental and simulated data	27
Figure 20	Comparison of simulated MMP and experimental MMP	29
Figure 21	Schematic of core flood setup	30
Figure 22	Comparison of oil recovery between slim-tube and core flooding experiment	33
Figure 23	Effluent profile of production fluid during CO ₂ flooding at 1317 psig and 110°F	34
Figure 24	Effect of rock type on recovery efficiency at 110°F	35

	<u>Page</u>
Figure 25	Effect of water saturation on oil recovery efficiency at 110°F 35
Figure 26	Porosity overlays of Well 4-16..... 41
Figure 27	Microlog (ϕ_{ML}) porosity cross plotted with (a) Neutron Porosity 42
Figure 28	Derived average porosity (a) and water saturation (b) plotted with depth for well 14-1..... 43
Figure 29	Contour grids of the Ogallah formation tops and the cross-section profiles ... 43
Figure 30A	Cross section of wells indicated as Line A-A' 44
Figure 30B	Cross section of wells indicated as Line B-B' 45
Figure 30C	Cross section of wells indicated as Line C-C' 45
Figure 30D	Cross section of wells indicated as Line D-D' 46
Figure 31	Isopach of the net-pay in Ogallah unit based on log interpretation 47
Figure 32	Porosity-permeability correlation of Arbuckle Group 47
Figure 33	Structure top map of Ogallah Unit 48
Figure 34	Example of cross section view of Ogallah Unit..... 49
Figure 35	Permeability and porosity of Arbuckle dolomite and Reagan sandstone..... 49
Figure 36	Production history of Lease 3, E. A. Scott 50
Figure 37	Relative permeability curves of oil and water 52
Figure 38	History match of oil production in well 3-2 53
Figure 39	History match of water production in well 3-2 53
Figure 40	History match of oil production in well 3-3 54
Figure 41	History match of water production in well 3-3 54
Figure 42	History match of oil production in well 4-12 55
Figure 43	History match of water production in well 4-12..... 55
Figure 44	History match of oil production in well 4-13 56
Figure 45	History match of water production in well 4-1356
Figure 46	Average reservoir pressures of Ogallah unit and Lease E. A. Scott 57
Figure 47	Grid system of Lease 3, E. A. Scott..... 59
Figure 48	Incremental oil production at well 3-2 when CO ₂ was injected at well 3-3 61
Figure 49	Reduction of water production at well 3-2 when CO ₂ was injected at well 3-3 61
Figure 50	Incremental oil production at well 3-3 when CO ₂ was injected at well 3-2 62

	<u>Page</u>
Figure 51	Reduction of water production at well 3-3 when CO ₂ was injected at well 3-2 .. 62
Figure 52	Pattern design of lease 3 for CO ₂ injection 63
Figure 53	CO ₂ distributions after 10 years of injection, Case A1 64
Figure 54	CO ₂ distributions after 10 years of injection, Case B1 65
Figure 55	CO ₂ distributions after 10 years of injection, Case C1 65
Figure 56	CO ₂ distributions after 10 years of injection, Case D1 66
Figure 57	CO ₂ distributions after 10 years of injection, Case E1 66
Figure 58	CO ₂ distributions after 10 years of injection, Case F1 67
Figure 59	Comparison of oil recovery factors at Lease 3 67
Figure 60	Average reservoir pressures at Lease 3 with/without CO ₂ injection..... 68
Figure 61	Lease 3 production performance without CO ₂ injection 73

1. INTRODUCTION

Carbon dioxide (CO₂) injection for improved oil recovery (IOR) is a proven technology. It is also considered as one of the most promising methods for carbon sequestration in geologic formations. CO₂ injections are normally operated at a pressure above the minimum miscibility pressure (MMP), which is determined by crude oil composition and reservoir conditions. However, many reservoirs in the United States and around the world are at shallow depths or geologic conditions exist such that they operate at pressures below the MMP. For example, one part of the Arbuckle reservoir in the Bemis-Shutts field has a MMP of 1400 psia while the current maximum operating pressure is at 1100 psia in a large portion of the field. Another part of Arbuckle reservoir in Ogallah unit has a MMP of 1350 psi while it is operating at current reservoir pressure in the neighborhood of 1150 psi.

Arbuckle reservoirs are a significant resource in Kansas for improved oil recovery. These reservoirs have produced an estimated 2.2 billion barrels of oil representing 35% of the 6.1 billion barrels of oil of total Kansas oil production (Franseen *et al.*, 2004). Most Arbuckle reservoirs have active water drives which have maintained reservoir pressure at 1000-1100 psig for nearly 50 years even though millions of barrels of fluid have been produced. Initial studies of CO₂ miscible flooding indicated that miscibility is not achievable at the reservoir operating pressure in most Arbuckle reservoirs. Currently, over a hundred of small producers are operating in Arbuckle reservoirs. Unless an alternative technology is introduced, many of these fields in central Kansas will be abandoned with substantial remaining oil left in place. For this reason, we proposed to use an oil field, Ogallah unit in this project as an example to demonstrate our approach to evaluate CO₂ displacement in the near miscible region. The goal of this project is to demonstrate near miscible CO₂ application can substantially increase oil productions with CO₂ injection at pressures below MMP. The application of CO₂ injection at near miscible conditions may lead to development of CO₂ projects for small producers in reservoirs where the MMP is not attainable at current operating reservoir pressures.

In this report, we summarize the results from our experimental and computational studies to characterize and demonstrate the phase behavior, the displacement process, the oil recovery and CO₂ sequestration under near miscible conditions.

In the experimental studies, the description of the experiments and results is divided into four sections: 1) slim-tube experiment, 2) swelling/extraction test, 3) phase behavior model and

4) core flow test. In the computational studies, the methodologies of developing a reservoir model and assessment of the potential recovery processes at near miscible condition by numerical simulation are discussed. The simulation results of oil recovery and CO₂ sequestration at near miscible condition in a 47 acre lease of oil field are reported.

Background Information

The target oil field, Ogallah unit is located at Trego County, Kansas (as shown in Figure 1). The unit is currently operated by Carmen Schmitt, Inc. The unit produces from Arbuckle formation (3950-4060 ft) and other formations above the Arbuckle (Marmaton and Lansing-Kansas City). The Arbuckle formation is associated with structural high at central Kansas uplift and is thin to absent in parts of Northeastern Kansas (Franseen, *et al.*, 2004). Reservoir temperature ranges from 92°F to 130°F with an average temperature of 110°F. Active water drives have maintained reservoir pressure at approximately 1150 psi.

Primary production of the Ogallah started in 1951. Well production history shows that no water was produced before 1960. Water breakthrough in producers started after 1960. Due to the high water production, wells were work over with well deepening, formation plug-back and perforation at upper interval. At the peak of production in 1969, the Ogallah field had 85 producing wells. The field was producing 1.07 MMBO/year with cumulative production of 11.37 MMBO by 1969. After 1969, the field commenced commingle-production from Lansing Kansas City formation (LKC) and half amount of those wells were shut in at 1989 due to economic decline. The Ogallah field was unitized in 1991 and the number of active producers since then was reduced to 18.

2. EXPERIMENTAL STUDY

The experimental study comprises fundamental studies of phase behavior for the CO₂/crude oil system and the displacement process at near miscible condition. Phase behavior studies between CO₂ and Arbuckle crude oil were carried out to define near miscible condition in Arbuckle formation at Ogallah unit. Slim-tube experiments were conducted to determine the MMP. Swelling tests were performed to determine the relationship between saturation pressure, swelling factor and CO₂ volume injected. Extraction tests were conducted to examine extraction of liquid hydrocarbon into CO₂-rich phase and the effect of pressure on the extraction. The

results from both tests were used to examine the phase behavior at near miscible conditions independently from slim-tube experiments, and to identify characteristics of phase behavior in CO₂ displacement process. A phase behavior model based on the Peng-Robinson equation of state was used to characterize the experimental phase behavior interaction between CO₂ and oil. Core flow tests were conducted at pressures at near miscible condition in which the effect of CO₂ injection pressure, water saturation on oil recovery was evaluated. Completion of these experimental studies allow us to develop a representative flow model to simulate near miscible displacement physics and extend it to simulate CO₂ injection process in a reservoir model of oil field.

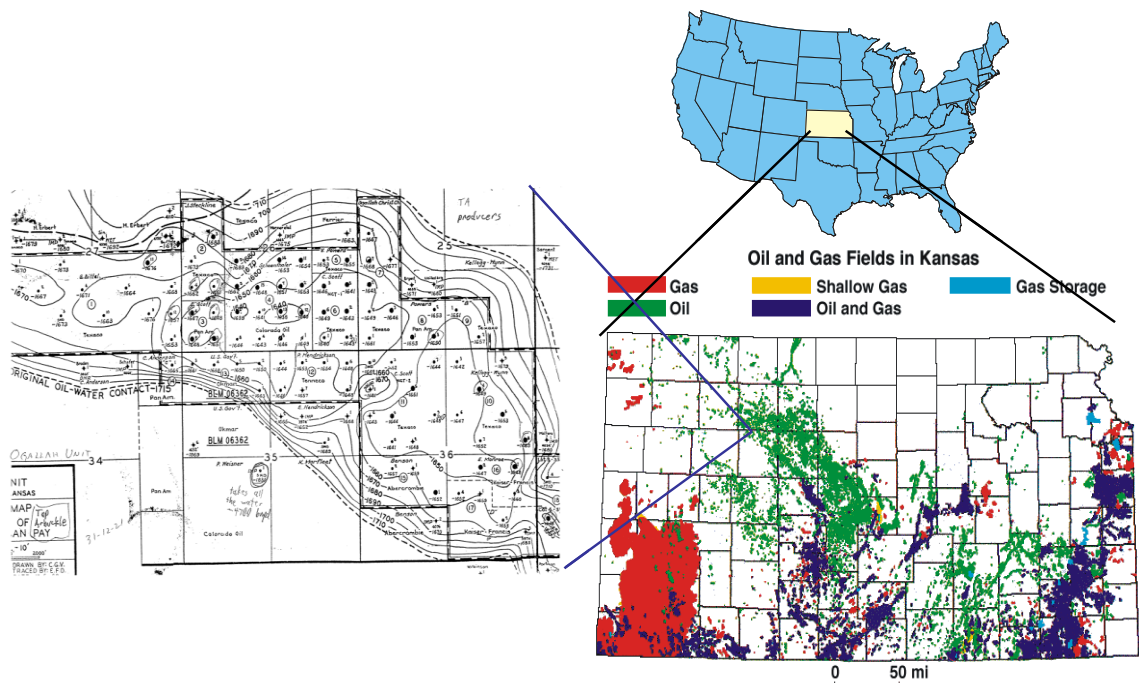


Figure 1 Ogallah unit, Trego County, Kansas

2.1 Slim-tube Experiments

The stock tank oil collected from tank battery from Ogallah unit was used for all the experiments. The crude oil was centrifuged and filtered in the laboratory. A compositional analysis of the crude oil using Gas Chromatography (GC) technique is shown in Figure 2. The physical properties of the oil are summarized in Table 1. Percentage of asphaltenes (heptane

insolubles) in this crude oil was determined approximately 0.93 % based on ASTM D 893-85 method.

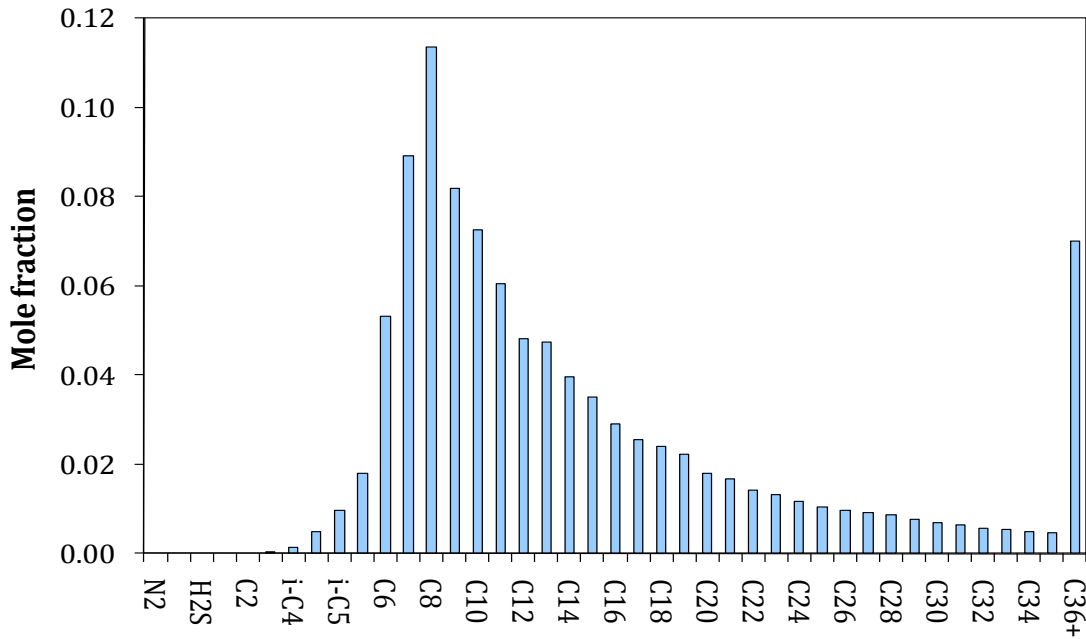


Figure 2 GC compositional analysis result of Ogallah crude oil

Table 1 Physical property of Ogallah crude oil

Molecular Weigh, g/mol	228.71
API gravity	33.34
Density @ 14.7 psi & 60°F, g/cc	0.8584
Viscosity @ 14.7 psi & 60°F, cp	13.4
C36+ molecular weight, g/mol	873.24
C36+ density @ 14.7 psi & 60°F, g/cc	0.9978

Minimum miscibility pressure was determined by performing displacement experiments in a 40-foot slim- tube. The lowest pressure at which oil recovery reaches 90% at 1.2 HCPV CO₂ injections is defined as the MMP. A series of slim-tube experiments were run at a suitable pressure increment to define the near miscible pressure range. Mixture density was measured using an in-line densitometer while the viscosity was measured with a high pressure viscometer independently.

Schematic of the slim-tube setup is shown in Figure 3. The system temperature is controlled and maintained in a Lindberg/Blue M oven with Eurotherm temperature controller. The system pressure is controlled and maintained by a back pressure regulator at the outlet. Back pressure regulator models BPR-50 is a dome-load type, which controls the upstream pressure at a setting pressure applied to the dome. The back pressure regulator has a working pressure of 5000 psi at 200°F.

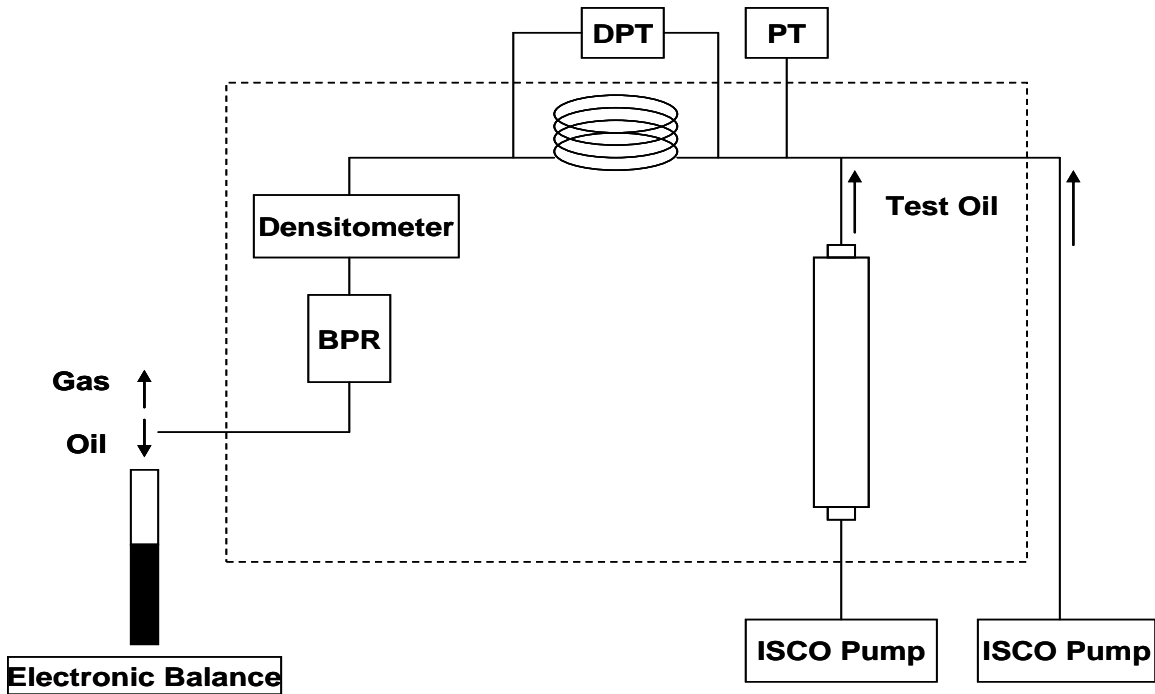


Figure 3 Schematic of slim-tube setup

Three Valydine pressure transducers are installed to measure pressures at different locations, such as pressure drop across the slim-tube, upstream pressures (CO_2 /oil pressure), and downstream pressure (back-pressure regulator pressure). The absolute pressure transducers have the capability of measuring pressures up to 2500 psi with the accuracy of 0.25% of their full scale (0-2500 psi) while the pressure range of the differential pressure transducer is 50 psi with the accuracy of 0.05% of its full scale.

The injection system consists of two ISCO 260DM syringe pumps (for CO_2 /crude oil transfer and injection at a desired rate) and a transfer cylinder (for crude oil storage). The

capacity of the transfer cylinder is 485 cc. The cylinder can withstand a maximum pressure of 3000 psi.

The slim- tube consists of a coiled 38.29 ft-long stainless steel tube with an ID of 0.24 in. packed with glass beads. Slim-tube properties are listed in Table 2.

Table 2 Slim-tube characteristics

Length, ft	38.29
O.D, in	0.31
I.D, in	0.24
Porosity	0.37
Bulk volume, cc	347.8
Pore volume, cc	127.76
Permeability, mD	4900
Packing beads	No. 2024

Density of the effluent is measured continuously by an inline densitometer. The densitometer consists of two units. The DPRn 422 density transducer measures the characteristic frequency of vibration. The Anton Paar mPDS 2003V3 Evaluation unit translates the characteristic frequency of vibration into a density value. The measuring range is 0-3g/cc within the temperature range of -13°F – 257°F and the pressure range of 0-2900 psi.

Effluent is continuously flashed to atmospheric conditions. The separator gas is connected to a flow meter. The separator liquid is collected in a graduated cylinder. The graduated cylinder is placed on an electronic balance which is connected to the data acquisition system.

Slim-tube displacements were conducted at 110°F and 125°F representing the range of temperatures reported from the field. Percentage of oil recovery at 1.2 PV of CO₂ injected was plotted against slim-tube average pressure to determine the MMP of the system at 110°F and 125°F. As shown in Figure 4, MMP of the system are estimated to be 1350 psig at 110°F and 1650 psig at 125°F. As expected, MMP increases with increasing temperature. This phenomenon is closely related to the dependence of CO₂ density on temperature and pressure and is explained in detail in the discussion of swelling/extraction experiment.

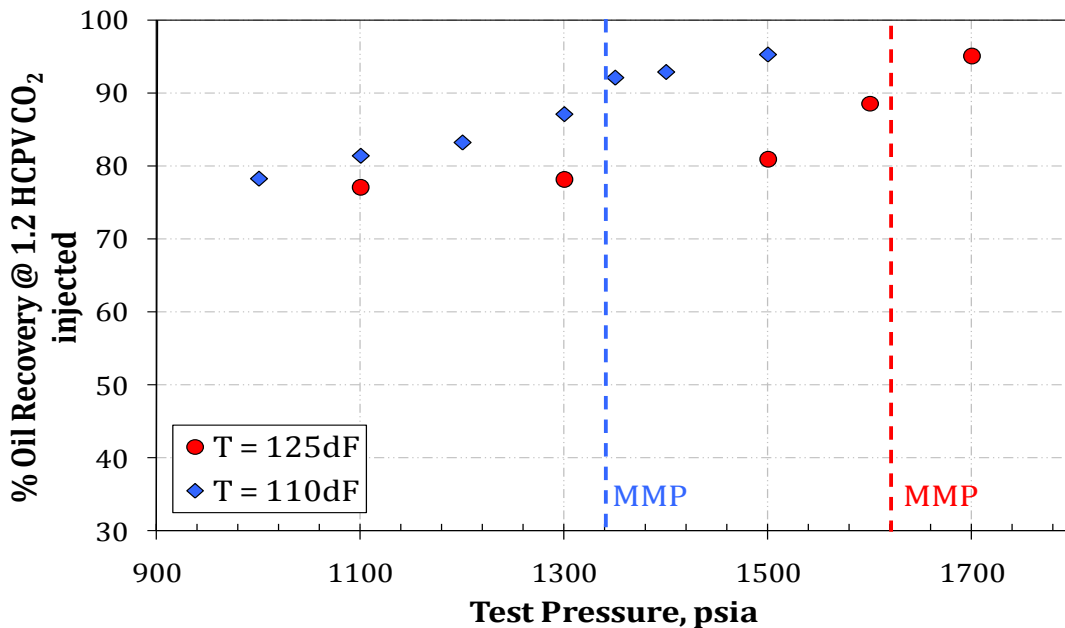


Figure 4 Minimum miscibility pressure determinations at 110°F and 125°F

Slim-tube experiment results indicate that miscibility is not achievable at the current reservoir pressure of 1150 psig which falls within a predefined near miscible pressure range between 1080 psig and 1350 psig (from 0.8 MMP to MMP). Nevertheless, the recovery efficiency at 1150 psig remains relatively high in a range of 78% to 83% at temperature between 110°F and 125°F.

Figure 5 shows the density profile of the effluent at pressures below MMP. Prior to the breakthrough of CO₂ the effluent density was equal to the oil phase density (0.834 g/cc) at reservoir temperature and slim-tube average pressure. The abrupt change in density of the effluent corresponds to the breakthrough of CO₂. Significant reduction of effluent density occurred at pressures below MMP following CO₂ breakthrough. After breakthrough of CO₂, average densities of the effluent were 0.434, 0.535 g/cc at average pressures of 1100, 1200 psig. At the same pressure and temperature, the densities of pure CO₂ are 0.221 g/cc and 0.275 g/cc. The increase of density in the effluent profile indicates that light hydrocarbon components from the oil continued to be vaporized or extracted by CO₂ which contributes to relatively high recovery efficiencies for near miscible CO₂ displacement.

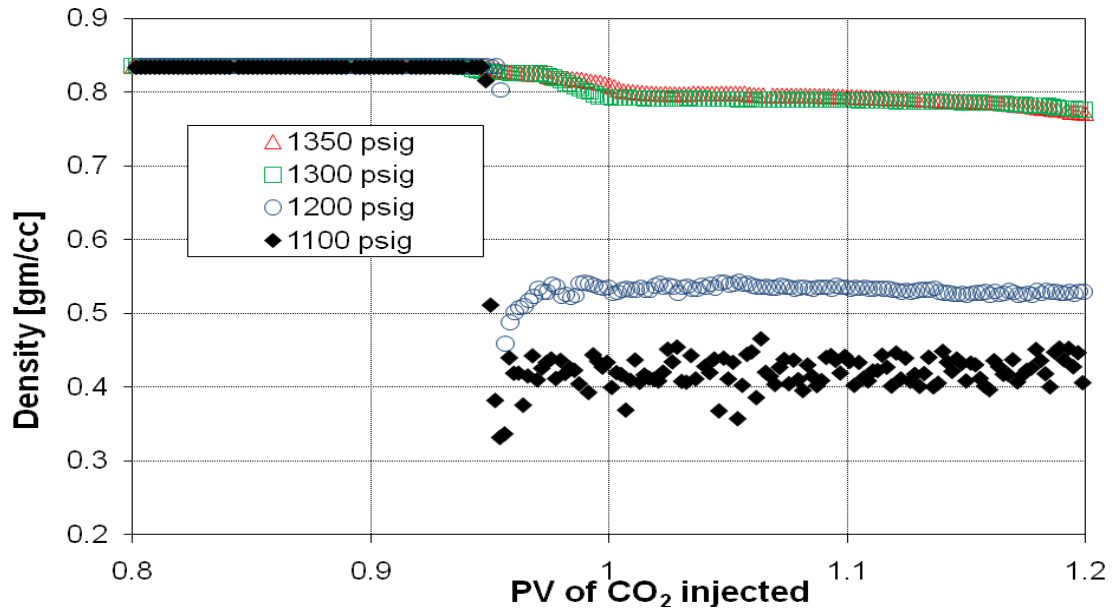


Figure 5 Density profile of the effluent at 110°F

Summary

- 1) The MMP was estimated to be 1350 psig at 110°F and 1650 psig at 125°F.
- 2) Miscibility is not achievable at the current reservoir pressure of 1150 psig.
- 3) The near miscible pressure conditions to be investigated in core flow test is defined from 1100 to 1350 psig.
- 4) At the current reservoir pressure of 1150 psig and at a temperature range of 110°F to 125°F, the recovery efficiency of the original oil in place from slim-tube experiment varied from 78 to 83% which is attributed to mass transfer mechanism between crude oil and carbon dioxide during the displacement process.

2.2 Swelling/Extraction Tests

Swelling/extraction tests were performed to examine the oil recovery mechanisms in the near-miscible region and to provide data to tune the phase behavior model. Swelling tests were conducted to determine the relationship between saturation pressure, swelling factor and CO₂ volume injected. Extraction tests were carried out to examine the extraction of liquid hydrocarbon into a CO₂-rich phase and the effect of pressure on the extraction.

Experimental Setup and Specifications

The schematic of swelling/extraction setup and its image are shown in Figure 6 and Figure 7. An ISCO 100DM syringe pumps is used for CO₂ injection. Temperature of the pump is controlled by a Fisher Isotemp circulator, model 3016 and measured by an Ertco-Eutechnic 5 digit thermister, model 4400 in the range of 0-100°C.

The gas lines are heated using fiberglass covered heating tape, controlled by two variable AC transformers, Staco Energy model 3PN1010B. Temperature of the gas lines is measured using T-type thermocouples. Fiberglass cloth tape is used to prevent heat dissipation to the surroundings.

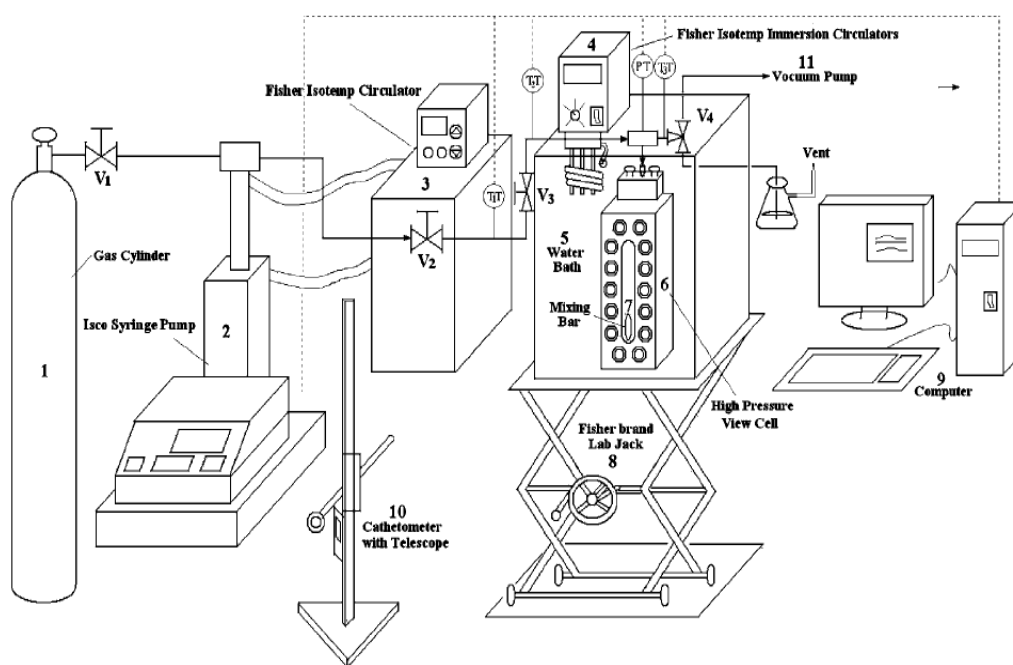


Figure 6 Experimental setup include (1) Gas cylinder (2) Isco Syringe pump (3) Fisher Isotemp circulator (4) Fisher Isotemp Immersion circulator (5) water bath (6) high pressure view cell (7) mixing bar (8) laboratory jack (9) computer (10) cathetometer with telescope (11) vacuum pump (Ren *et al.*, 2008)

The key component of this setup is the high pressure view cell with high pressure gauge glass window allowing visual observations of fluids under experimental conditions. The view cell is made of stainless steel and has a volume of 26 cc. The gauge glass window allows a maximum temperature of 280°C and pressure of 4000 psi. Pressure in the view cell is measured by a 5000 psi Heise DXD Series 3711 precision digital pressure transducer. A 3.2mm diameter

× 12.7 mm PTFE coated stir bar is placed inside the view cell. Mixing is achieved by an external rare-earth magnet in a slot behind the cell raised and lowered by a pulley system.

The view cell is immersed into the water bath by raising/lowering the platform jack. The temperature of the water bath is adjusted by an immersion circulator Haake DC30/DL3 and a Fisher Isotemp circulator, model 3016. An Eberbach 5160 cathetometer is used to measure the height of the liquid in the view cell.



Figure 7 Image of the swelling/extraction experimental setup

Experimental Procedures

In a typical swelling experiment, the ISCO pump is filled with CO₂. Pressure of the pump is set at the maximum anticipated pressure with a constant-pressure mode. The pump automatically adjusts the volume of CO₂ to maintain the desired pressure. Temperatures of the gas lines are maintained above the critical temperature of CO₂ to avoid CO₂ condensation inside the lines. Temperature of the water bath is set at the desired temperature. A predetermined volume of crude oil is carefully injected into the view cell to avoid liquid droplets on the wall of the view cell. The view cell is connected to the gas lines and then immersed into the water bath. The height of the liquid sample inside the view cell is measured using the cathetometer. The volume of the liquid sample is calculated using a pre-calibrated curve which correlates the volume with the measured height.

When the system is thermally equilibrated, the gas lines and the view cell are flushed with CO₂ at low pressure to remove any residual gas or air. The cell pressure is increased in discrete steps by CO₂ injection from the top of the view cell. CO₂ injection is stopped when a desired pressure is achieved. During pressurization process, the stir bar inside the view cell is used to mix the liquid and vapor phases, accelerating the mass transfer between the gas and liquid phase. When the system is in equilibrium, the height of the liquid sample in the view cell is measured with a cathetometer. Equilibrium between pressure changes takes from 30-60 minutes after vigorous mixing. The pump condition (temperature, pressure & final volume of CO₂), temperature of gas lines and the view cell condition (temperature & pressure) are recorded. All the data are transferred into a specially designed spreadsheet to calculate the solubility, density of the liquid solution, molar volume and volume expansion. The material balance calculations are based on the assumption that the amount of hydrocarbon extracted into the vapor phase is negligible. The composition of the liquid phase is based on the mass balance by determining the amount of CO₂ dissolved in the liquid. This assumption appears to be valid over a wide range of pressures. This method yields high resolution of solubility data (often better than ± 0.0001), pressure with accuracy of ± 3 psi, temperature of ± 0.01 °C, density up to $\pm 0.4\%$ and volume expansion to $\pm 0.05\%$ (Ren *et al.*, 2007). At the end of the experiment after depressurization, the view cell is cleaned with methylene chloride, acetone solution and blown dry with compressed air.

Experimental Principles

The phase equilibria data were obtained based on a mass balance and the following assumptions: 1) the pressure of CO₂ is much greater than the vapor pressure of the crude oil and 2) vapor phase composition of the hydrocarbon component is much less than CO₂. The mass balance equation of CO₂ is as follows:

$$m_g = m_{pump} - m_{lines} - m_{headspace} + m^o_{lines} + m^o_{headspace}$$

$$m_{pump} = \Delta V_{pump} \rho(T_{pump}, P_{pump})$$

$$m_{lines} = \Delta V_{lines} \rho(T_{lines}, P)$$

$$m_{headspace} = \Delta V_{headspace} \rho(T, P) = (V_{cell} - V_{liquid}) \rho(T, P)$$

$$m^o_{lines} = \Delta V_{lines} \rho(T_{lines}, P^o)$$

$$m^o_{headspace} = \Delta V_{headspace} \rho(T, P^o) = (V_{cell} - V_{liquid}) \rho(T, P^o)$$

where

m_g : the mass of CO₂ dissolved in the liquid

m_{pump} : equal to the product of volume of CO₂ displaced from the pump and density of CO₂ at the pump constant temperature & pressure

m_{lines} : the product of volume of the lines and density of CO₂ at temperature of the lines & system equilibrium pressure

m^o_{lines} : the product of volume of the lines and density of CO₂ at temperature of the lines & system initial pressure

$m_{headspace}$: the product of volume of the headspace and density of CO₂ at temperature & pressure of the equilibrium system. The volume of the headspace is the difference between volume of the cell and volume of the liquid in the cell.

$m^o_{headspace}$: the product of volume of the headspace and density of CO₂ at temperature & pressure of the initial system. The volume of the headspace initially is the difference between volume of the cell and initial volume of the liquid in the cell.

CO₂ density was calculated using REFPROP database (developed by the National Institute of Standards and Technology) which used the ultra-accurate Span-Wagner equation of state. Mole fraction of CO₂ in the liquid phase was calculated as follows:

$$x_g = \frac{n_g}{n_g + n_l} = \frac{m_g / M_g}{m_g / M_g + m_l / M_l}$$

Apparatus Validation

The apparatus was verified by comparing experimental data obtained from this apparatus with literature data for n-decane/CO₂ mixture at 71.1°C. (Ren *et al.* 2008). The experimental data

had excellent agreement with the literature data obtained from different experimental methods. Phase equilibrium data of CO₂/n-decane at 71.1°C was obtained and shown in Table 3.

Analysis of this data was based on the assumption that the amount of liquid component in the vapor phase is negligible. Although the composition of the vapor phase was not actually analyzed in our experiments, it had been demonstrated earlier by Ren *et al.* (2007) that the percentage of n-decane in CO₂ vapor phase was less than 0.13%. Figure 8 shows that the p-x phase equilibrium of CO₂/n-decane generated using this apparatus were reproducible and in excellent agreement with literature data by Nagarajan *et al.* (1986) and Jennings *et al.* (1996). As a consequence, the apparatus was validated and used for the measurement of vapor liquid equilibrium data of crude oil/CO₂ system.

Table 3 Phase equilibrium data of CO₂/n-decane at 71.1°C

Run 1		Run 2	
Pressure, psi	x _{CO2}	Pressure, psi	x _{CO2}
192.18	0.09609	209.43	0.10900
425.25	0.21070	434.97	0.22498
701.98	0.34940	643.68	0.32669
1005.55	0.50260	866.89	0.44391
1270.24	0.61657	1080.39	0.52821
1448.35	0.69121	1321.58	0.64927
1531.45	0.72330	1495.77	0.71555
1666.05	0.77723	1612.38	0.76148
		1709.41	0.80048
		1771.35	0.82829

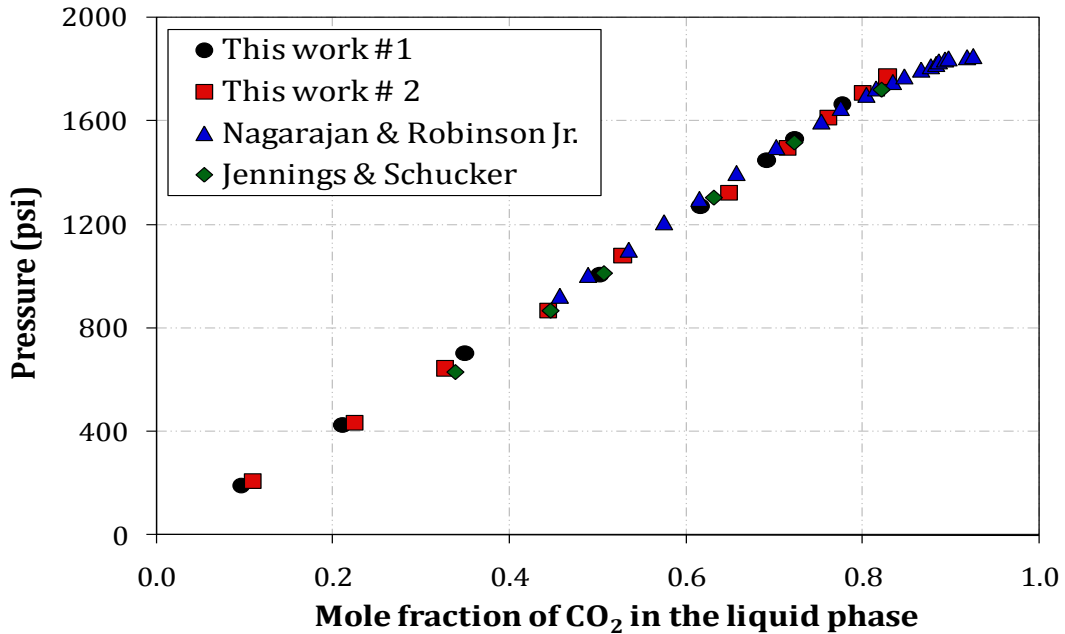


Figure 8 Comparison of liquid phase compositions for CO₂+ n-decane system at 71.10°C (160°F) with literature data (○) this work (□) this work (Δ) Nagarajan & Robinson Jr. (◇) Jennings & Schucker

Effect of System Pressure

Figure 9 illustrates the observations of Ogallah oil/CO₂ phase behavior. The volume of oil in the liquid phase increases with the increasing pressure (P_1) as CO₂ dissolves in and swells the oil. As the pressure (P_2) further increases, CO₂ density increases. Since the ability of CO₂ to extract hydrocarbon components from crude oil is enhanced as its density increases with the pressure, CO₂ starts extracting hydrocarbons from the crude oil. The volume of oil in the liquid phase is reduced at pressure above P_1 as the rate of extraction becomes greater than the rate of swelling.

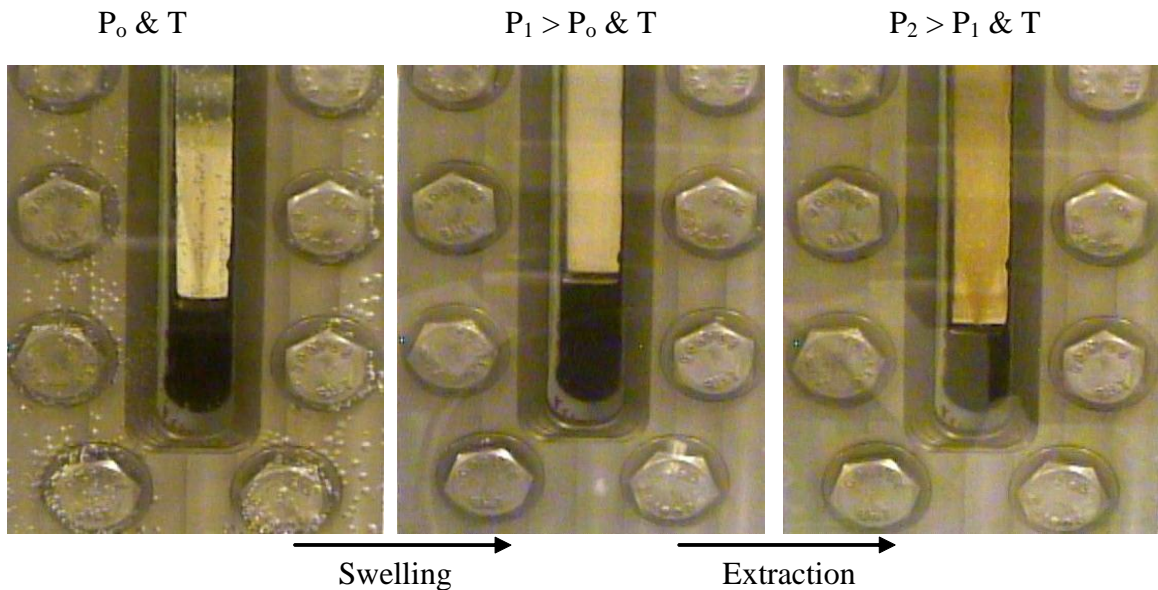


Figure 9 Change of initial oil volume with pressure

Figure 10 shows the swelling/extraction curve for Ogallah/ CO_2 system at 110°F with the sample size of 3 cc. The sample volume was about 12 % volume of the view cell. The swelling factor (SF) of oil is the ratio of liquid volume at test pressure divided by the liquid volume at atmospheric pressure and at 110°F . This value is determined by measuring the change of the interface level as a result of CO_2 dissolution in the oil or as a result of hydrocarbon extracted into the CO_2 rich vapor phase. Swelling factor was equal to 1 at initial conditions. As a result of CO_2 dissolution into the liquid phase, the liquid phase swelled and the swelling factor was greater than 1. Maximum swelling occurred at 1158 psi, when volume of the liquid phase became 1.21 of its original volume with 0.728 mole fraction of CO_2 dissolved in the liquid phase.

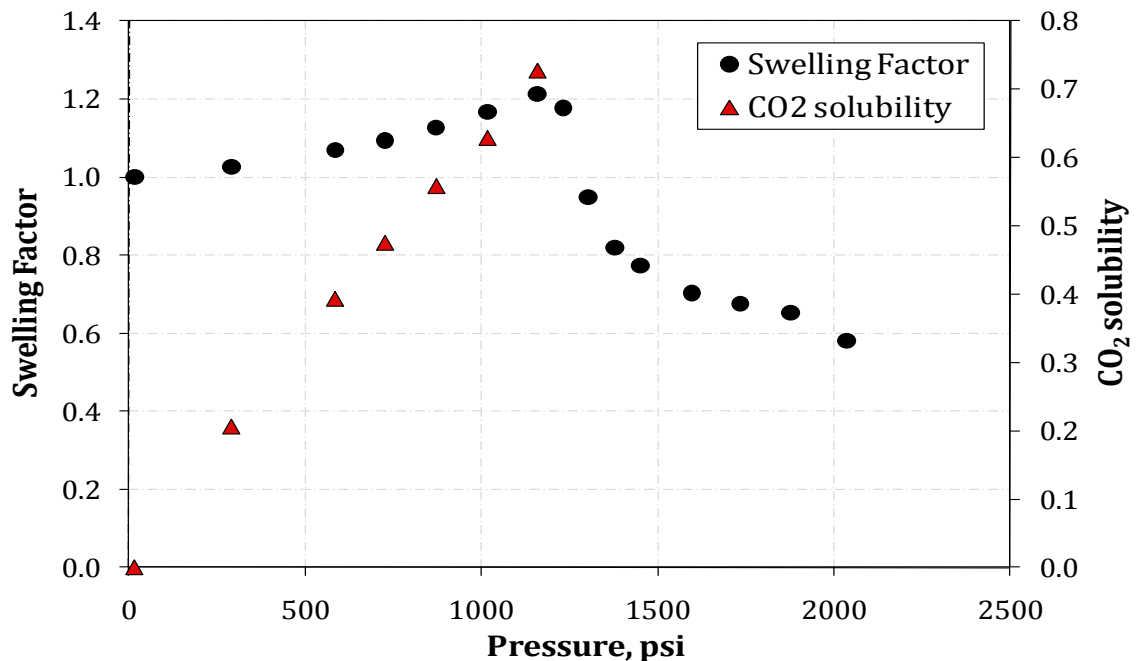


Figure 10 Effect of pressure on CO₂ solubility and swelling factor at 110°F

Major extraction started at approximately 1158 psi. As pressure increased, hydrocarbon components of the crude oil were removed from the liquid phase, the liquid phase shrank and swelling factor was reduced. At 2035 psi, the volume of CO₂ rich liquid phase shrank as much as 39.2 % of its original volume. CO₂ solubility is also plotted in Figure 10 as a function of pressure up to 1158 psi. Calculations of CO₂ solubility at pressures above 1158 psi are invalid since the assumption that the components of the liquid phase do not vaporize does not hold true. In the pressure range from 1100 psig to 1350 psig which is within 0.80 MMP, the extraction or vaporization of hydrocarbon components from crude oil appears to be the primary mechanism in phase behavior between the interaction of CO₂ and oil.

Effect of System Temperature

Swelling/extraction experiments were performed under various temperatures from 105°F to 125°F. Effects of temperature on CO₂ solubility and oil swelling/extraction curve are shown in Figure 11 and Figure 12. CO₂ solubility increases with increasing pressure and decreases with increasing temperature. The rate of oil swelling decreases with increasing temperature. The pressure at which oil swelling reaches maximum or at which CO₂ begin extracting components from crude oil increases with increasing temperature, ranging from 1159 psi to 1260 psi at a

temperature range of 105°F to 125°F. The rate of oil shrinkage decreases with increasing temperature.

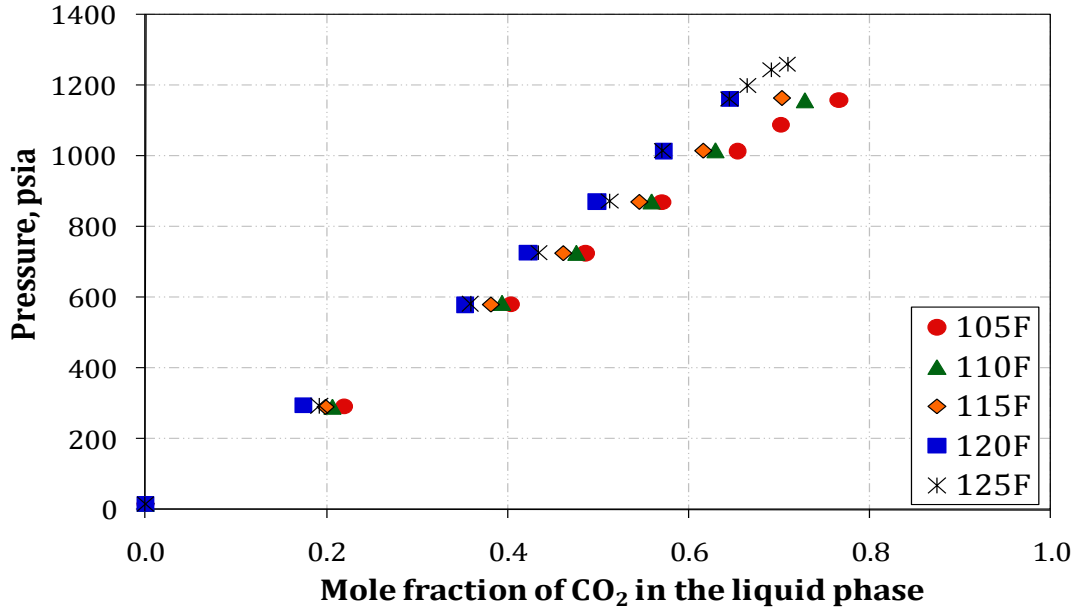


Figure 11 Effect of temperature on CO₂ solubility

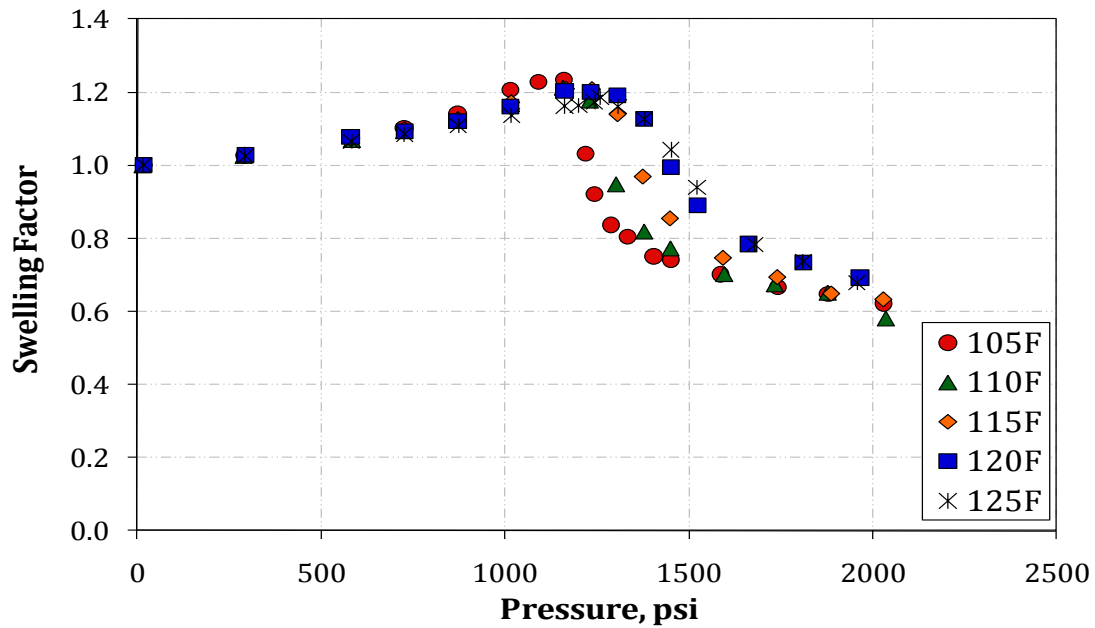


Figure 12 Effect of temperature on Swelling/ Extraction curves

The ability of CO₂ to extract hydrocarbon from the crude oil depends on its density. At higher temperature, a higher pressure results in a density equivalent to its density at a lower temperature. Holm and Josendal (1982) reported that the extraction of liquid hydrocarbons into CO₂-rich vapor phase occurs when the density of CO₂ is at least 0.25 to 0.35 gm/cc. The extraction of oil starts at density of CO₂, 0.26 gm/cc at 105 °F and 1150 psig. At 125 °F, the pressure of CO₂ needs to increase to have an equivalent density to start the extraction and it is in the neighborhood of 1300 psia.

2.3 Viscosity Measurements

A high pressure viscometer (ViscoPro 2000 System 4-SPL-440 with Viscolab software) manufactured by Cambridge Applied System was used to measure the viscosity of crude oil and crude oil/CO₂ mixture at different pressures.

The viscometer utilizes the principles of annular flow around an axially oscillating piston. It contains two magnetic coils inside a stainless steel body. A low mass stainless steel piston inside the measurement chamber is magnetically forced back and forth in the fluid. As the piston is pulled toward the bottom of the measurement chamber, it forces the fluid at the bottom of the chamber to flow around the piston toward the sensor opening where it interchanges with the normal flow of the fluid. On the upward piston stroke, fresh process fluid is pulled around the piston to the bottom of the measurement chamber. The time required for the piston to move a fixed distance is related to the viscosity of the fluid in the chamber. Temperature is measured continuously with the use of a platinum Resistance Temperature Detector (RTD) mounted at the base of the measurement chamber.

Experimental Setup and Specifications

The schematic of the setup is shown in Figure 13 along with its image in Figure 14. The high pressure sensor is placed inside a temperature-controlled oven and connected to a manual high pressure syringe pump (Model No. 50-575-30; 30,000 psi). The sensor is capable of measurements from 0.2 to 10,000 cp at a maximum pressure of 137.9 MPa and in a temperature range of 233.15K to 463.15K. The measurement chamber of the high pressure sensor is connected to a rupture disk (RD) and a precision pressure transducer (PT). When the setup is used for viscosity measurements of pure crude oil as a function of pressure, a high-pressure

generator is required. When it is used for viscosity measurements of crude oil/CO₂ mixture, the pressure of the system is increased by CO₂ injection. ISCO 260D pump is used for CO₂ transfer/injection. A view cell placed inside the oven allows observations of crude oil/CO₂ interaction. During pressurization process, the time required for the contents in the system to equilibrate under a particular pressure and temperature is minimized by a circulation pump-Micropump, Inc. Model 415A.

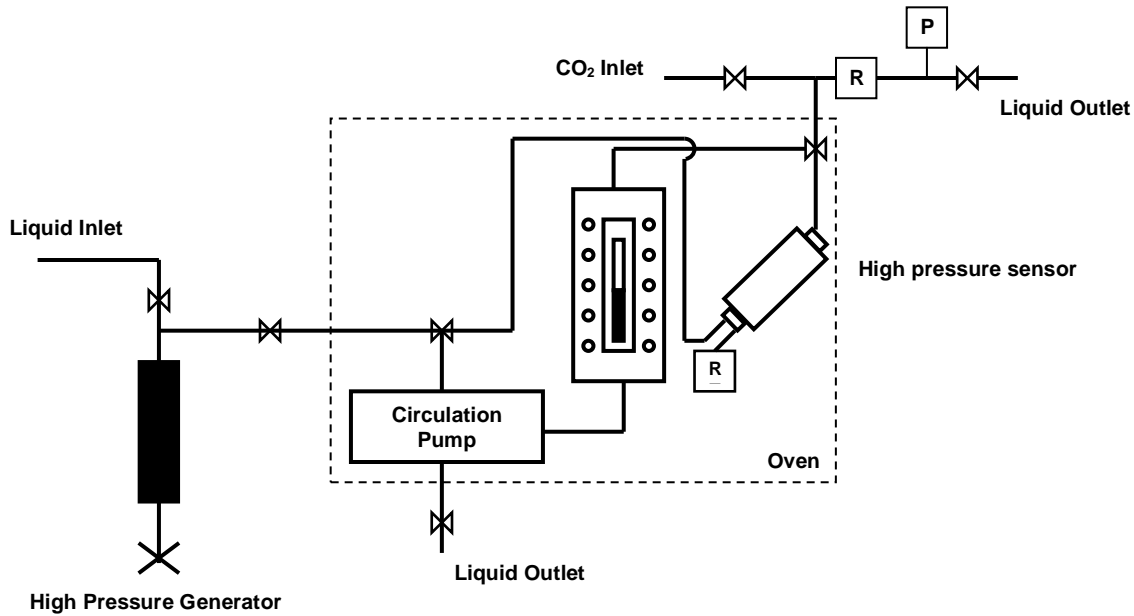


Figure 13 Schematic of high-pressure viscosity measurement setup

Figure 15 shows the effect of pressure on the viscosity of pure crude oil at 110°F which indicates the viscosity of oil is increased with the pressure. Figure 16 demonstrates the effect of CO₂ dissolution into crude oil on the viscosity of CO₂ saturated oil at 110°F. Dissolution of CO₂ into the crude oil reduces the viscosity of crude oil to as much as a factor of five. The reduction of oil viscosity observed in the near miscible pressure range, from 1100 psig to 1350 psig, reduces the mobility ratio between CO₂ and oil in the displacement process and consequently viscous fingering.

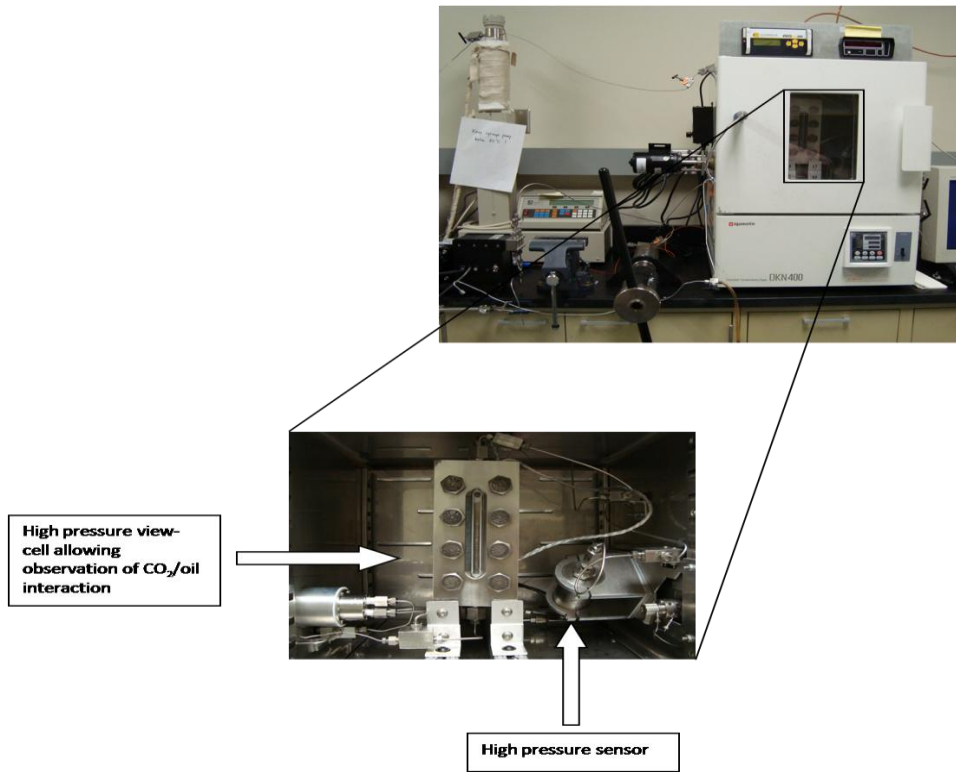


Figure 14 Image of the high-pressure viscosity measurement setup

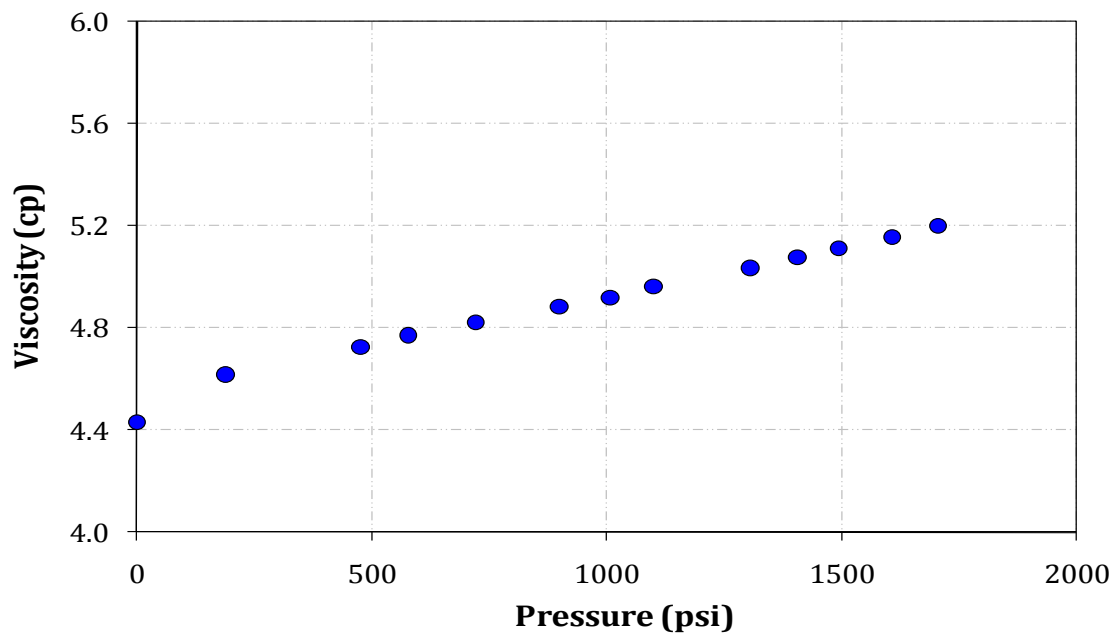


Figure 15 Effect of pressure on Ogallah oil viscosity at 110°F

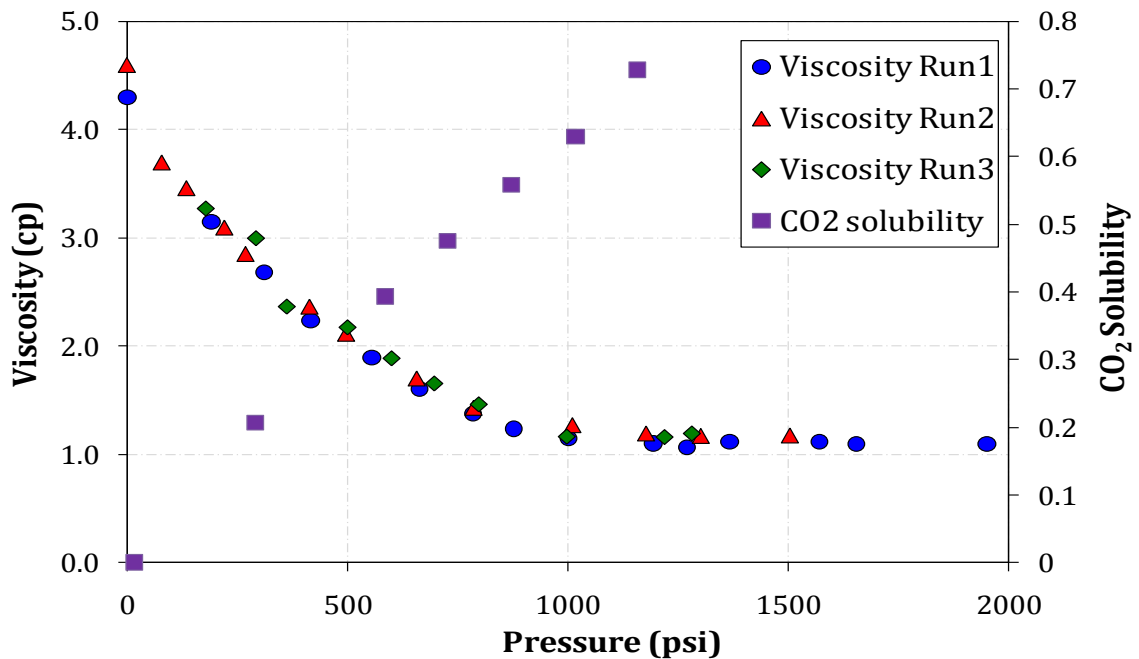


Figure 16 Viscosity of crude oil saturated with CO₂ at 110°F

2.4 Estimation of MMP

The relationship between the phase behavior observed in swelling/extraction tests and MMP measured by slim-tube experiment has been investigated by several researchers. Harmon and Grigg (1988) reported a relationship between the pressure required to initiate significant extraction in swelling/extraction tests and the MMP from slim-tube experiment. They proposed that a rapid rise in CO₂ upper-phase density of measurement due to the extraction of hydrocarbon components from the crude oil corresponds to the process by which multiple-contact miscibility is developed. However, Hand and Plnczewski (1990) concluded no such direct relationship between the two tests because the vapor phase density, dominated by high solvent CO₂ concentration, is not a sensitive indicator of the onset of major extraction, or of MMP. In this work, we observed MMP can be graphically derived from the extraction test. By examining the extraction test results with MMP measured from the slim-tube experiment, a relationship exists between these two tests if the initial oil volume tested in view cell is small (12%) and the relative volume of oil due to extraction falls below 0.8 over the pressure range investigated. Figure 17 present swelling/extraction test curves of oil/CO₂ system at 110 °F and 125 °F. The rate of slope changes in two distinct stages in each of the two extraction curves. Drawing lines through the

major extraction and secondary stages, the pressure at the intersection of these two lines is close to MMP determined with the slim-tube experiment. As shown in this figure, the pressures at the intersection point are 1340 psig and 1640 psig at 110 °F and 125 °F, respectively. The MMP determined from slim-tube for oil B/CO₂ were 1350 psig and 1650 psig.

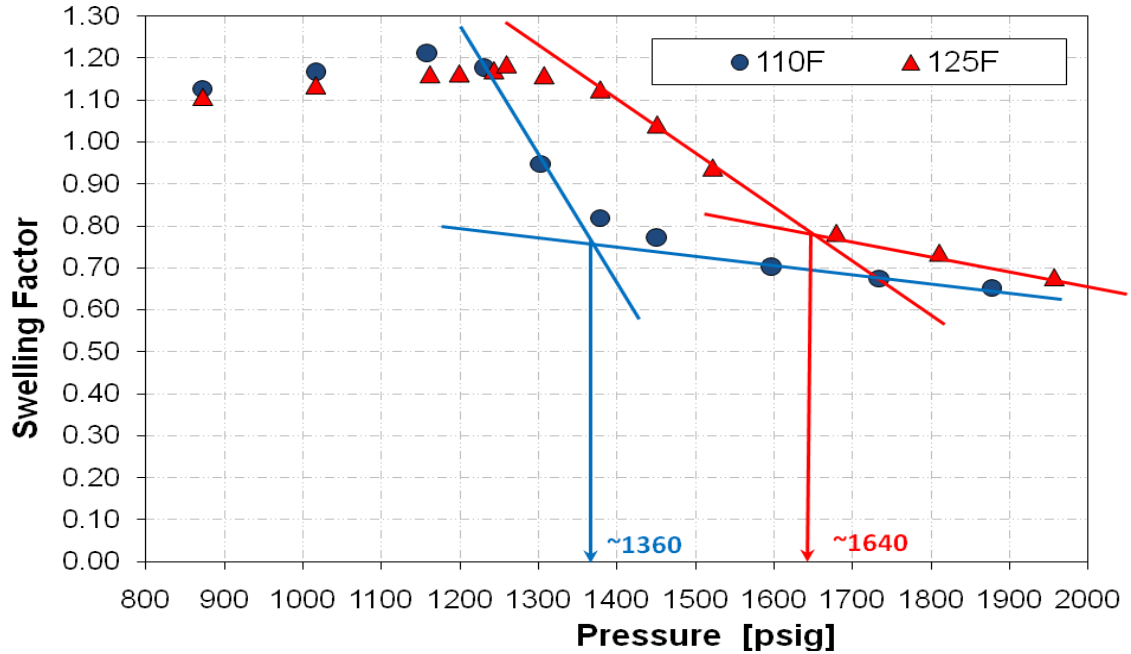


Figure 17 Estimation of MMP from extraction test of Ogallah crude oil

Summary

- 1) CO₂ solubility increases with increasing pressure and decreases with increasing temperature. As a result of CO₂ dissolution into the liquid phase, the liquid phase swells. The degree of swelling depends on pressure and temperature.
- 2) The pressure at which CO₂ begins to extract significant amounts of hydrocarbons from crude oil increases with increasing temperature. The amount of extraction increases with increasing vapor-phase volume (decreasing initial oil volume) and decreases with increasing temperature.
- 3) Significant extraction started at pressure of 1150 psig and 110°F. Extraction or vaporization of hydrocarbons into the CO₂ rich phase is the primary mechanism for oil recovery in the near-miscible region, from 1100 psig to 1350 psig at 110°F

- 4) Swelling/extraction tests provide valuable phase behavior data which is used later to tune the phase behavior model.
- 5) A nearly five-fold reduction in oil viscosity was achieved in the near-miscible region with CO₂ injection.
- 6) The reduction of oil viscosity improved the total mobility ratio between reservoir oil and the displacing fluid, which will affect the recovery efficiency in a favorable way.
- 7) Viscosity measurements are useful in tuning the phase behavior model.
- 8) The MMP estimated by the swelling/extraction test graphically is close to what determined from the slim-tube experiment.

2.5 Phase Behavior Model

A phase behavior model based on the Peng-Robinson equation of state was used to characterize the phase behavior interaction between CO₂ and oil. The model was adjusted to match the saturation pressure and swelling factors derived from the swelling tests. This phase behavior model was used in a compositional reservoir simulator GEM (from Computer Modeling Group, Inc.) to match slim-tube experiments. Parameters in the model were adjusted accordingly to obtain the best match. The final tuned model was to be used to in compositional simulator to describe CO₂ injection process for potential field applications.

Equation of State

Equations of State (EOS) have been introduced widely to model and predict CO₂-crude oil phase behavior. An EOS is an algebraic relationship between pressure, temperature, and molar volume for a single component or a mixture. Peng-Robinson EOS was used in this study to describe the fluid properties and the oil/CO₂ interaction.

$$P = \frac{RT}{v - b} - \frac{a}{v^2 + 2vb - b^2}$$

The parameters a and b are defined using the following mixing rule for mixtures,

$$a = \sum_i x_i S_i$$

$$S_i = \sqrt{a_i} \sum_j x_j (1 - d_{ij}) \sqrt{a_j}$$

$$b = \sum_i x_i b_i$$

where, d_{ij} is an empirically determined interaction coefficient.

For pure components, the parameter a_i and b_i are expressed in terms of the critical properties and the acentric factor:

$$\sqrt{a} = \sqrt{a_c \alpha}$$

$$\sqrt{a_c} = \sqrt{\Omega_a (RT_c)} / \sqrt{p_c}$$

$$\sqrt{\alpha} = 1 + \kappa \left(1 - \sqrt{T/T_c}\right)$$

$$b = \Omega_b RT_c / p_c$$

Where, Ω_a and Ω_b are the EOS parameters with the default values of 0.45723553 and 0.077796074 for the PR EOS.

The κ is obtained from the following empirical correlations,

$$\kappa = 0.379642 + 1.48503 \omega - 0.164423 \omega^2 + 0.016666 \omega^3$$

While the application of the EOS to simple mixtures is relatively straightforward, crude oil systems pose many seemingly insurmountable problems. The essential infinite number of components contained in a typical crude oil makes it impossible to obtain a complete chemical analysis. Standard oil analysis lumps all components heavier than C36 into a single C36+ pseudo-component characterized by its average molecular weight and density. Therefore, the parameters of the EOS were adjusted so that the EOS could reproduce the laboratory-determined oil properties and the observed oil/CO₂ interaction.

Slim-tube model was constructed using 1-D compositional simulator with the tuned EOS. Simulated slim-tube results were compared with experimental slim-tube results. The following sections describe in detail the development of phase behavior model/slim-tube model in CMGTM software and the application of this phase behavior model to match with experimental PVT data and slim-tube results.

Phase Behavior Modeling Using WINPROP

WinProp, a CMG software was utilized to build the phase behavior model. The EOS requires the following properties for each component, critical pressure (P_c), critical temperature (T_c), acentric factor (ω), and interaction coefficients between different components (d_{ij}) to perform phase equilibrium calculations. The molecular weight (MW) is also required to calculate mass densities. Additional factors such as the volume shifts τ , and the equation-of-state parameters Ω_a and Ω_b can also be adjusted for each component to enhance the equation of state predictions.

Pure hydrocarbon components were selected from the software library list, as well as generalized single carbon number (SCN) petroleum fractions FC6 through FC45. The specific gravities, molecular weights and boiling points of the SCN fractions were obtained from Whitson *et al.* (2000). The critical properties of these fractions were calculated with the Lee-Kesler correlation. The heavy lumped component C36+ was defined using specific gravity and molecular weight. Physical and critical properties of C36+ were assigned using Twu and Lee-Kesler correlation respectively. For accentric factors, the Lee-Kesler correlation was recommended for petroleum fractions. Equilibrium phase viscosities were calculated with the Pedersen viscosity corresponding states model. The Pedersen viscosity correlation uses the principle of corresponding states to calculate the viscosity of a component or mixture, knowing the viscosity of a reference substance at the same conditions of reduced pressure and temperature. The deviation from simple corresponding states is accounted for by a “rotational coupling coefficient”, α . The reference substance for the Pedersen model is methane. The viscosity of the mixture is calculated according to the following formula:

$$\frac{\mu_{mix}(P, T)}{\mu_o(P_o, T_o)} = \frac{T_{c,mix}^{-1/6}}{T_{c,o}} \frac{P_{c,mix}^{2/3}}{P_{c,o}} \frac{MW_{mix}^{1/2}}{MW_o} \frac{\alpha_{mix}}{\alpha_o}$$

When the components representing the fluid model had been selected and their compositions had been specified, a grouping scheme was performed primarily for the purpose of speeding up the simulation running time. Whitson suggested that C7+ should be grouped into NH pseudo-components given by,

$$N_H = 1 + 3.3 \log(N - 7)$$

The groups are separated by molecular weights MI given by,

$$M_I = M_{C_7} (M_N / M_{C_7})^{1/N_H}$$

where N = CN of the heaviest fraction in the fluid description and I = 1 to NH

Therefore, NH = 5 pseudo-groups

Group 1 < M1 = 138.303

M1 < Group 2 < M2 = 191.276

M2 < Group 3 < M3 = 264.539

M3 < Group 4 < M4 = 365.865

Finally an 8-component EOS fluid model was obtained after grouping the components as
 Group 1: C3 + iC4 + nC4; Group 2: nC5+ iC5; Group 3: C6 ; Group 4: C7 – C9
 Group 5: C10 – C13; Group 6: C14 – C18; Group 7: C19 – C25; Group 8: C26 – C36+

Equation of State Characterization

Figure 18 and Figure 19 present the experimental data and the simulated data after tuning EOS parameters. Molecular weight (MW) of the heavy fraction was adjusted to match the oil density. Coefficients of Pedersen viscosity correlation were adjusted to match the oil viscosity. Binary interaction coefficients (BIC) between CO₂ and the hydrocarbon components as well as CO₂ volume shift factor were adjusted to match saturation pressure and swelling data. Table 4 shows the adjustment of each parameter to achieve the match. The maximum percentage error between simulated data and experimental data after tuning the EOS is presented in Table 5.

Table 4 Adjustments of EOS parameters

Variable	Lower Bound	Upper Bound	Initial Value	Final Value
MW C26 to C36+	5.07E+02	7.60E+02	6.34E+02	5.98E+02
Volume shift of CO ₂	-1.54E-01	9.20E-01	0.00E+00	9.11E-01
BIC (C7-C9)-CO ₂	0.00E+00	2.00E-01	1.50E-01	0.00E+00
BIC (C10-C13)- CO ₂	0.00E+00	2.00E-01	1.50E-01	0.00E+00
Coefficient of viscosity correlation # 4	1.00E+00	2.22E+00	1.85E+00	1.04E+00
Coefficient of viscosity correlation # 5	4.14E-01	6.21E-01	5.17E-01	6.21E-01

Table 5 Maximum percentage errors between simulated and experimental data

	Maximum error percentage
Viscosity	3 %
Density	1 %
Saturation pressure	7 %
Swelling factor	1 %

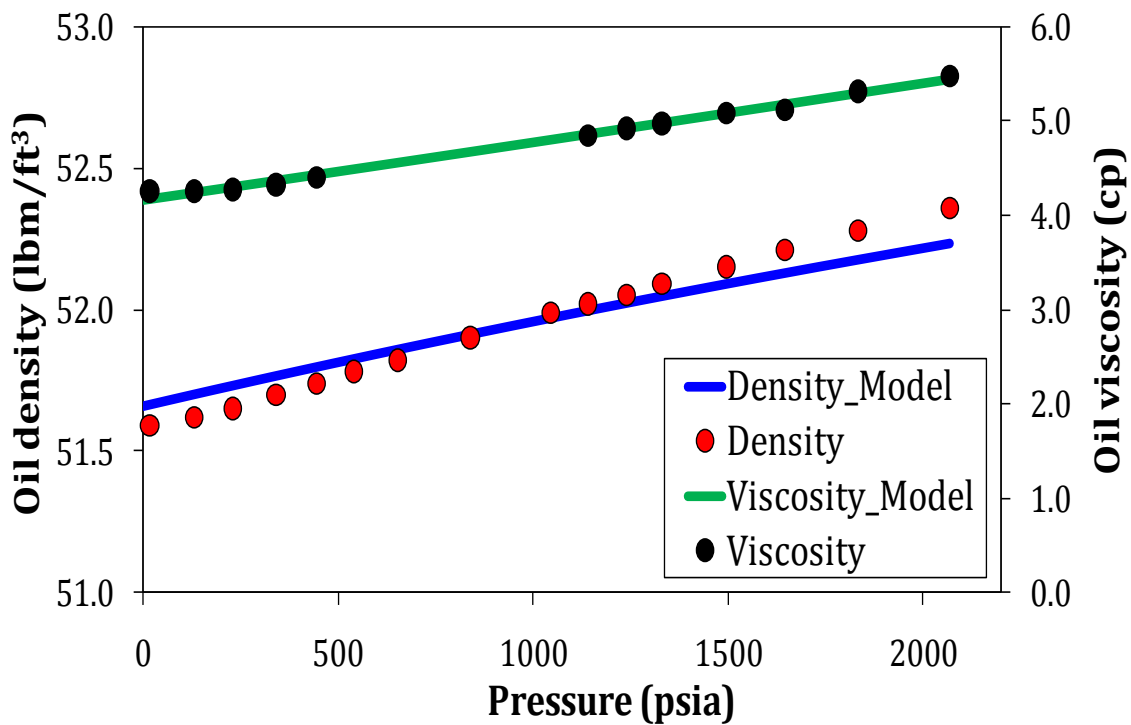


Figure 18 Comparison of viscosity/density experimental data and simulated data

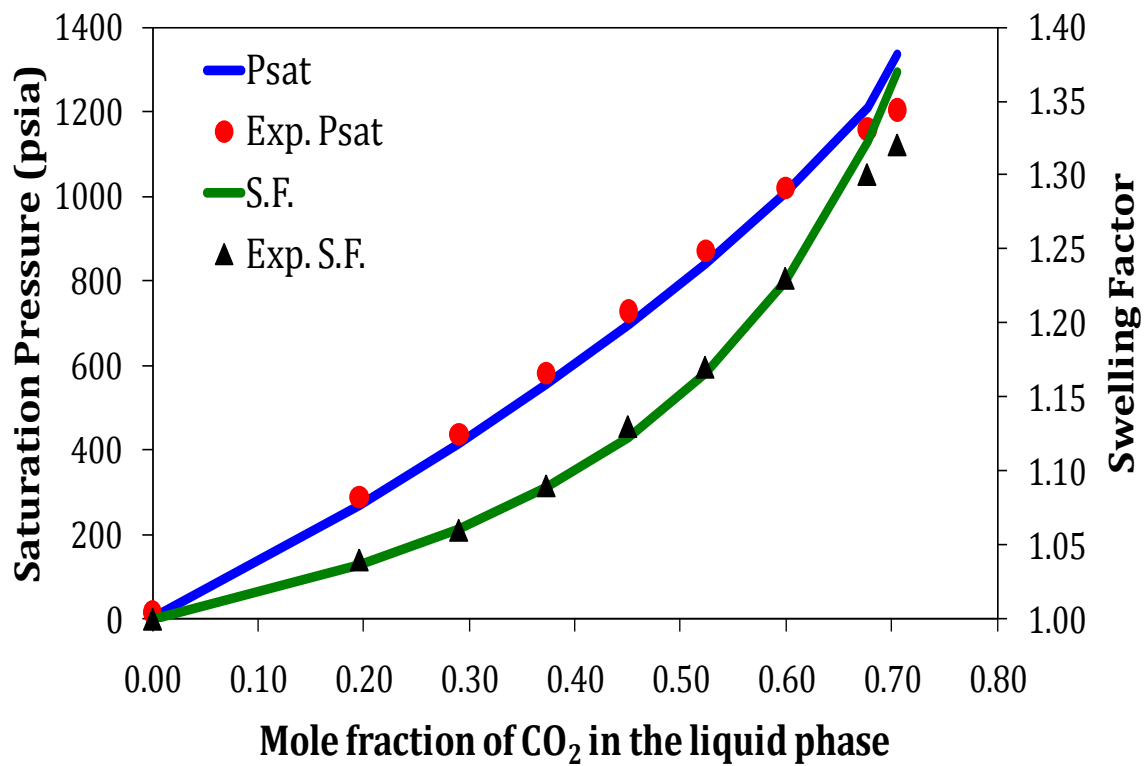


Figure 19 Comparison of saturation pressure/swelling factor experimental and simulated data

Slim-Tube Experiment Modeling Using GEM

A slim-tube model was created in compositional model simulator of GEM from CMG package with the phase behavior model derived from this phase behavior study. The slim-tube was represented by a one dimensional linear model using 320 grid blocks. The grid block sizes were 0.125 ft, 0.0185 ft and 0.0185 ft in I, J, K direction respectively. One injector and one producer were incorporated at the ends of the model. Some relevant information of slim-tube model is summarized in Table 6.

Table 6 Slim- tube model properties

Length, ft	40
Porosity, PV	0.367
Permeability, mD	4900
Pore Volume, cc	142.3
No. of blocks	320
Grid size in I direction, ft	0.125
Cross section, ft ²	0.0003423
Grid size in J and K direction, ft	0.0185
Geometry	Square Cross-section

The slim-tube gas/oil relative permeability data used in this model were obtained from Negahban and Kremesec (1992). A number of slim-tube displacements were simulated. Figure 20 compares the recovery efficiency from simulation and experimental work at 1.2 PV of CO₂ injected. As shown by Figure 20, the phase behavior model predicts the MMP and the oil recovery reasonably well.

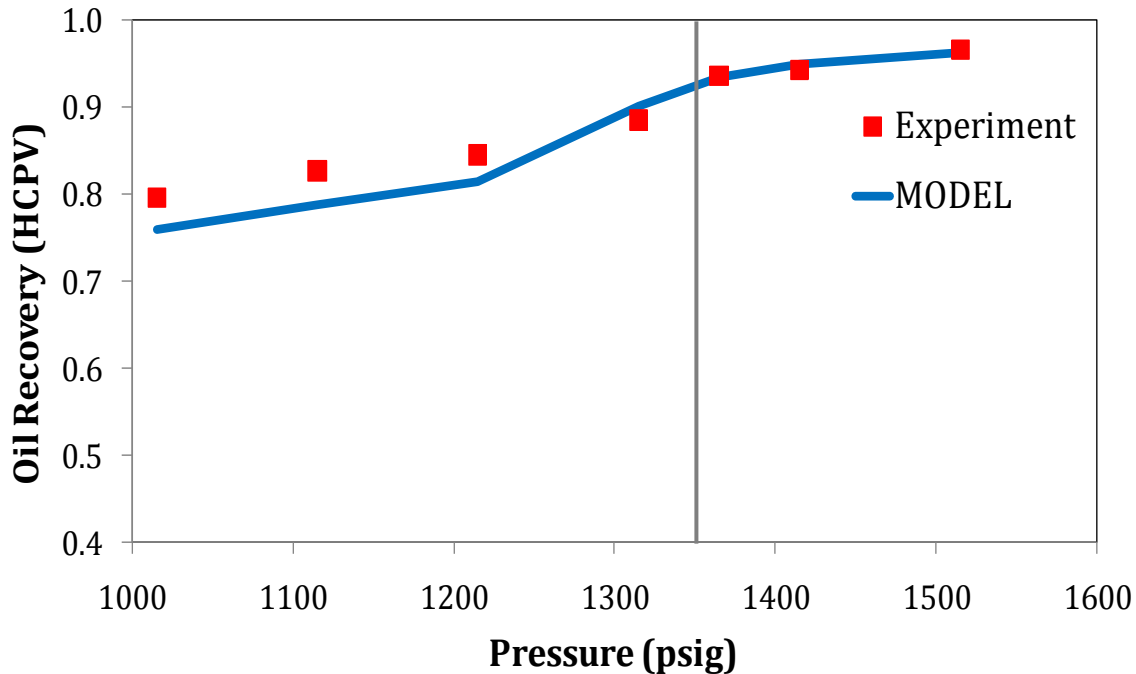


Figure 20 Comparison of simulated MMP and experimental MMP

Summary

- 1) A phase behavior model based on the Peng-Robinson equation of state was used to characterize the phase behavior interaction between CO₂ and oil.
- 2) The parameters were adjusted to match the saturation pressure and swelling factors derived from the swelling tests.
- 3) The phase behavior model successfully modeled the measurement of MMP from the slim-tube experiment. This 8 pseudo-component of hydrocarbon phase behavior model was further reduced to one with 4 pseudo-components and used in compositional reservoir model to simulate CO₂ injection process.

2.6 Core Flow Test

Arbuckle reservoir rock and two queried rock samples, Berea sandstone and Baker dolomite were used in a series of core flow tests. Secondary and tertiary CO₂ flooding experiments were conducted to evaluate the recovery efficiency at operating pressure in the near miscible condition at reservoir temperature.

Core Floods Experimental Setup

The core flood setup is shown in Figure 21. The core flood displacement setup consists of a core holder, injection system, a high-pressure densitometer, a production system and a computerized data acquisition system. The temperature of the system is maintained in a Lindbergh/Blue M oven with Eurotherm temperature control.

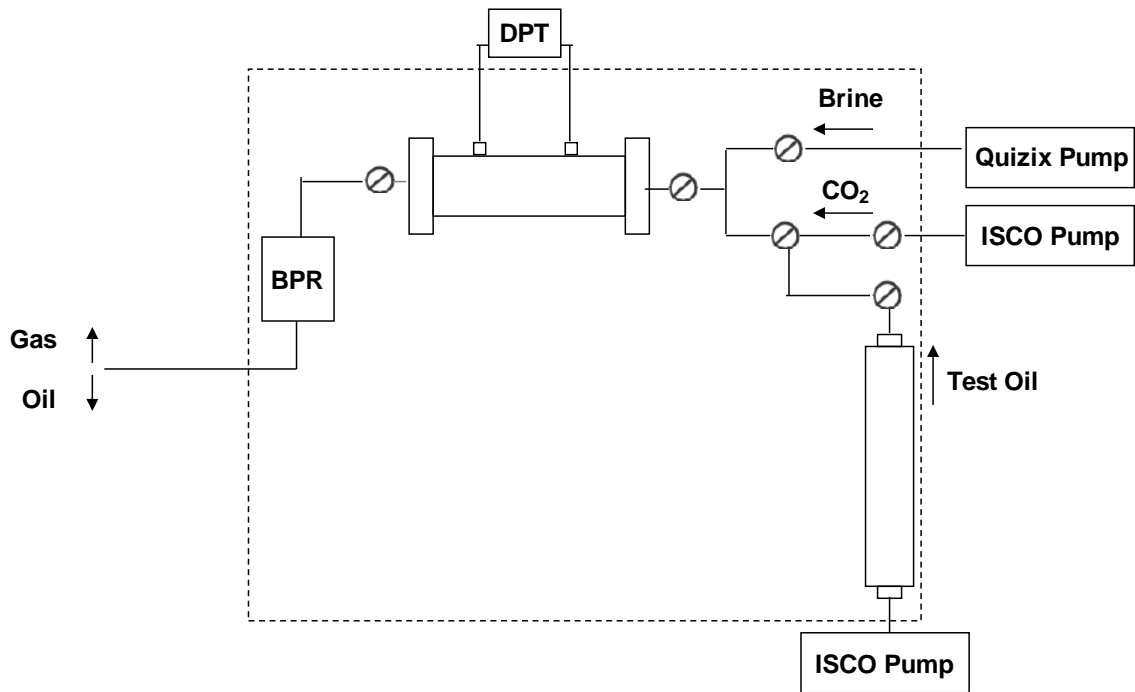


Figure 21 Schematic of core flood setup

The injection system consists of a Parker transfer cylinder (oil storage), two ISCO 260DM syringe pumps (oil/CO₂ transfer and injection) and a Quizix Pump (brine transfer and injection). The capacity of the transfer cylinder is 485 cc. The cylinder can withstand a maximum pressure of 3000 psi.

The production system consists of a back-pressure regulator, connected to the outlet of the core holder, to set/control the system pressure. Back pressure regulator models BPR-50 is a dome-load type, which controls the upstream back pressure to the pressure applied to the dome. It is designed to operate using compressed gas in the dome and water, oil, gas in the body. The back pressure regulator has a working pressure of 5000 psi at 200°F (93°C).

During the experiment, the core effluent was flashed to atmospheric pressure at the outlet of the back-pressure regulator. The separator fluid was collected in glassware designed for

different stages of displacement. The amount of fluids produced was determined volumetrically and/or gravimetrically.

Three Valydine pressure transducers are installed to measure pressures at different locations, such as pressure drop across the core, upstream pressures (CO₂/oil/brine pressure), and downstream pressure (back-pressure regulator pressure). Pressure drop was recorded during the brine flow test and used to calculate permeability of core sample.

Cores from Arbuckle reservoirs are limited. Core flow tests were made using Berea sandstone, Baker dolomite and Arbuckle dolomite. Berea sandstone and Baker dolomite were quarried rock samples whereas Arbuckle dolomite was cored sample from Hadley well, Bemis-Shutts Field at Ellis County, Kansas. Cores were epoxy encased and cast inside an aluminum cylinder with high strength epoxy. The core properties are tabulated in Table 7. The pore volumes of the cores were determined by measuring the volume of brine imbibed by the evacuated core and confirmed by tracer test with 1 wt% MgNO₃ as the tracer. The cores were cleaned and reused after completion of each CO₂ flood. During core cleaning, the core was flushed with 10 PV of methylene chloride followed by 10 PV of methanol. The sequence was repeated at least three times and finally the core was flushed with 10 PV of brine prior to be used for the flow test. All flow tests were conducted with 1wt% total dissolved solids (TDS) brine consisting of 0.5 wt% MgCl₂ and 0.5 wt% CaCl₂ in deionized water. Density and viscosity of brine measured at 110 °F and atmospheric condition were 0.9959 g/cc, 0.7250 cp, respectively.

Table 7 Core plug properties

Type	Berea sandstone A1	Berea sandstone A2	Arbuckle dolomite	Baker dolomite
Length (cm)	5.86	14.67	5.97	8.07
Cross section (cm)	2.53	3.86	2.46	2.34
Area (cm ²)	5.01	11.67	4.75	4.30
Pore volume (cc)	5.80	34.72	6.05	7.20
Porosity (%)	19.7	20.28	21.3	20.7
Permeability mD)	238.5	369.04	2.5	89.7

Secondary and tertiary CO₂ flooding experiments were conducted to evaluate the recovery efficiency at operating pressure in the near miscible condition. Injection of CO₂ was controlled at flow rate of 0.1cc/min at operating pressure. The amount of fluid recovered by CO₂ displacement was compared at 6 PV of injection.

Secondary CO₂ Flooding

Berea sandstone was used in this series of experiments with the core saturated with oil prior to injection of CO₂. The recovery efficiency was determined by the amount of oil recovered at 6 PV of CO₂ injections. The recovery efficiency is presented in Figure 22 where the recovery efficiency from slim-tube experiment is also plotted for comparison. The recovery efficiency in a short core was much less than that from slim-tube displacements. The lower recovery at pressure above MMP is probably due to lack of development of multiple-contact miscibility in a short core. At pressure below MMP, the extraction was also less effective as the dispersion is dominated for flow in the core plug as compared to that in a slim-tube. Nevertheless, the density profiles of core flooding effluents showed similarity in density profiles of slim-tube effluents at pressure below MMP. Density of effluent during the displacement was higher than density of pure CO₂ at near miscible pressure. The density behavior of the effluent suggested that the vaporization process took place during core flooding process despite the length of core is short.

Tertiary CO₂ flooding

Core plugs of Arbuckle dolomite, Baker dolomite and Berea sandstone, were used in this series of experiments. Each core sample was saturated with brine at the test pressure and permeability was measured. The core was then flooded with oil to connate water saturation at flow rate of 0.1cc/min. After connate water saturation was established, the core was water flooded at same rate to residual oil saturation. At least 10 PV of brine and crude oil were used in each sequence of displacement to establish a steady state residual fluid saturation. Carbon dioxide was finally injected to displace the remaining oil in the core. The amount of oil recovered by CO₂ flooding was determined volumetrically. A typical result of CO₂ flooding is presented in Figure 23 where the recovery history of fluid is plotted. Most of recovery occurred before 4 PV of CO₂ injection. No significant fluid recovery was observed after 6 PV of CO₂ were injected.

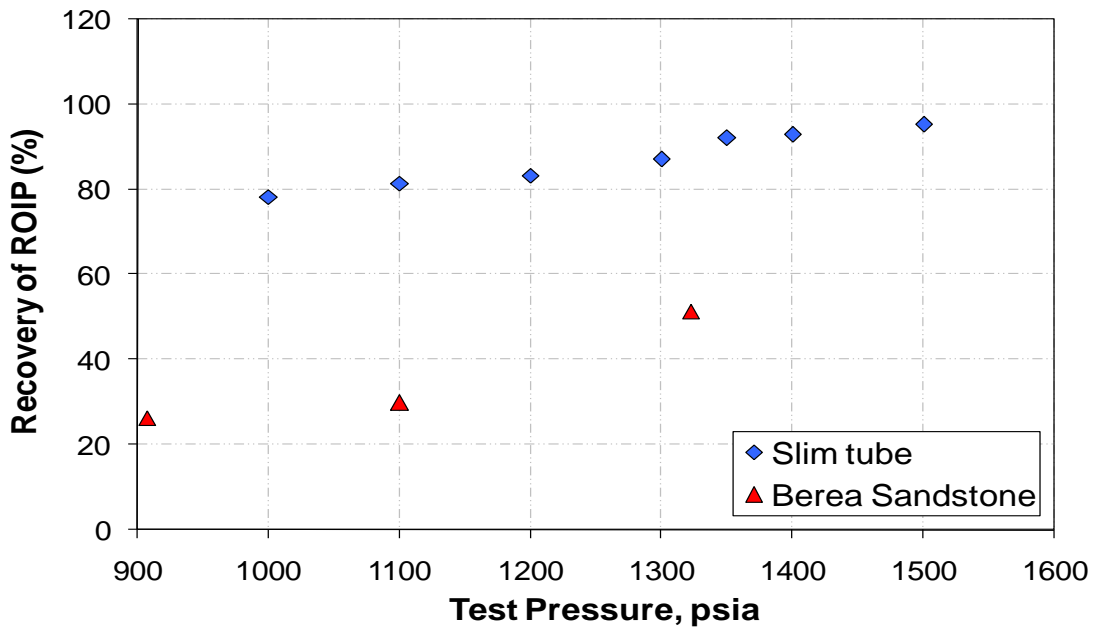


Figure 22 Comparison of oil recovery between slim-tube and core flooding experiment (Oil recovery @ 6 PV of CO₂ injected in core flow tests and oil recovery @ 1.2 PV of CO₂ injected in slim-tube tests at 110°F)

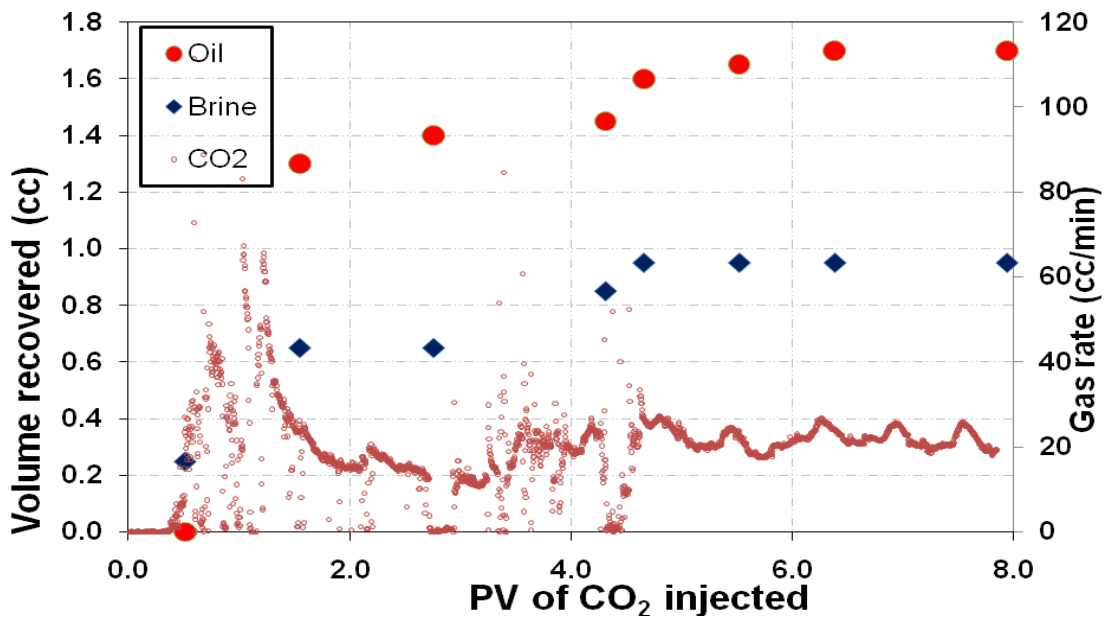


Figure 23 Effluent profile of production fluid during CO₂ flooding at 1317 psig and 110°F

The results of tertiary CO₂ flood in different cores are summarized in Table 8 to 10. Relatively high values of S_{orCO₂}, 0.21 to 0.29 were found in Berea sandstone as it had an unusual high S_{orw}, 0.48 to 0.50 prior to CO₂ injections. On the other hand, the S_{orw} of the dolomite core was found to vary from 0.32 to 0.41 with the S_{orCO₂} from 0.07 to 0.17 at the near miscible condition. Figure 24 presents the comparison of recovery efficiency among the cores tested. The recovery efficiency of ROIP varied from 60% to 80% for dolomite cores while it varied from 35% to 58 % for sandstone core as pressure increased from 900 psig to 1400 psig. Although the recovery efficiency differed among the rock types, substantial recovery was observed for Arbuckle rock at current reservoir operating pressure of 1150 psig.

Figure 25 gives a comparison of recovery efficiency between secondary and tertiary CO₂ flooding with Berea sandstone. Higher recovery efficiency of remaining oil in place (ROIP) in tertiary CO₂ flooding indicates the existence of water phase is not necessarily detrimental to CO₂ displacement efficiency due to its blocking effect. Instead, the relative permeability of CO₂ at presence of water might be reduced. Coupled with the reduction of the oil viscosity, the mobility ratio between the oil and CO₂ is reduced and therefore the recovery efficiency is improved.

The recovery efficiency was similar between two dolomite cores and was substantially higher than that in Berea core. Wylie and Mohanty (1998) in their study of effect of wettability on oil recovery by gas injection concluded that the mass transfer from the bypassed region to the flowing gas inside a core is enhanced under oil-wet conditions over water-wet conditions. Although the wettability of core was not determined in this study, it is generally believed that Berea sandstone is strongly water wet whereas the dolomite is less water wet. After CO₂ breakthrough from the core, the extraction or the mass transfer between the bypassed region and flowing CO₂ becomes more important to extract the remaining oil inside the core. The findings from Wylie's study may explain why the recovery efficiency is slightly higher in dolomite than that in sandstone tested in this study.

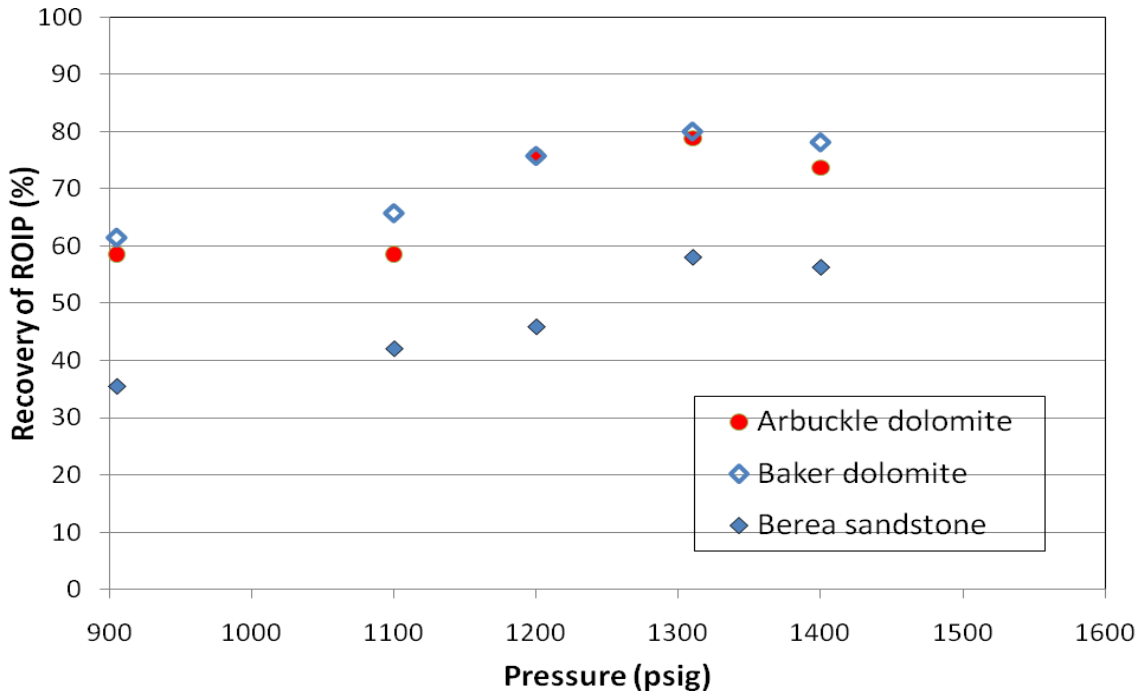


Figure 24 Effect of rock type on recovery efficiency at 110°F

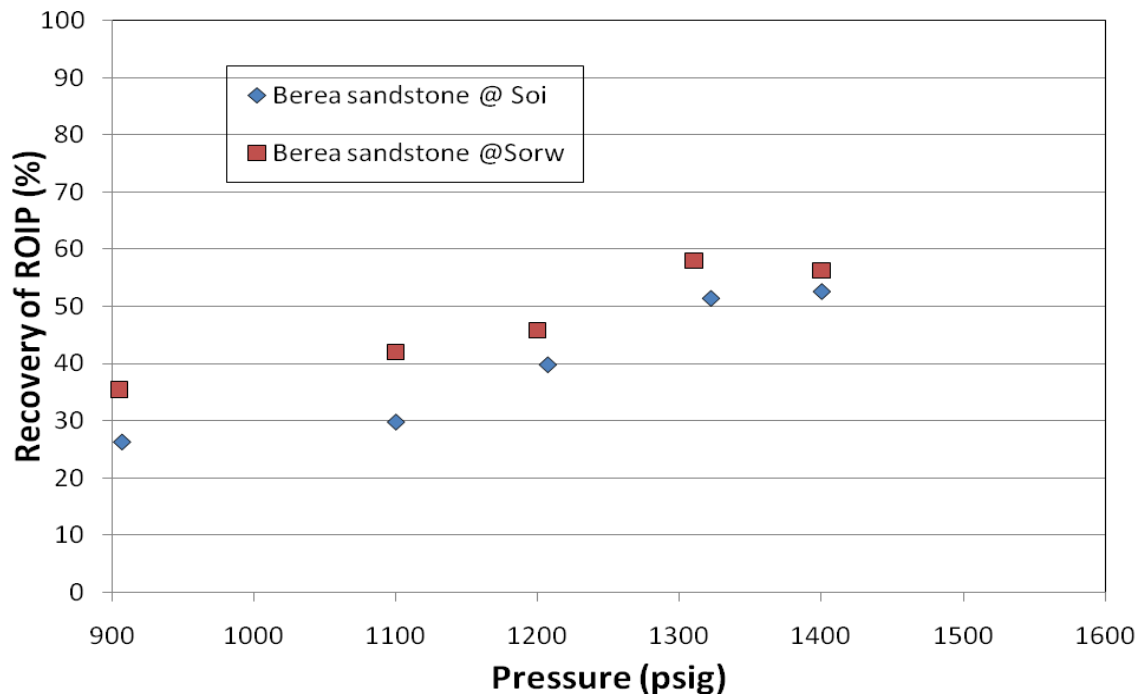


Figure 25 Effect of water saturation on oil recovery efficiency at 110°F

Table 8 Tertiary CO₂ flood results of Berea sandstone

Pressure (psig)	S _{wr}	S _{orw}	S _{orco2}	S _{wf}	Recovery 1-(S _{orco2} /S _{orw})
905	0.318	0.483	0.311	0.370	35.71
1104	0.318	0.500	0.293	0.388	41.38
1198	0.318	0.483	0.259	0.405	46.43
1317	0.318	0.500	0.207	0.336	58.62
1413	0.318	0.483	0.207	0.336	57.14

Table 9 Tertiary CO₂ flood results of Arbuckle dolomite

Pressure (psig)	S _{wr}	S _{orw}	S _{orco2}	S _{wf}	Recovery 1-(S _{orco2} /S _{orw})
901	0.380	0.414	0.165	0.512	60.00
1100	0.380	0.414	0.165	0.553	60.00
1200	0.446	0.331	0.083	0.636	75.00
1305	0.446	0.331	0.066	0.636	80.00
1407	0.380	0.380	0.099	0.529	73.91

Table 10 Tertiary CO₂ flood results of Baker dolomite

Pressure (psig)	S _{wr}	S _{orw}	S _{orco2}	S _{wf}	Recovery 1-(S _{orco2} /S _{orw})
905	0.284	0.389	0.153	0.437	60.71
1109	0.312	0.375	0.125	0.409	66.67
1201	0.340	0.347	0.097	0.451	72.00
1303	0.368	0.347	0.069	0.534	80.00
1402	0.368	0.320	0.069	0.465	78.26

Summary

- 1) Tertiary oil recovery efficiency varied among rock types, from 65% to 80% for dolomite cores and lesser from 45% to 60 % for sandstone core in the near-miscible region, from 1100 psig to 1350 psig & at 110°F.
- 2) Recovery of more than 60% of the waterflood residual oil was obtained using Arbuckle reservoir core when CO₂ was injected at the current average reservoir pressure 1150 psig & 110°F.
- 3) Experimental works showed that the presence of water phase improved the relative permeability of CO₂, which coupled with the reduction of the oil viscosity reduced the mobility ratio between the oil and CO₂ and therefore the recovery efficiency was improved.

3. COMPUTATIONAL STUDY

The discussions on computational study are divided into two main sections: 1) methodologies to develop a geological model, and 2) reservoir simulations to assess the oil recovery and CO₂ sequestration by CO₂ injection at near miscible condition. The geological model was developed by well-log interpretation and cross-plotting method. The reservoir simulations were conducted to investigate the pattern design of CO₂ injection on the oil recovery and carbon sequestration. The simulation results of oil recovery and CO₂ sequestration at near miscible condition in a 47 acre lease of oil field are reported.

3.1 Geological Model

The geological model developed is a primitive model based on well-log interpretation and cross-plotting method. The database of the field operation contained logs of pre-60's gamma ray, resistivity and microlog from most wells. Only one infill drilled well was logged with modern gamma-ray, resistivity and neutron-density log in year 2000. All the logs were digitized on foot-by-foot basis to prepare the log measurements for analysis.

Fourteen cored well data were available across the Ogallah field when the wells were drilled in the early 1950. From the lithology description presented in the core analysis report, the upper carbonate sequence (Arbuckle) was found to form a few streaks of dolomite-sand with variable thickness of crystalline-dolomite. The dolomite was characterized by permeability in the range of 0.01 to 150 md and low porosity from 1 to 12%. The lower Precambrian sequence of the reservoir was deposited with Reagan sandstone showing good permeability ranging from 0.01 to 400 md and higher porosity varied from 1 to 20%.

Due to the lack of advanced log data in the early 1950 when the Ogallah unit was developed, the reservoir porosity was calculated by resistivity log interpretation and calibrated with a correlation developed from a modern suite of logs of an infill drilled well in 2000. The permeability estimation was based on a correlation published by Byrnes *et al.* (1999) in which the permeability and porosity relationship is developed from measurement of core plug representing the Arbuckle group petro facies. The initial water saturation was calculated using Archie equation along with data derived from the calibrated resistivity logs.

Log Interpretation

Prior to estimating the reservoir properties quantitatively, a preliminary analysis was conducted to identify the Arbuckle formation by reviewing the well logs, formation information described by the geologists and log measurements. The logs available for analysis include gamma-ray, resistivity (laterolog, microlog, microlaterolog and guard), and neutron-gamma logs. Table 11 lists the number of different type of logs available for this study. From the visual-investigation of formation signature among the logs, the formation lithology is defined by characteristic of log trend between two or more logs. Table 12 describes the guideline used to identify the formation by this visual investigation method in which four groups of rock type, shale, dolomite, sandstone and granite-wash are classified.

The initial reservoir description and interpretation of the well logs were developed based on the lithology description from each well. Mapping of the Ogallah unit stratigraphy surface, the sequence of the deposition and correlation of formation tops relied on lithology information which is not available from most of the wells. The number of wells with lithology information available is summarized in Table 13 in which 11 wells contain identifiable data of top of Graite-wash while 17 wells have information available for Reagan formation top and 28 wells have data available for Arbuckle formation top.

Table 11 Type of well logs available at Ogallah unit

Well Log Description	No. of Wells
Neutron-gamma	13
Microlog, micro resistivity	15
Resistivity	28
Gamma-ray	28

Table 12 Visual indication of rock type: shale, dolomite, sandstone, and granite-wash

Rock-Type	Gamma-ray	Neutron-gamma	Resistivity logs (resistivity, guard, laterolog, microlog, microlaterolog)
Shale	High	High	Low
Dolomite	Low	Low	High, oil-bearing zone.
Sandstone	Low	Low	Low, assuming that sandstone containing highly conductive pore fluid.
Granite-wash	High	Low	High

Table 13 Ogallah wells with lithology information available

Formation Identified	No. of Wells
Arbuckle	28
Reagan	17
Granite-wash	11

Neutron-gamma (GRN) Log Analysis

Neutron-gamma log were recorded in counts per second (CPS) or API unit. A logarithmic scale was derived using the high-low porosity method. The high porosity value (ϕ_h) was in the range of 0.20-0.30 and the low porosity (ϕ_l) was in the range of 0.01-0.05. The equation for porosity computation is shown as follows,

$$m = \frac{\log(\phi_h/\phi_l)}{(CPS_h - CPS_l)}$$

$$c = \frac{\phi_h}{10^{(CPS_h \times m)}}$$

$$\phi_n = c \times 10^{(NCPS \times m)}$$

where CPS_h is GRN counts at high porosity point, CPS_l is the GRN counts at low porosity point, and NCPS is the neutron log readings.

Microlog and Microlaterolog Analysis

The microlog and microlaterolog porosity (ϕ_{ml}) was derived from the rearrangement of classical Archie equation. No shale correction was applied to the equation. The mud filtrate resistivity (R_{mf}) at formation of interested was used to calculate the porosity, which was obtained from log header and calibrated at formation temperature. The microlog and microresistivity porosity is estimated as,

$$\phi_{xo} = \left[\frac{A}{(R_{xo}/R_{mf}) \times S_{xo}^n} \right]^{1/m}$$

where S_{xo} is assumed to be 1.0 for low porosity zone and 0.70 for the hydrocarbon bearing zone.

Water Saturation

The water saturation was estimated from Archie equation. To compute the water saturation, R_t was read from the resistivity logs (laterolog and guard log), R_w was estimated at

the temperature of interested formation depth, and effective porosities was calculated from porosity log and microlog.

$$S_w = \left[\left(\frac{A}{\phi^m} \right) \times \left(\frac{R_w}{R_t} \right) \right]^{1/n}$$

In this study, R_w , 0.130 was estimated at formation temperature, 110 °F. Parameters of carbonate values, $m = 2$, $n = 2$, and $a = 1$ were applied to compute the water saturation profile for each well.

Cross-plotting Method

Porosity is normally derived from single porosity method for wells with good porosity logs such as neutron density and sonic log. However, very limited porosity data were available in the early 1950 when the Ogallah unit was developed. Most logs in Ogallah unit were either micrologs or microlaterlogs which are used as porosity indicators. The porosity derived from these logs is generally affected by the R_{xo} measured at the formation surrounding the tool. In year 2000, a modern suit of logs was conducted in an infill drilled well, 4-16 at Schoenthaler lease. It provided the opportunity to correlate the porosity derived from neutron density, sonic porosity log with resistivity logs in this well. With the new correlation developed from well 4-16, the porosity estimation from all the old resistivity logs becomes feasible.

Well 4-16 was drilled with a total depth of 4100 ft. It was logged with modern gamma-ray, neutron, density, spontaneous potential, resistivity log and microlog. From the geological report, Arbuckle formation was located approximately at 3990 – 4050 ft. Fair oil staining was observed for the first eight feet sandy-dolomite in the interval.

Porosity derived from neutron and density log in well 4-16 was cross-plotted with porosity determined from microlog to develop a reasonable correlation between porosity log and microlog. This cross-plotted relationship was used to derive the porosity from microlog in wells where no porosity log was available.

Well 4-16 Cross-plot Porosity

Graphical comparison of well 4-16 porosity logs using porosity overlay is illustrated in Figure 26. Both neutron porosity and density porosity are recorded in limestone porosity unit. The separation of the porosity curves is an indicative of a certain type of lithology. At the interval of 3972-4003ft, the separation of curves where ϕ_N (PHIN) > ϕ_D (PHID) is corresponding

to shale. A sandstone interval with $\phi_N < \phi_D$ is found at 4004-4019 ft and 4033-4051 ft. Lack of curve separation at interval of 4033-4051 ft, is an indication of dolomite streak.

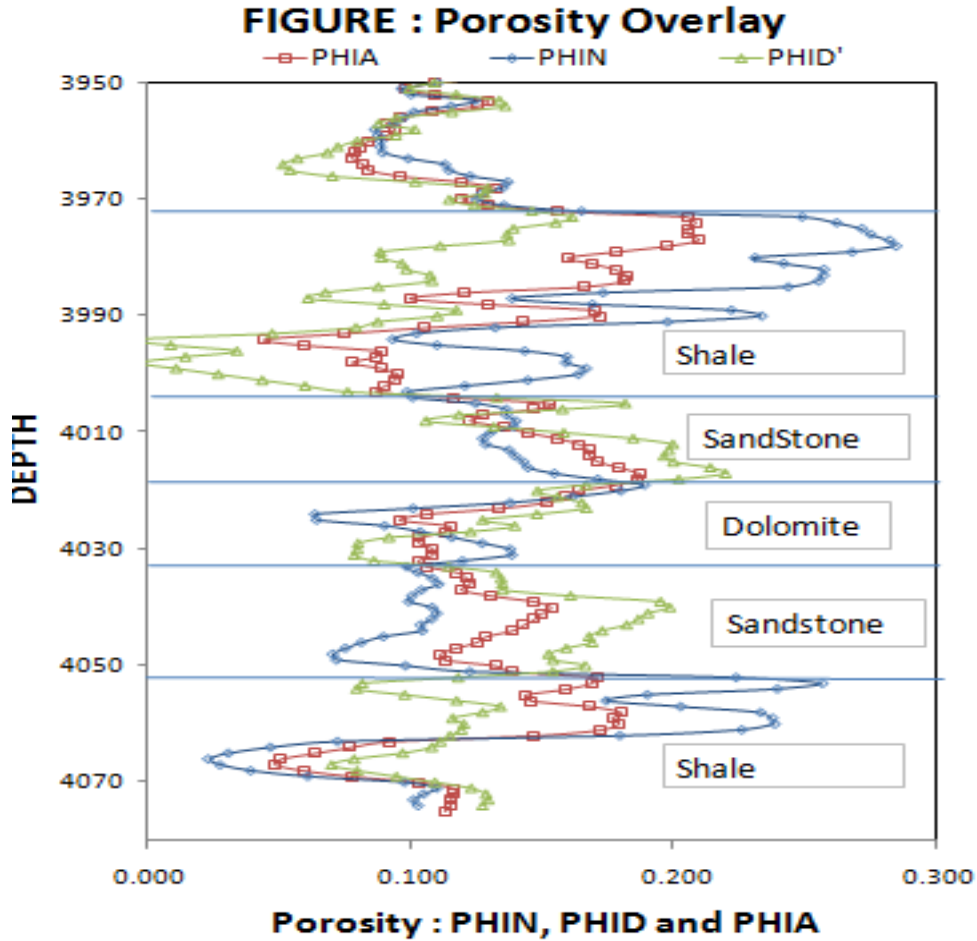


Figure 26 Porosity overlays of Well 4-16

In Figure 26, dolomite and sandstone layers indicate an average porosity (PHIA) of 0.12 and 0.14, respectively. The calculated average porosity data from this well is then cross-plotted with microlog porosity at each corresponding depth interval to derive the correlation between the averaged porosity log and microlog. Figure 27 shows the relationship between the porosity response of microresistivity logs (ϕ_{ML}) with the neutron porosity (ϕ_N), density porosity (ϕ_D) and average porosity (ϕ_{AV}). The cross-plot demonstrates a conversion relationship of the porosities corresponding to reservoir rock lithology. The developed correlation is used accordingly to convert porosities derived from resistivity logs to representative porosities in other wells.

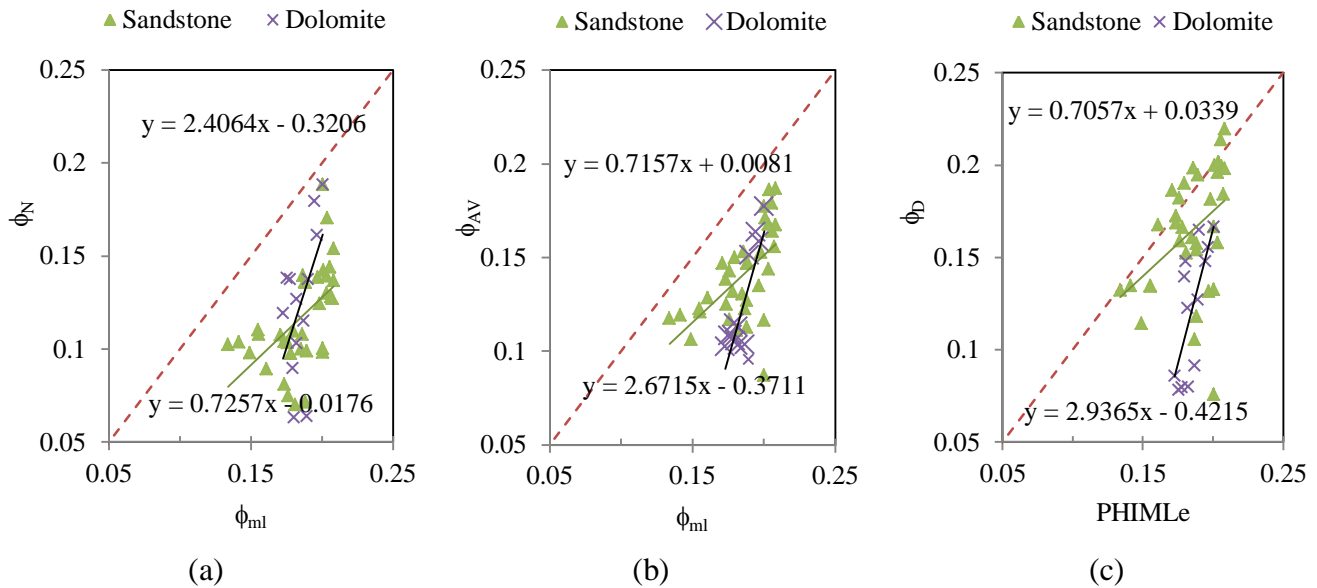


Figure 27 Microlog (ϕ_{ML}) porosity cross plotted with (a) Neutron Porosity (ϕ_N) (b) Average Porosity (ϕ_{AV}) (c) Density Porosity (ϕ_D) for the Arbuckle of well 4-16. The shale effect was included.

Example of well 14-1 Porosity Calculation

Example of converting microlog data to averaged porosities by means of the cross plotting method is described with a set of microlog data from well 14-1. This well was logged with gamma-ray, resistivity and microlog. It was drilled in year 1952 with Arbuckle top identified at 3989 ft. The procedure of porosity and water saturation calculation is described as follows,

1. The lithology of well 14-1 was first defined based on geology description from geological report and the visual interpretation method given in Table 12.
2. The microlog porosity was computed using microlog of well 14-1.
3. The microlog porosity was converted to neutron porosity, average porosity and density porosity using the derived relationship from well 4-16.
4. The water saturation was calculated with the average porosity derived in step 3.

The converted porosity and water saturation profiles of well 14-1 are presented in Figure 28 where (a) shows the final converted porosity profile and (b) shows the derived water saturation profile.

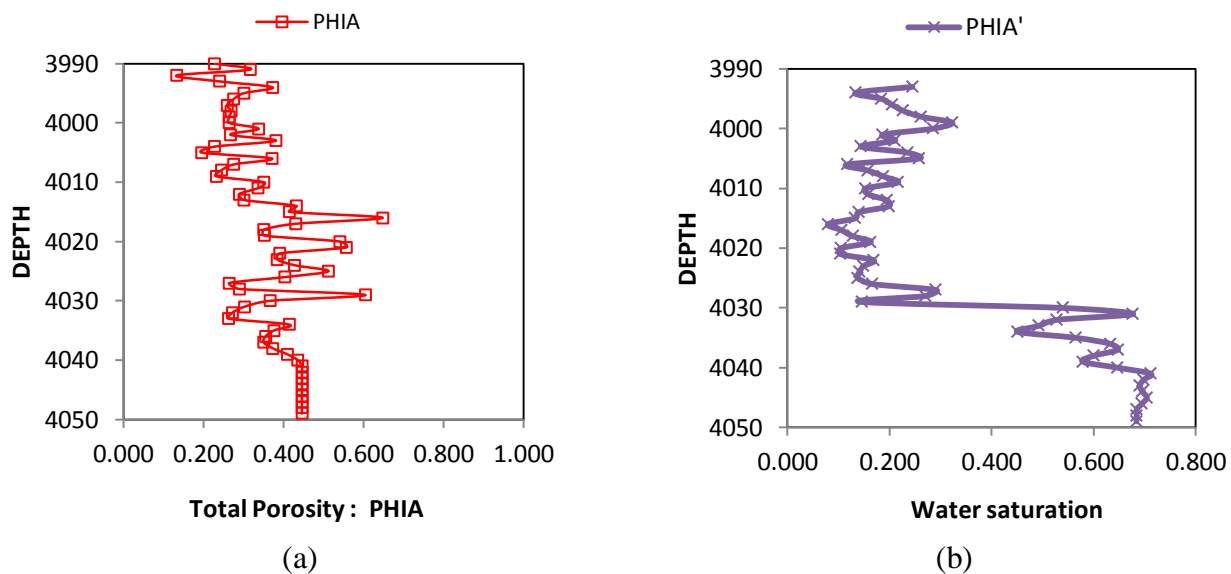


Figure 28 Derived average porosity (a) and water saturation (b) plotted with depth for well 14-1

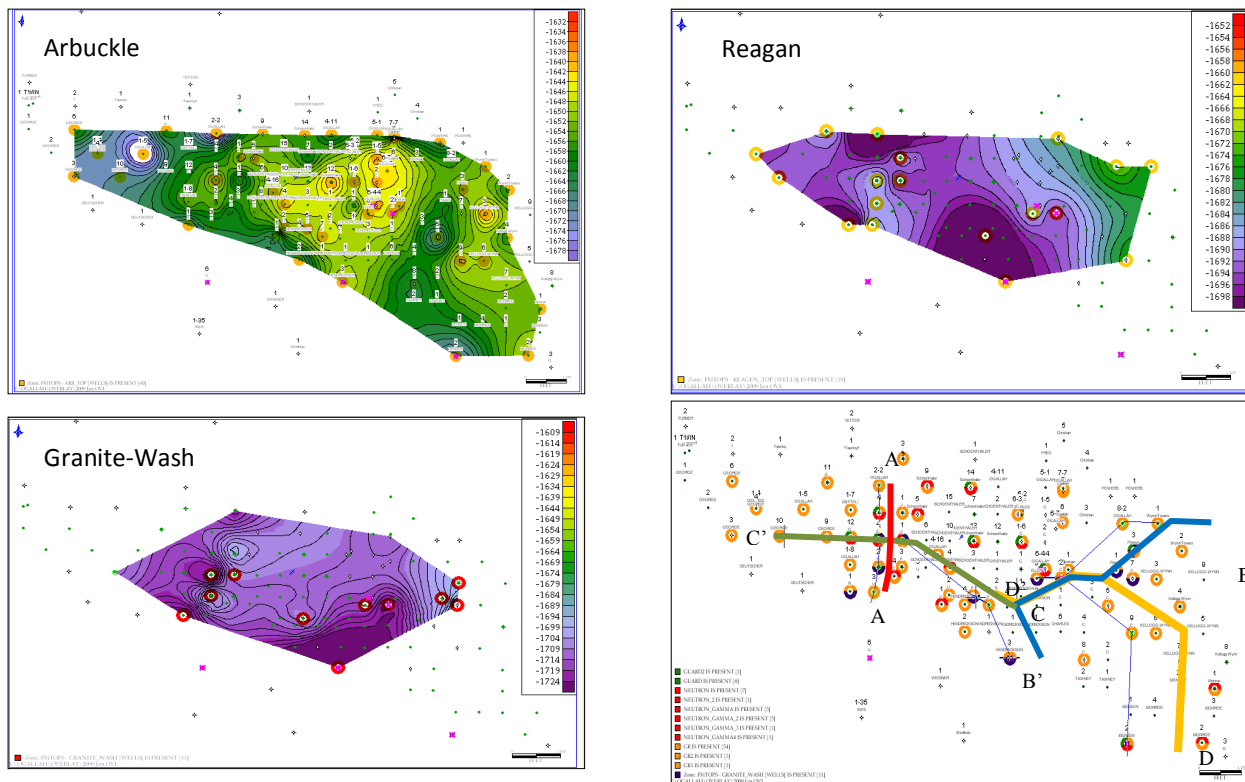


Fig. 29 Contour grids of the Ogallala formation tops and the cross-section profiles

Stratigraphy and Cross-section Profiles

The stratigraphy and lithology profile of wells were constructed based on the formation top markers. The Ogallah net-pay mapped based on the sequence of deposition is shown in Figure 29.

The cross sections of Ogallah are presented in Figure 30A to Figure 30D. From the cross section, it is seen that Arbuckle formation is generally located at high structure underlain by Reagan sandstone and Granite-wash. Reagan formation is absent in some area in the lease where Arbuckle formation is found at low structure. The isopach maps of the net-pay for Arbuckle and Reagan formations are also shown in Figure 31.

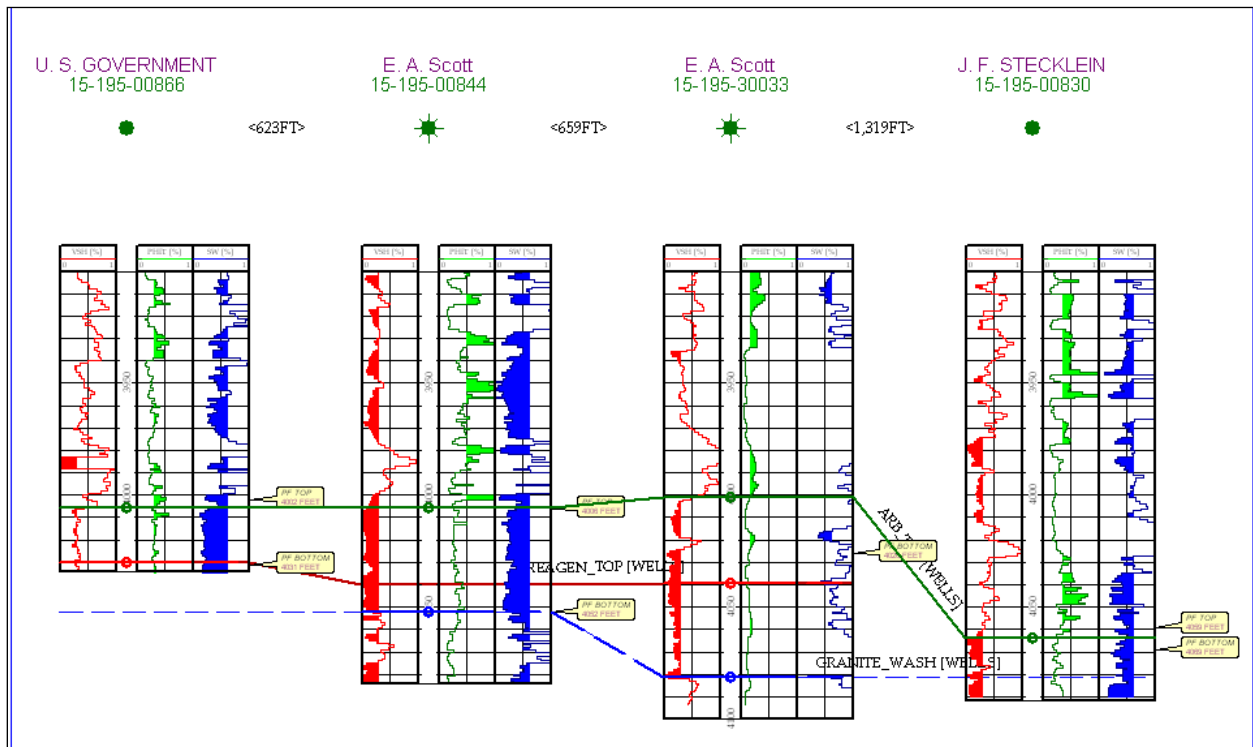


Figure 30A Cross section of wells indicated as Line A-A' (red line in Figure 29)

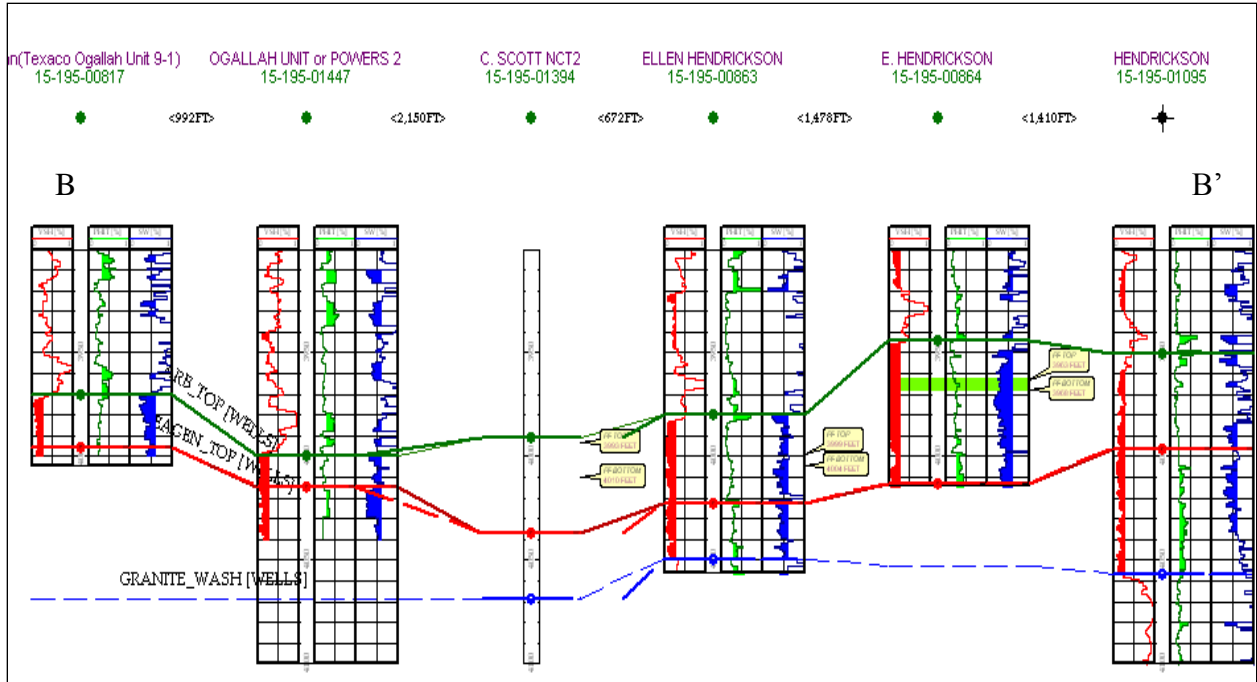


Figure 30B Cross section of wells indicated as Line B-B' (blue line in Figure 29)

Well UWI: 15-195-01394 has incomplete laterolog and microlog.

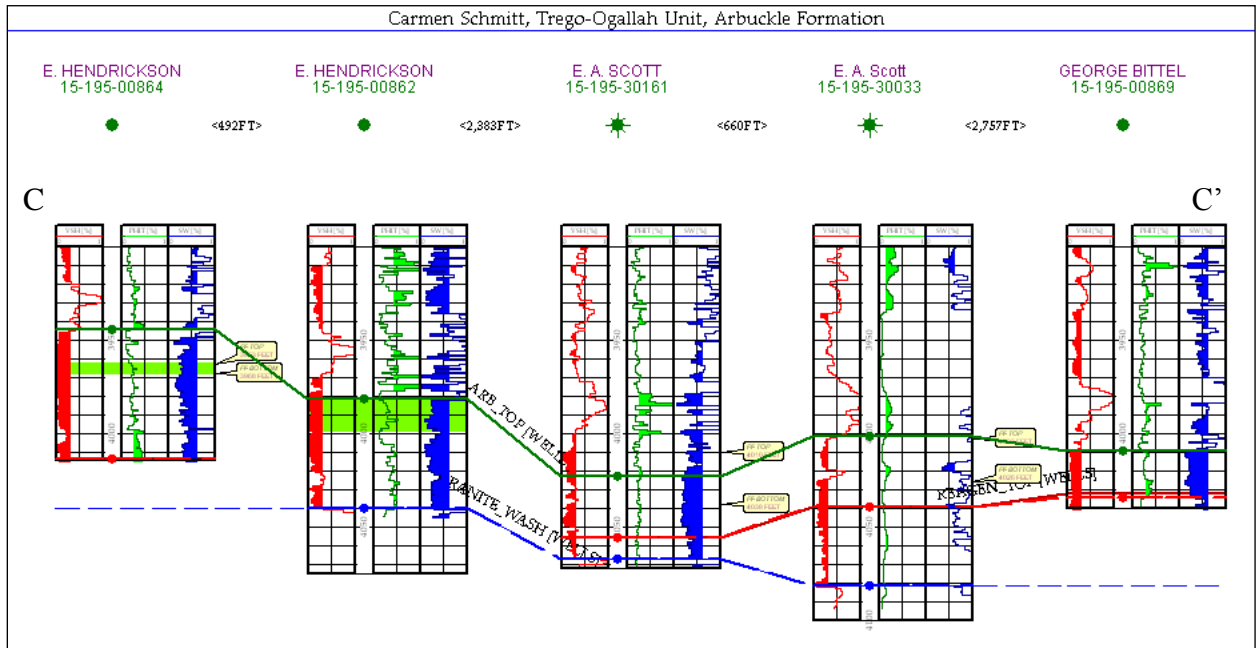


Figure 30C Cross section of wells indicated as Line C-C' (green line in Figure 29)

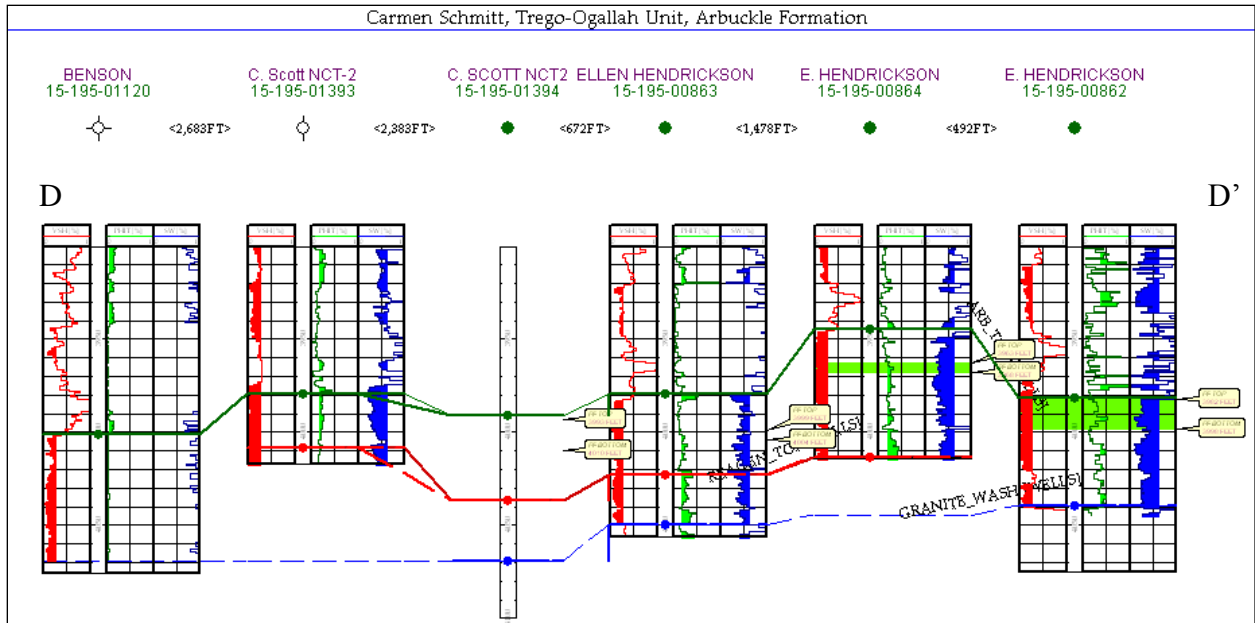
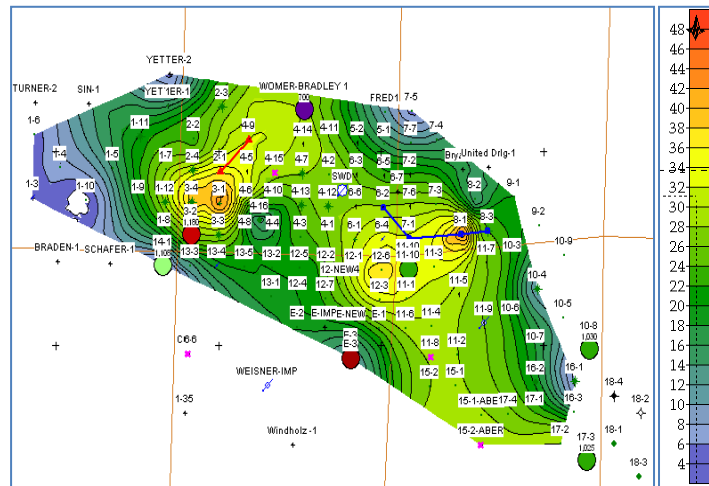
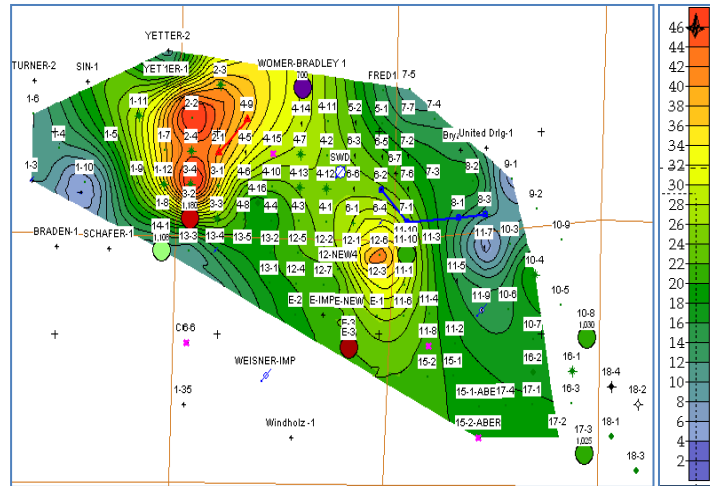


Figure 30D Cross section of wells indicated as Line D-D' (yellow line in Figure 29)

Well UWI: 15-195-01394 has incomplete laterolog and microlog.



(a) Arbuckle dolomite



(b) Reagan sandstone

Figure 31 Isopach of the net-pay in Ogallah unit based on log interpretation

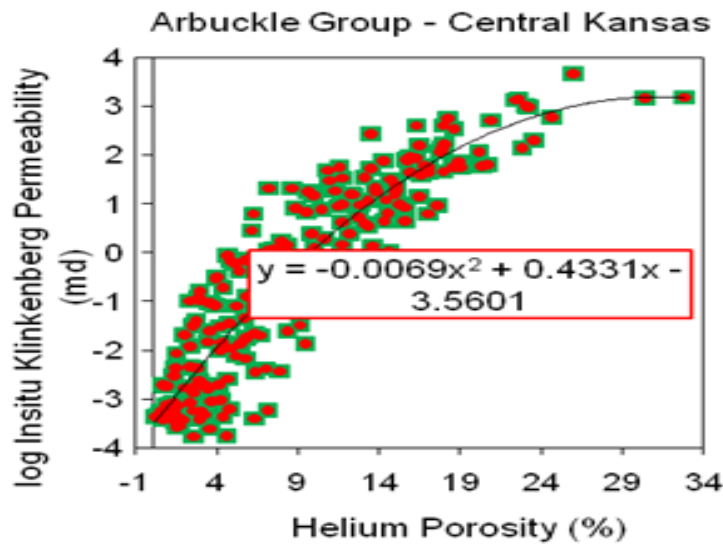


Fig. 32 Porosity-permeability correlation of Arbuckle Group (Byrnes *et al.*, 1999)

Porosity-Permeability Distribution

The permeability calculation was based on the permeability correlation of Arbuckle Group, Central Kansas which was published by Byrnes *et al.* (1999). In that study, Byrnes *et al.* collected petrophysical data from a number of core-plug samples of different Arbuckle facies and related the facies and matrix properties to reservoir character. The equation shown in Figure 32 represents the typical correlation of petrophysical property in Arbuckle formation. The correlation was adopted to calculate the permeability as a function of porosity for Arbuckle formation in Ogallah unit.

Geological software, PETRA (HIS Inc.) was used to construct the geological model with all the reservoir properties collected through the aforementioned methods. The spatial distribution of the Ogallah reservoir properties such as porosity, permeability, water saturation and net-pay gridded surfaces were subsequently exported to Builder, a pre-processing application of commercial simulator, IMEX (Computer Modeling Group, Inc.) for further construction of a reservoir model.

3.2 Reservoir Model and Simulation

Black oil simulator, IMEX was used to perform history match of primary production in Ogallah unit. The geological model was exported to Builder to construct a reservoir model along with PVT data, relative permeability data and recurrent data such as well location, perforation depth and production history. The model was discretized with 127 blocks in east-west direction, 70 blocks in north-south direction and 8 layers in vertical direction. The grid block size was 110 feet in length and 110 feet in width. The thickness of each grid varied. Figure 33 presents the structure top of the oil field and the location of 103 wells. Figure 34 shows an example of the cross-section view of the layers consisting of Arbuckle dolomite and Reagan sandstone. The Granite wash was not included in the model as it is assumed to be part of the aquifer underling the reservoir. The aquifer was modeled with Carter-Tracery method to simulate the aquifer as a bottom water drive aquifer.

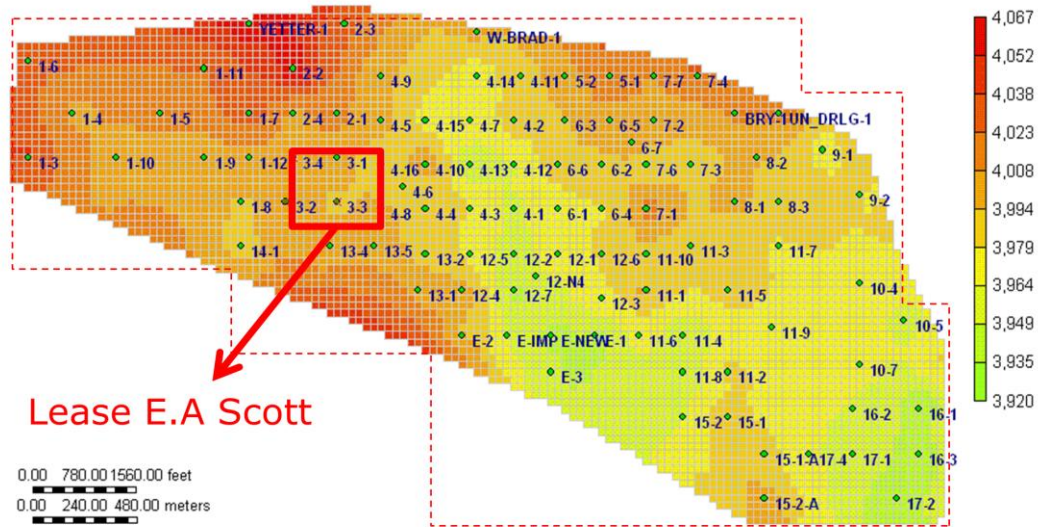


Figure 33 Structure top map of Ogallah Unit

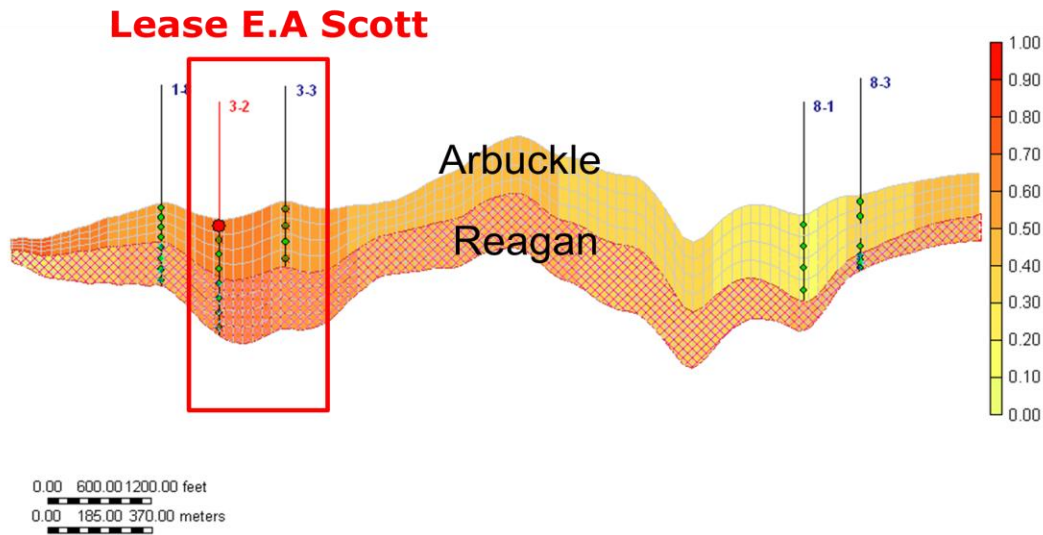


Figure 34 Example of cross section view of Ogallah Unit

Figure 35 presents the permeability and porosity distribution in the Arbuckle and Reagan layer of the model. High permeability and porosity are generally observed in the central-southwest part of the field which includes part of Lease 1, (G. Bittle), Lease 3, (E.A. Scott), and Lease 13, (U.S. Government).

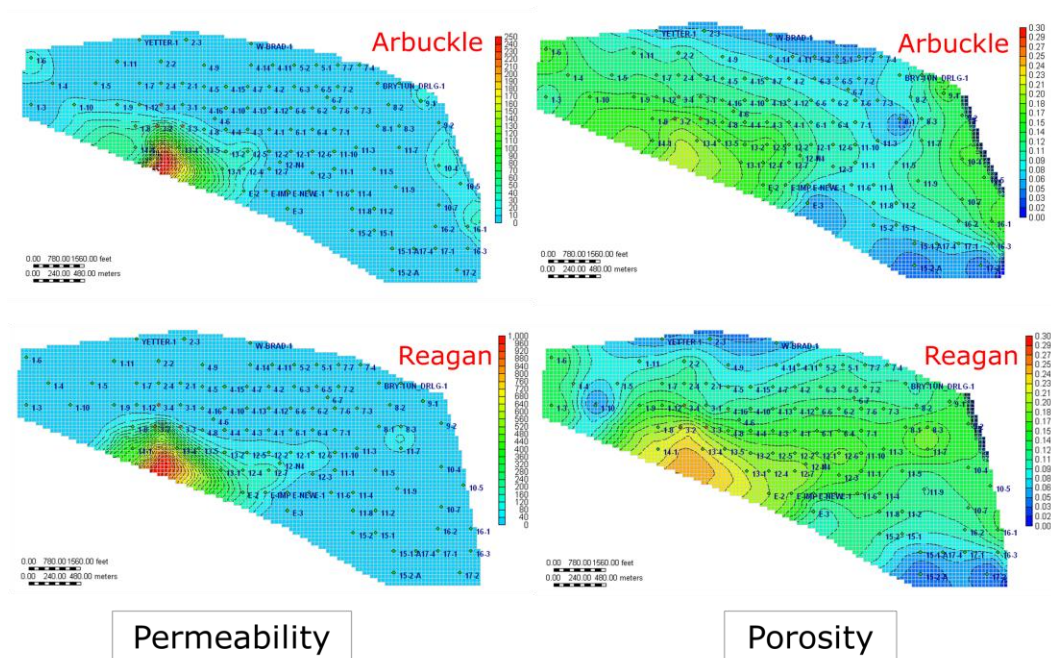


Figure 35 Permeability and porosity of Arbuckle dolomite and Reagan sandstone

3.2.1 History Match of Primary Production

Primary production of the Ogallah started in 1951. Well production history shows that no water was produced before 1960. Water breakthrough in producers started after 1960. At the peak of production in 1969, the Ogallah field had 85 producing wells. The field was producing 1.07 MMBO/year with cumulative production of 11.37 MMBO by 1969. After 1969, the field commenced commingle-production from LKC formation and approximately half number of these wells were shut in at 1989 due to economic decline. The Ogallah field was unitized in 1991 and the number of active producers since then was reduced to 18.

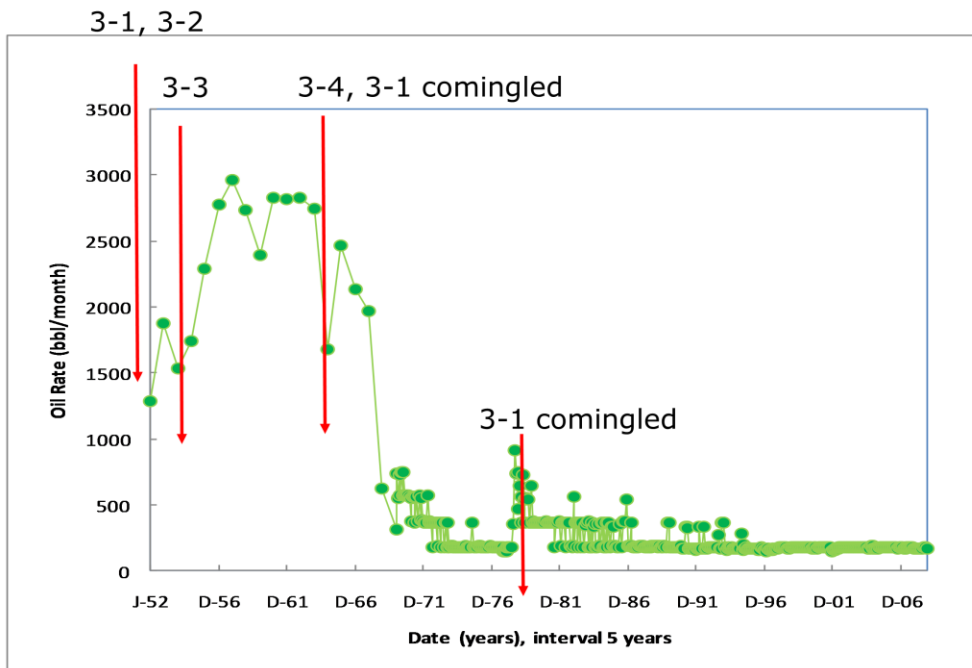


Figure 36 Production history of Lease 3, E. A. Scott

Individual well production history in Ogallah unit was not recorded in the early years of production. Most recent record for individual active producer was from 1991 onwards. Nevertheless, Kansas Geological Survey database has production record of each lease in the unit. Figure 36 shows the production history of Lease 3, E. A. Scott. Production in Lease 3 started in 1952 when well 3-1 and 3-2 were first drilled and produced from Arbuckle formation. Well 3-3 started production from Arbuckle in 1955. The total production rate from all three wells stabilized at around 2700 BO/month. The production rate started to decline from 1963. In 1965, well 3-4 was drilled and produced from Arbuckle and Lasing-Kansas City (LKC). At the late of

1965, LKC-F was perforated in well 3-1 to have a comingle production with Arbuckle. The production rate started decline significantly after water breakthrough. Another apparent rate increase occurred in 1977 when well 3-1 was perforated at upper formations, LKC-A and Topeka.

It is challenging to history match the primary production performance of the whole unit as there is insufficient field data for each individual producer, and in most cases, the production is commingled with other formations on top of the Arbuckle group. Because of the limitation of data, the effort to history match was directed toward wells with detailed production record from the Arbuckle group only. Two wells, well 3-2 and 3-3 in Lease 3 (E.A Scott), and two wells, 4-12 and 4-13 in Lease 4 (Schoenthaler), are produced from Arbuckle formation. The history match on these four wells is discussed in the following sections.

The production of the Ogallah unit is primarily attributed to natural water drive as the reservoir pressure has been maintained at above 1150 psi for more than 50 years. To simulate the primary production by the bottom water drive, black oil simulator, IMEX was used to history match the production performance. The volumetric performance of reservoir fluids at various pressure levels are tabulated in Table 14. These data are derived from the laboratory studies of PVT of reservoir fluid in a companion technical report (Tsau, *et al.* 2010)

Table 14 PVT data used in simulator

P (psia)	Rs (scf/stb)	Bo (rb/stb)	z	viso (cp)	visg (cp)
15	3.5	1.021	0.999	4.124	0.0124
412	62.8	1.039	0.964	2.906	0.0127
809	136.7	1.063	0.933	2.176	0.0133
1206	218.6	1.091	0.908	1.735	0.0140
1603	306.1	1.122	0.889	1.445	0.0148
2000	398.1	1.157	0.878	1.241	0.0157

Relative permeability curves for two flow units (Arbuckle and Reagan) were modeled using modified Corey-type equations (Corey, 1954) where S_{wc} was obtained from the laboratory measurement. The modified Corey relative permeability equations used were:

$$k_{ro} = k_{ro_{S_{wi}}} (1 - S_{WD})^m$$

$$k_{rw} = k_{rw_{S_{ORW}}} (S_{WD})^n$$

$$S_{WD} = (S_w - S_{WC}) / (1 - S_{ORW} - S_{WC})$$

where m is the exponent of the oil relative permeability and n is the exponent of water relative permeability. Figure 37 shows the oil-water relative permeability curves used in the simulation. The m - and n -exponent used are 5 and 2 respectively. The end-points residual oil and water saturation are both 0.25. For Arbuckle formation parameters used were: $k_{ro_{S_{wi}}} = 1.0$, $k_{rw_{SORW}} = 0.18$; for Reagan formation parameters used were: $k_{ro_{S_{wi}}} = 1.0$, $k_{rw_{SORW}} = 0.07$.

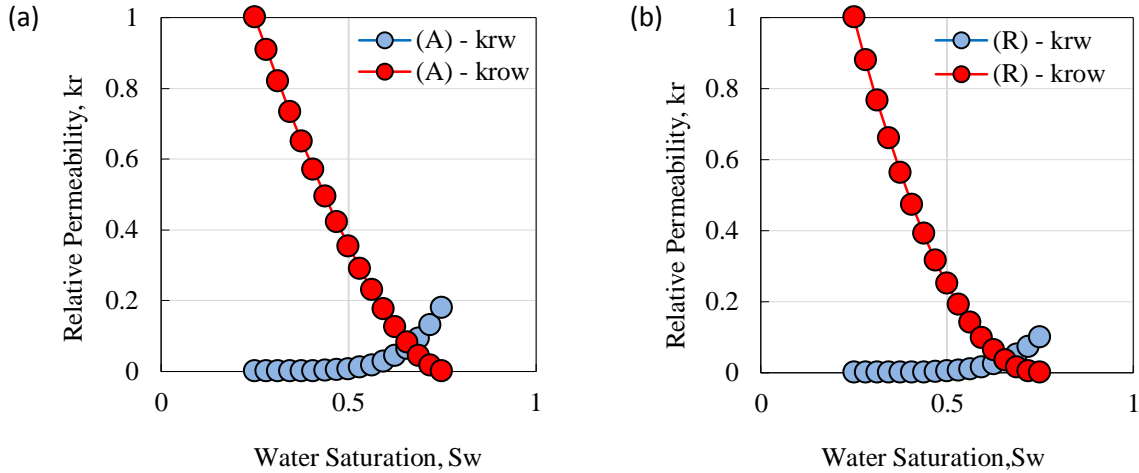


Figure 37 Relative permeability curves of oil and water. (a) Arbuckle formation, (b) Reagan formation.

The initial reservoir pressure was assumed to be 1200 psia based on DSTs conducted in the early years of production. The rate constraint was applied to the wells when prorate production was imposed. Otherwise, the pressure constraint was applied to the producers at a given bottomhole pressure when the record was available or pumped off when it was not available. During the process of history match, properties being adjusted include horizontal permeability, end point of relative permeability and initial water saturation.

Some of the production history match results are presented in Figure 38 to Figure 45 where the symbols represent the field data while the curves represent the simulation results. In most of these plots, the production rate of each individual well is not available prior to 1991. At the early time of simulation, the oil production was controlled at a given rate in the model to represent the prorate production stipulated by the government at the early stage of the development. In general, the production history is reasonably well matched.

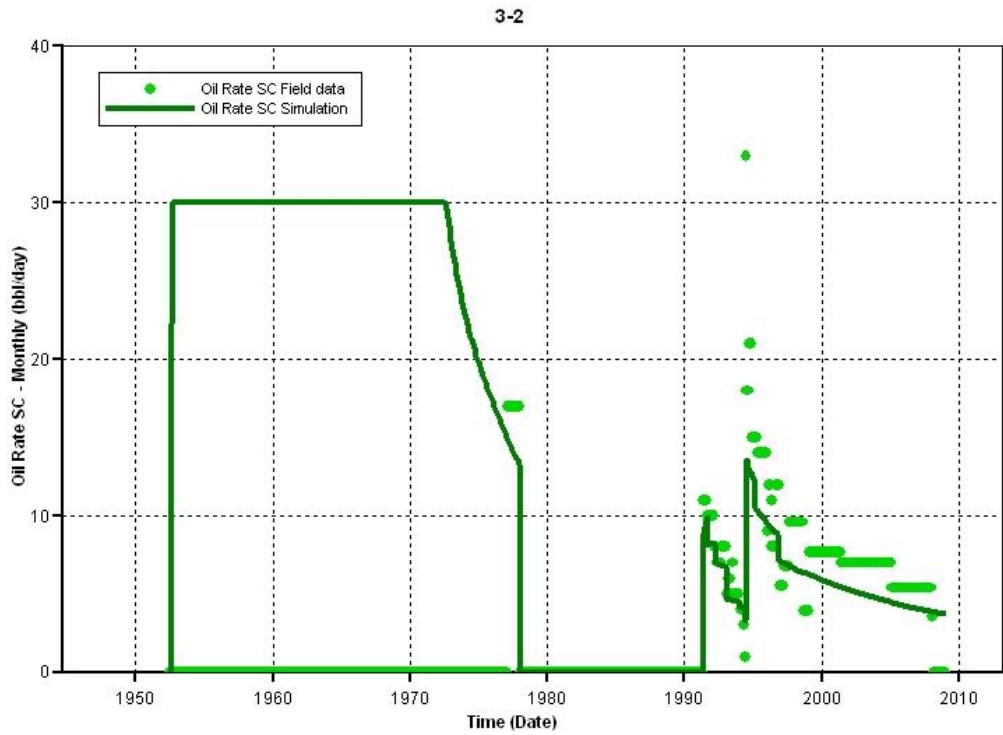


Figure 38 History match of oil production in well 3-2

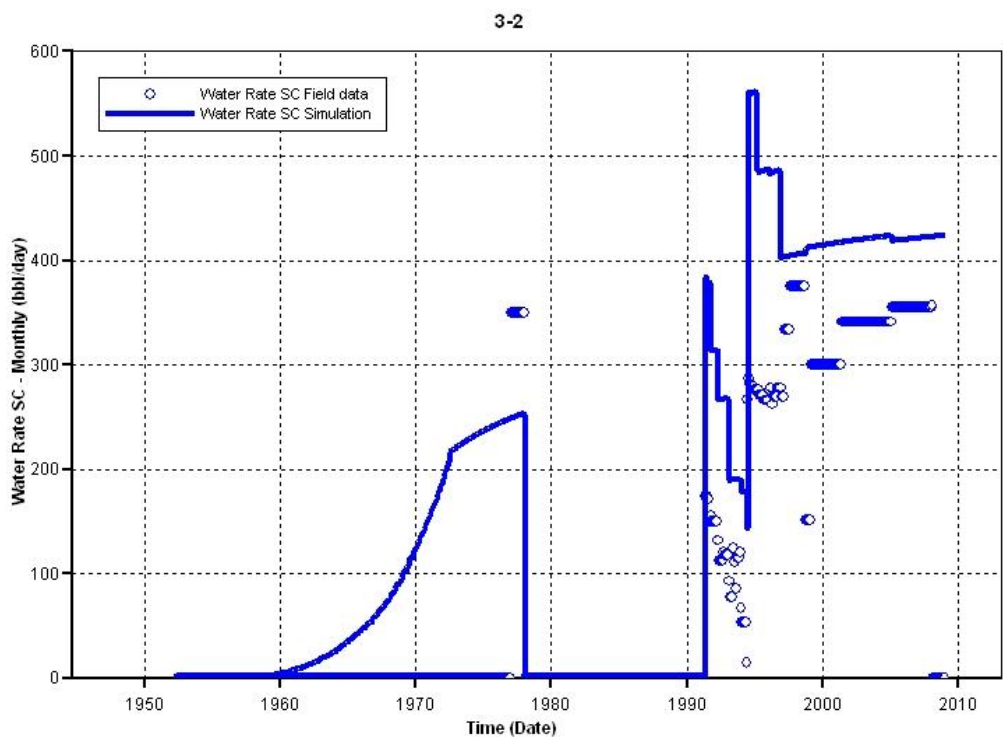


Figure 39 History match of water production in well 3-2

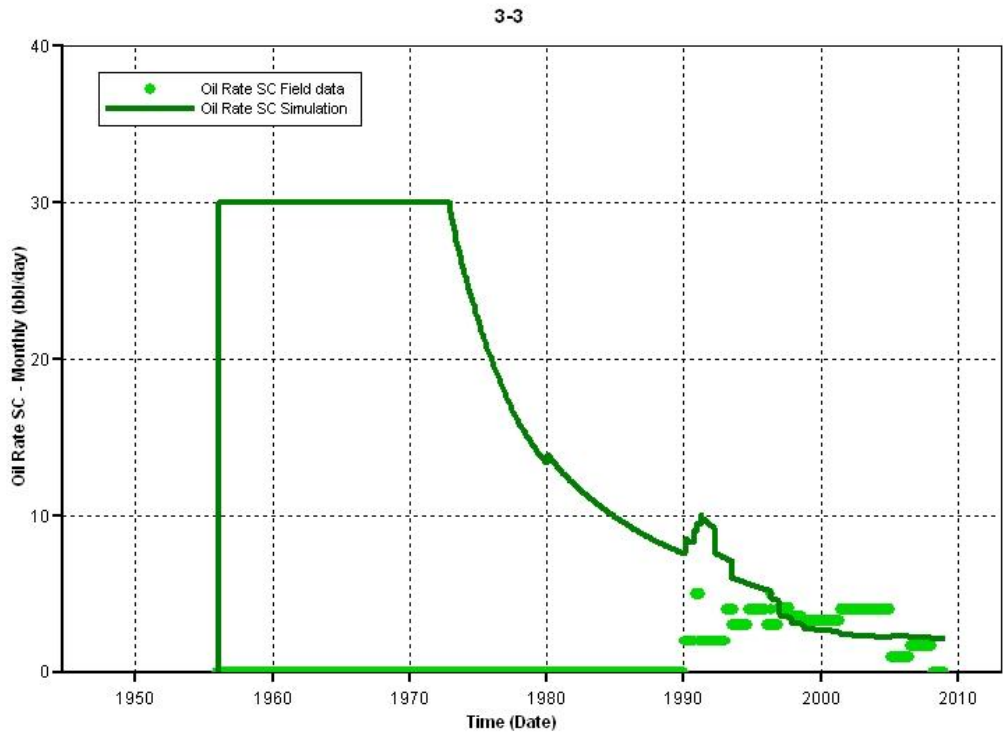


Figure 40 History match of oil production in well 3-3

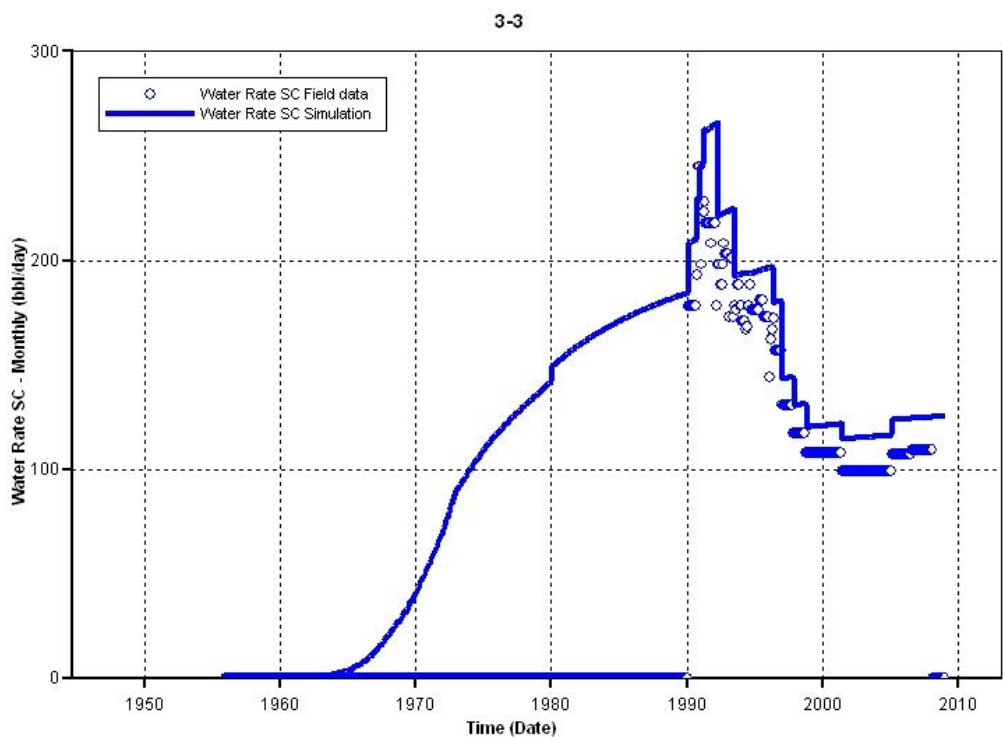


Figure 41 History match of water production in well 3-3

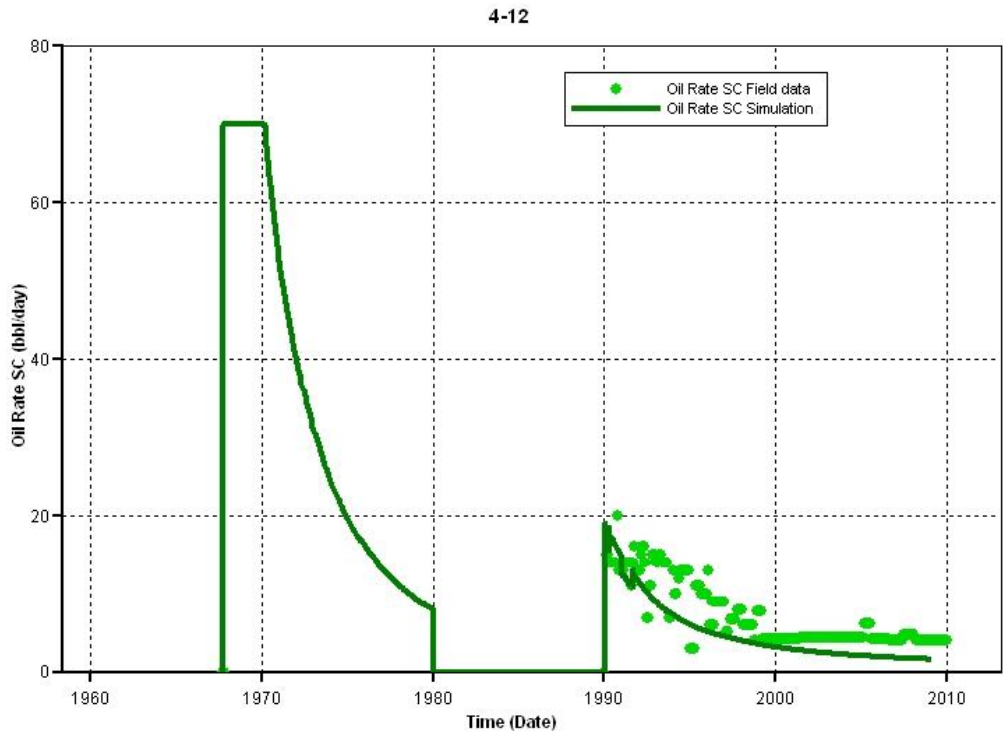


Figure 42 History match of oil production in well 4-12

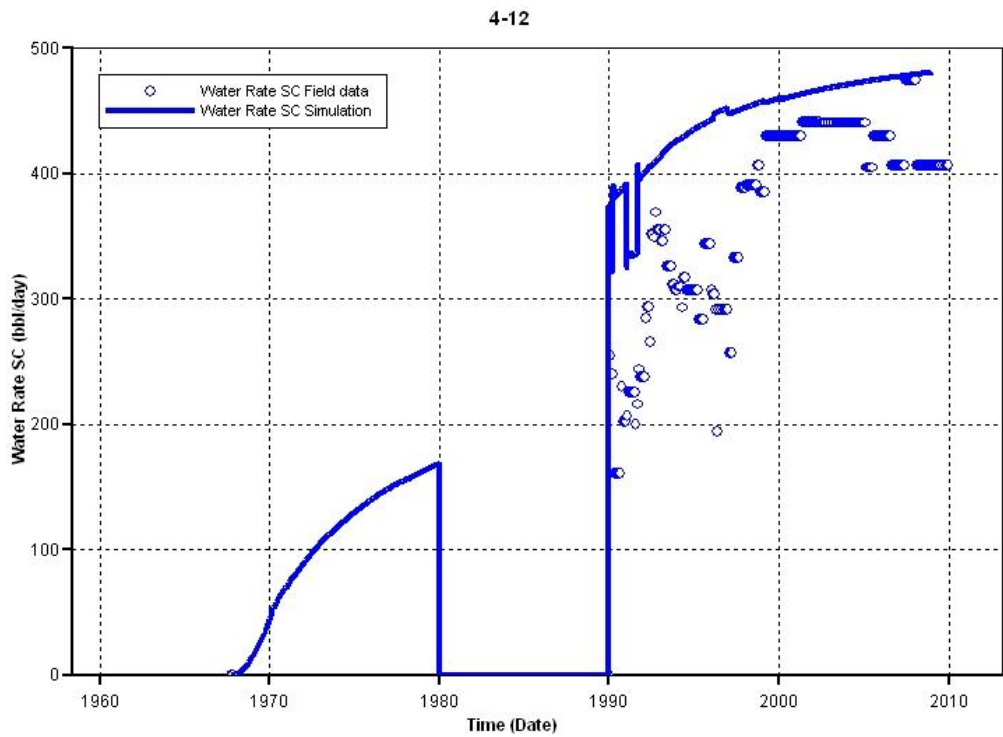


Figure 43 History match of water production in well 4-12

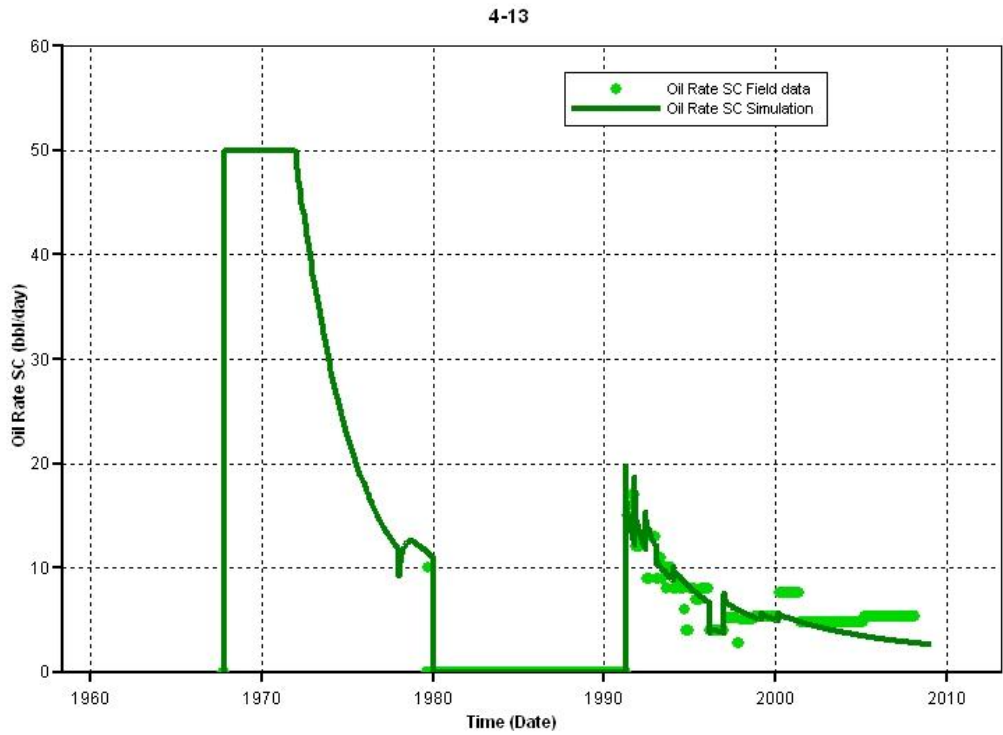


Figure 44 History match of oil production in well 4-13

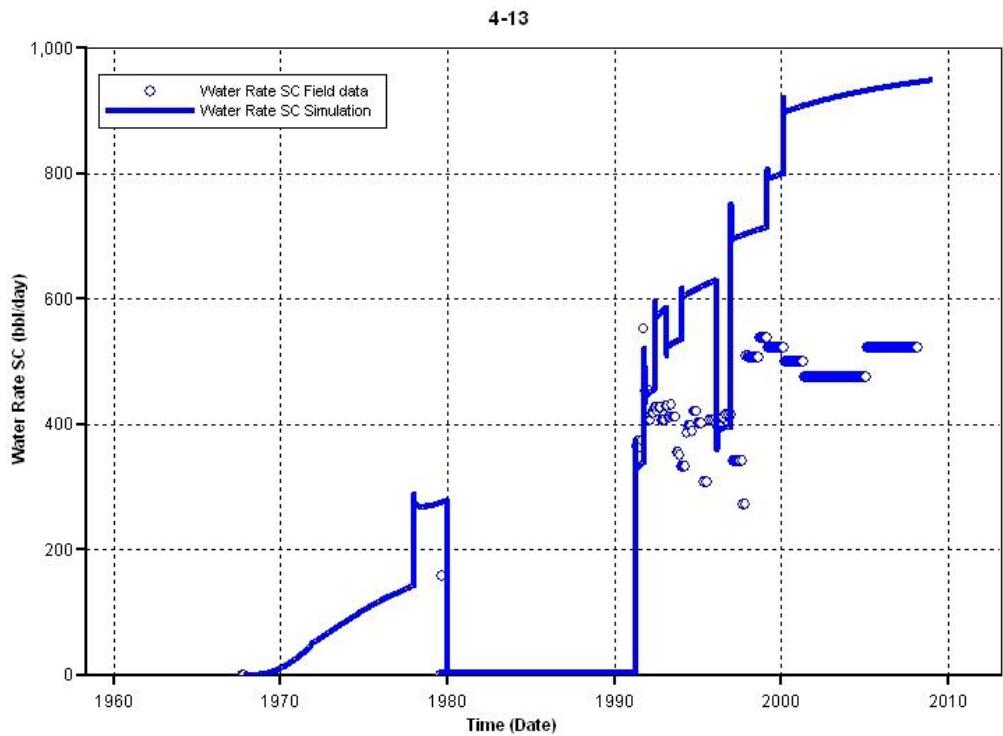


Figure 45 History match of water production in well 4-13

Although the Ogallah unit has been in production since 1951, the average reservoir pressure was not changed significantly. Figure 46 shows the average reservoir pressure based on the model calculation which decreases from 1200 psi to 1180 psi in 50 years of production. This confirms the assertion that the reservoir is underlain by an aquifer and the Carter-Tracery method is adequate to simulate the pressure support needed by the reservoir performance. As shown in the same figure, the average reservoir pressure in Lease 3, E. A. Scott varies between 1200 psi and 1150 psi.

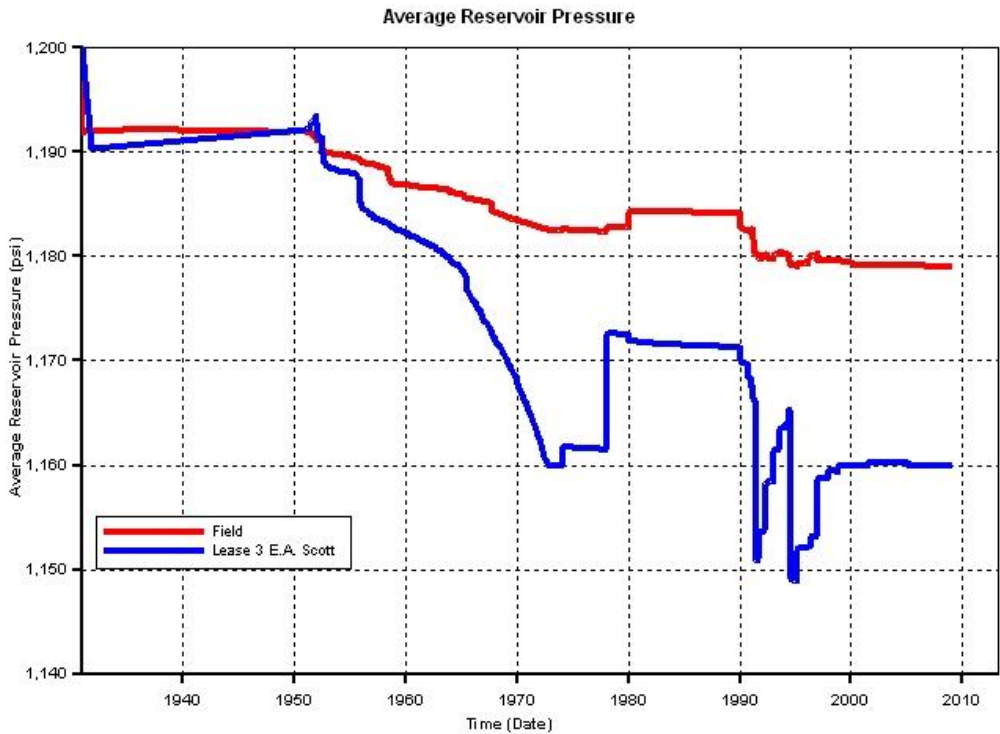


Figure 46 Average reservoir pressures of Ogallah unit and Lease E. A. Scott

3.2.2 Simulation of Carbon Dioxide Injection

The objective of CO₂ injection simulation is to investigate the feasibility of using CO₂ to improve oil recovery at near miscible condition in Ogallah unit. The reservoir model constructed in IMEX for history match was converted to GEM, a compositional simulator to simulate phase behavior of reservoir fluids for CO₂ injection process. All the reservoir properties after adjustment for the history match were kept intact in the compositional simulator. Compositional model was applied with the fluid system consisting of oil in four components, water and carbon dioxide.

In the process of history match, verification of the modeling results was limited to a few wells having detailed production record. As a result, simulation of CO₂ injection is continued on selected wells with a reasonably well matched history. The Lease 3 was selected for further case study as it contains two wells with reasonably well matched production history in the model. The lease 3 is located in central- west part of the field as shown in Figure 33. It is surrounded by lease 1, 2, 4 and 13. Figure 47 shows the grid system of the lease (colored in purple) presented in the reservoir model. The lease has four producers, well 3-1, 3-2, 3-3, and 3-4. Two producers (3-2 and 3-3) produces from Arbuckle, the other two (3-1 and 3-4) produces from Arbuckle and LKC. The size of the lease is approximately 47 acre. The pore volume calculated by the model was 3.64 MM bbl. At year 1951, the average oil saturation in the lease was 0.472 and the OOIP was 1.72 MM bbl. The properties of well blocks at these wells are summarized in Table 15. The properties at well 3-2 and 3-3 were adjusted for history match during the primary production whereas the properties at well 3-1 and 3-4 were maintained the same as that in the geological model. The scenarios designed for CO₂ injection in this lease are described as follows.

Table 15 Well block properties at well locations

Description	Well 3-2		Well 3-3	Well 3-1	Well 3-4
	Arbuckle	Reagan	Arbuckle	Arbuckle	Arbuckle
ϕ	0.164	0.201	0.203	0.123	0.119
k (md)	52.94	252.01	258.46	5.25	4.22
S _w	0.382	0.417	0.413	0.486	0.593

Grid Top (ft) 1994-12-01 K layer: 1

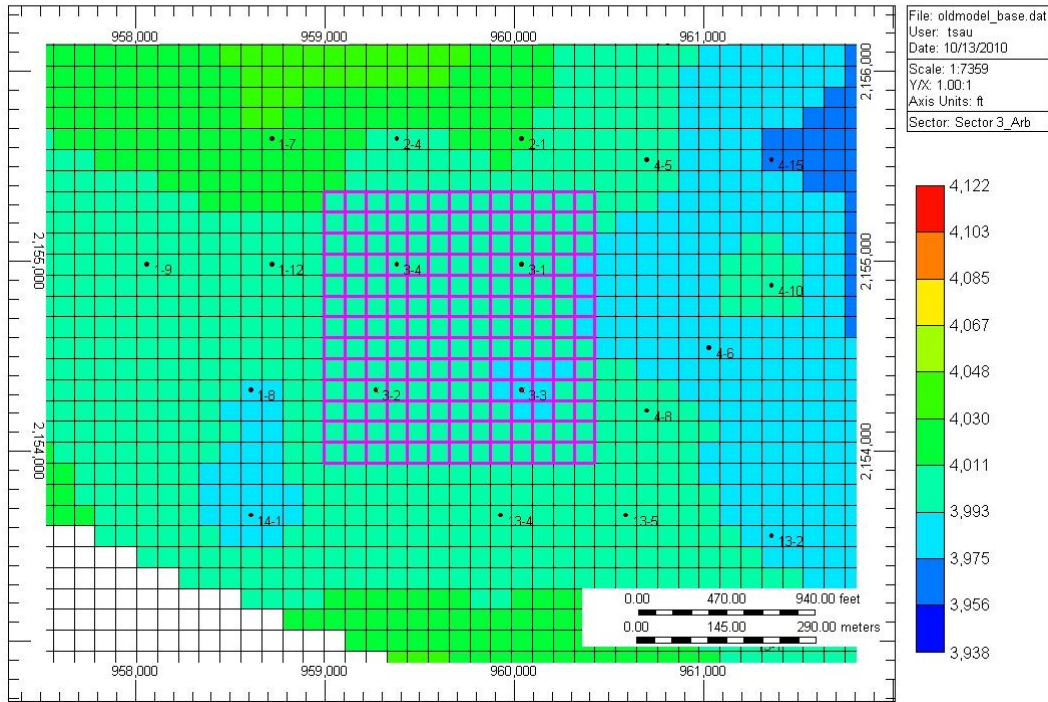


Figure 47 Grid system of Lease 3, E. A. Scott

One CO₂ Injector

The current status of well 3-1 is shut-in in the field while all other three remains open. Well 3-2 and 3-3 are producing from Arbuckle group whereas well 3-4 is in comingle production from Arbuckle and LKC. Therefore, only well 3-2 and 3-3 are considered to be converted to injector in the case study of one CO₂ injector.

Four cases were designed to simulate CO₂ injection process with one injector. In case 1, well 3-2 was converted to injector. CO₂ was injected at a maximum bottomhole pressure (BHP) of 1300 psi and a maximum rate of 200 MSCF/day. In case 2, well 3-2 injected CO₂ at BHP of 1200 psi and rate of 200 MSCF/day. In case 3, well 3-3 was converted to injector and injected CO₂ at BHP of 1300 psi with rate of 200 MSCF/day. In case 4, well 3-3 injected CO₂ at 1200 psi with a rate of 200 MSCF/day. In all cases, the CO₂ injection started on February 1, 2009 and continued for 10 years until February 1, 2019. When one injector injected CO₂, the remaining producers were open to production except well 3-1 was shut in. As a base case, the lease production was modeled without CO₂ injection until February 1, 2019

Figure 48 shows the production performance of well 3-2 when CO₂ was injected into well 3-3. The incremental oil is produced prior to the breakthrough of CO₂ when CO₂ is injected at 1300 psi. The water production of the same well is reduced (see Figure 49) as a result of CO₂ injection. Similar results are observed in well 3-3 when CO₂ is injected into well 3-2 (Figure 50 and 51). The comparisons of the results between two injection pressures with the base case are summarized in Table 16 and 17. The incremental oil in the base case is primarily produced by the natural water drive whereas in the other cases, it is attributed to CO₂ injection. It is apparent that the oil production is increased and water production is reduced when CO₂ is injected at pressure below MMP, 1350 psi. Since the average pressure of lease 3 at the start of CO₂ injection is 1160 psi in the model (as shown in Figure 46), less CO₂ is injected at a lower pressure. Nevertheless, fair amount of incremental oil is recovered as a result of CO₂ injection which shows the benefits of using CO₂ as a displacing agent to recover oil at near miscible condition. The gross utilization of CO₂ in all of the cases varies from 17 to 33 MCF/STB whereas net utilization of CO₂ varies from 12 to 27 MCF/STB. The CO₂ retention efficiency, which is the amount of CO₂ remained in the reservoir after 10 years of injection and production, varies from 59 to 83%.

Table 16 Comparison of incremental oil and water production in 10 years of CO₂ injection

CO ₂ injected at well 3-3 and produced at well 3-2					
	CO ₂ Injected	CO ₂ Produced	CO ₂ Remained	Oil	Water
	(SCF)	(SCF)	(SCF) (%)	(STB)	(STB)
Base case				11237	2319200
Case 1 @1300 psi	7.25E+08	3.01E+08	4.24E+08 (59)	34205	1984420
Case 2 @1200 psi	4.88E+08	1.55E+08	3.33E+08 (68)	28412	2106800

Table 17 Comparison of incremental oil and water production in 10 years of CO₂ injection

CO ₂ injected at well 3-2 and produced at well 3-3					
	CO ₂ Injected	CO ₂ Produced	CO ₂ Remained	Oil	Water
	(SCF)	(SCF)	(SCF) (%)	(STB)	(STB)
Base case				7266	684100
Case 1 @1300 psi	7.30E+08	1.44E+08	5.86E+08 (80)	21895	431070
Case 2 @1200 psi	6.53E+08	1.12E+08	5.41E+08 (83)	19809	464930

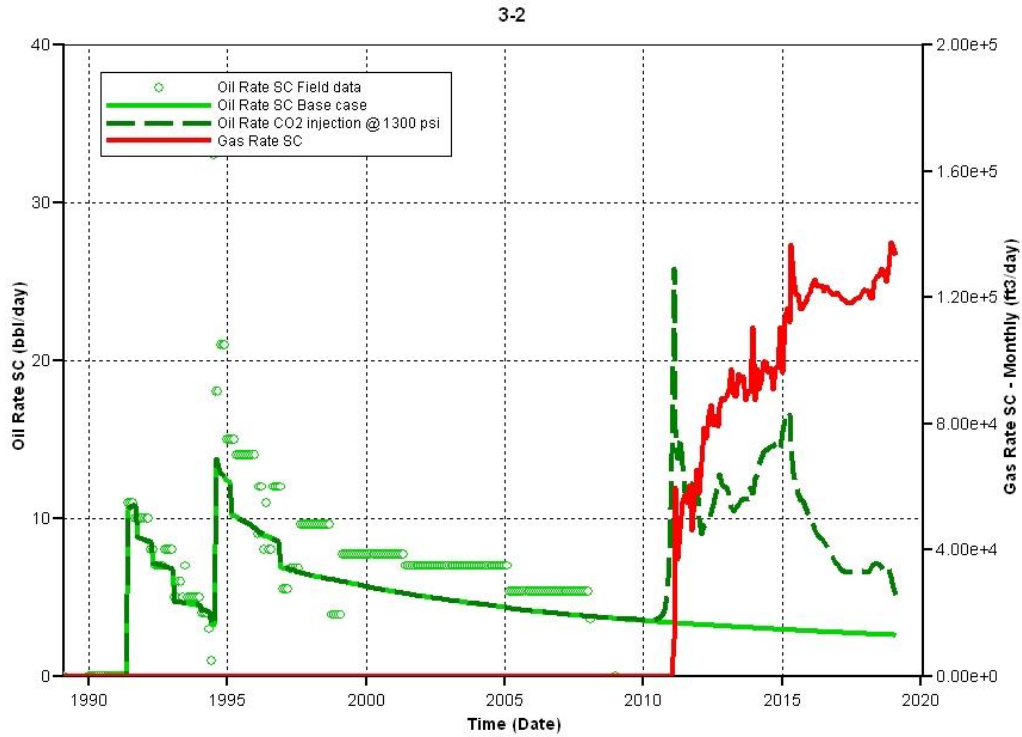


Figure 48 Incremental oil production at well 3-2 when CO₂ was injected at well 3-3

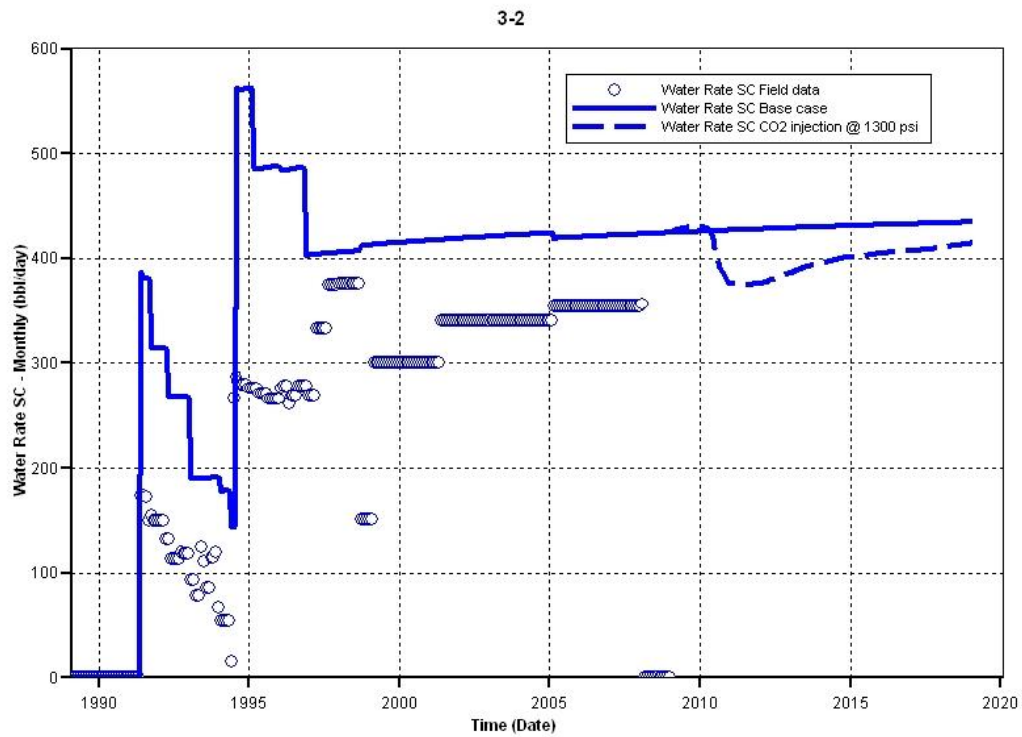


Figure 49 Reduction of water production at well 3-2 when CO₂ was injected at well 3-3

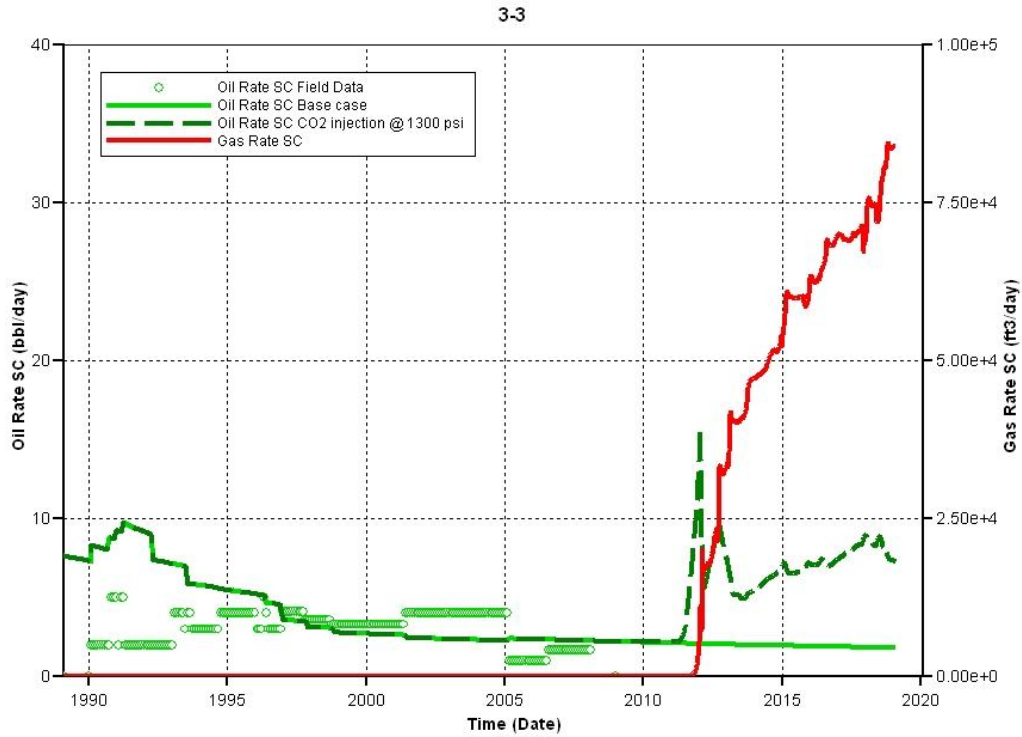


Figure 50 Incremental oil production at well 3-3 when CO₂ was injected at well 3-2

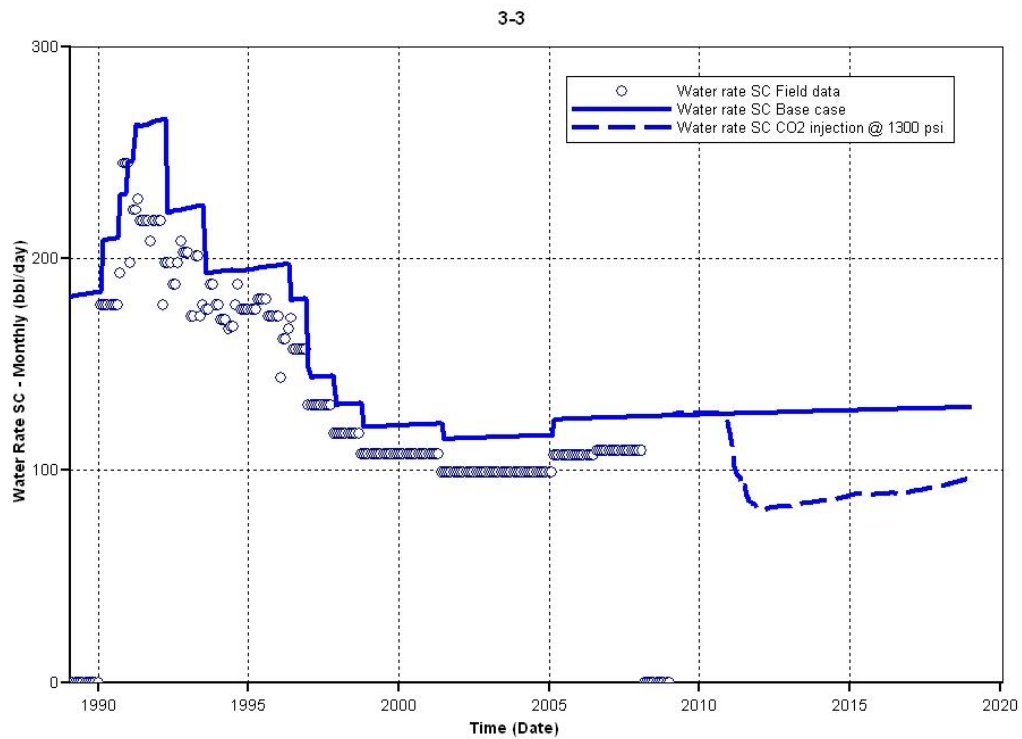


Figure 51 Reduction of water production at well 3-3 when CO₂ was injected at well 3-2

Two CO₂ Injectors

The modeling of CO₂ injection at Lease 3 was extended with two injectors to study the effect of injection pattern on oil recovery and CO₂ sequestration in the reservoir. The pattern design is shown in Figure 52 where the ratio of injector to producer is one to one. The lease itself is surrounded by lease 1, 2, 4 and 13. Field production data indicate that well 3-2 and well 3-3 are two of the better producers in the lease. When either one is converted to a CO₂ injector, 200 MSCF/day of CO₂ can be injected without exceeding the formation fracture pressure. In each of the injection pattern, the maximum injection rate of each injector was set at 200 MSCF/day. The bottomhole pressure was set at either 1200 or 1300 psi. The simulated injection rate, however, varied from case to case depending on the injectivity of the well and the flow pattern of the CO₂ which is affected by the reservoir heterogeneity.

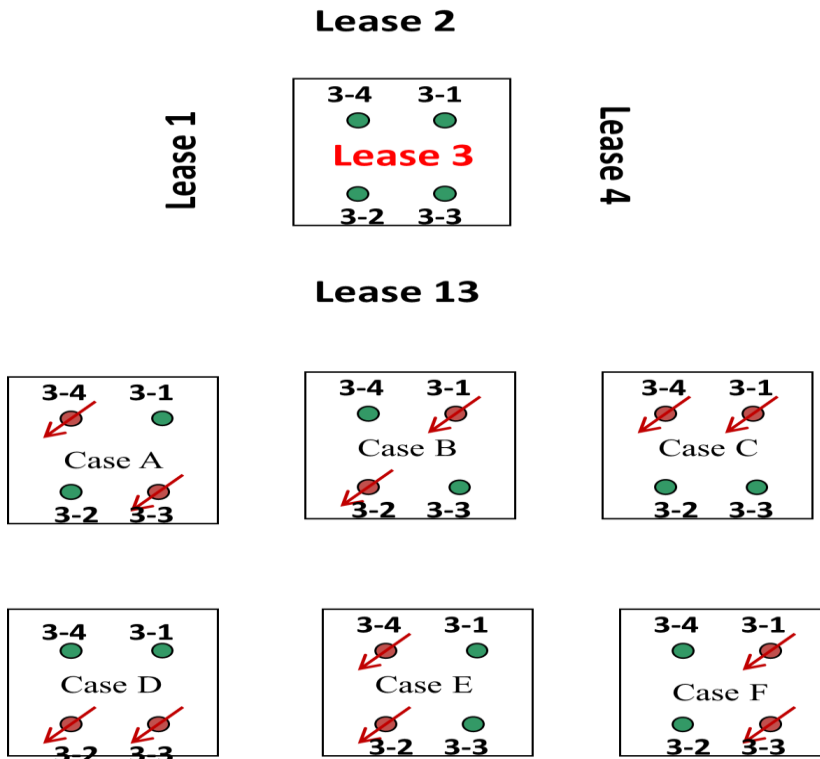


Figure 52 Pattern design of lease 3 for CO₂ injection

The primary production without CO₂ injection was simulated with all four producers open for production. The production performance from February 1, 2009 to February 1, 2019 was referred as a base case in which the recovery mechanism is relied on the natural water drive

from the underlying aquifer. The recovery efficiency from the primary production in this 10 year span was compared with the results from CO₂ IOR at near miscible condition.

Generally, the incremental oil recovery is increased with the injection pressure as more CO₂ is injected and interacted with oil during the displacement process. The recovery results differ in each case which is attributed to the variation in remaining oil in place at the beginning of CO₂ injection and the flow path of the displacing agent. Because there is no water injector around the lease to confine CO₂, CO₂ concentration remained in the lease at the end of injection depends on the flow direction and capacity of CO₂. Figure 53 to Figure 58 present remaining CO₂ concentrations on the top layer of Arbuckle formation in the lease 3 and its surrounding leases at the end of injection. It shows that CO₂ tends to move towards lease 13 and lease 1 which is located at west and south part of lease 3 as the permeability in that area is relatively higher. As a result, the incremental oil produced from these surrounding leases is attributed to the CO₂ injection. When the injection pressure is limited at 1300 psi, the highest incremental oil recovery occurs in case A where CO₂ was injected in wells 3-4 and 3-3. The recovery factor increases from 32.7 to 36.3% (Figure 59). At a lower injection pressure, 1200 psi, the recovery factor is reduced to 34%. If the maximum injection rate, 200 MCF/day were maintained for each injector in the designed pattern, the recovery efficiency becomes 37.5%, an increase of 4.8%.

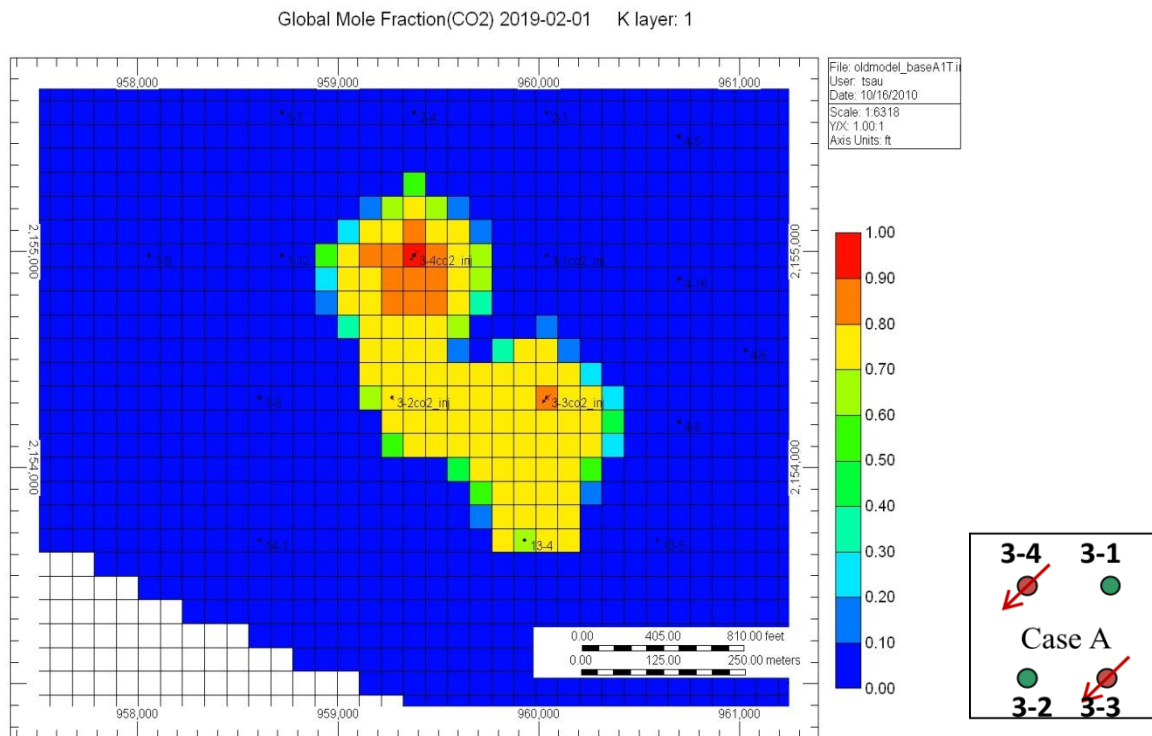


Figure 53 CO₂ distributions after 10 years of injection, Case A1

Global Mole Fraction(CO2) 2019-02-01 K layer: 1

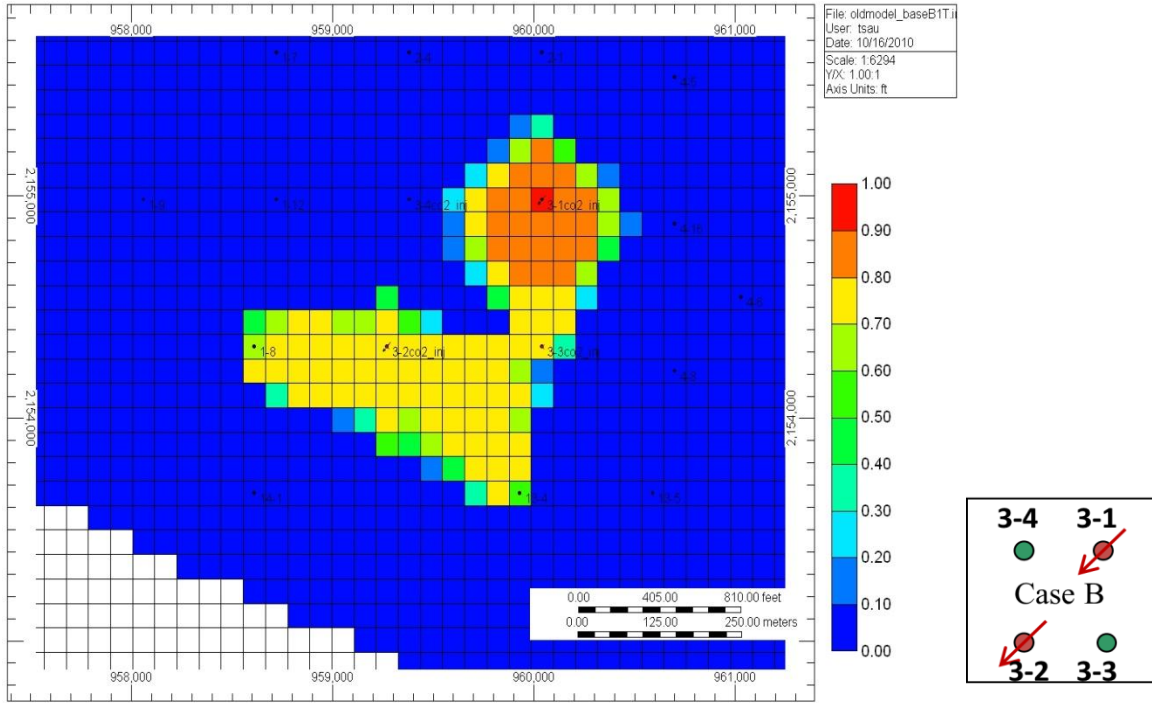


Figure 54 CO₂ distributions after 10 years of injection, Case B1.

Global Mole Fraction(CO2) 2019-02-01 K layer: 1

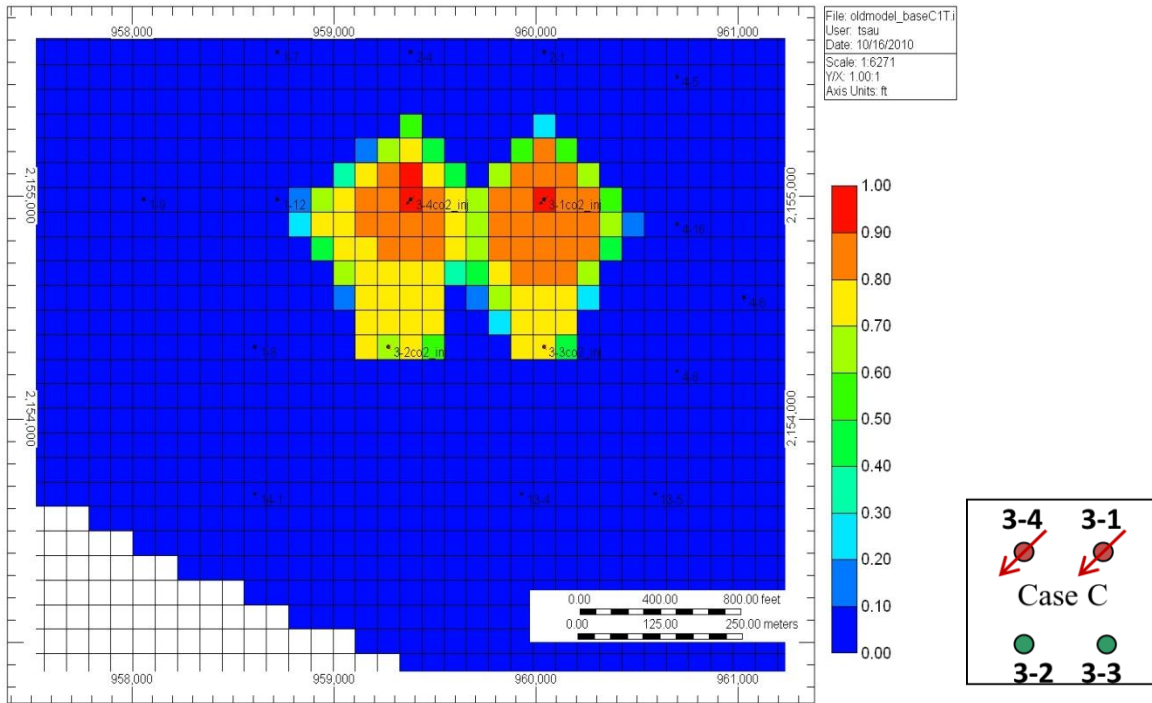


Figure 55 CO₂ distributions after 10 years of injection, Case C1.

Oil Mole Fraction(CO2) 2019-02-01 K layer: 1

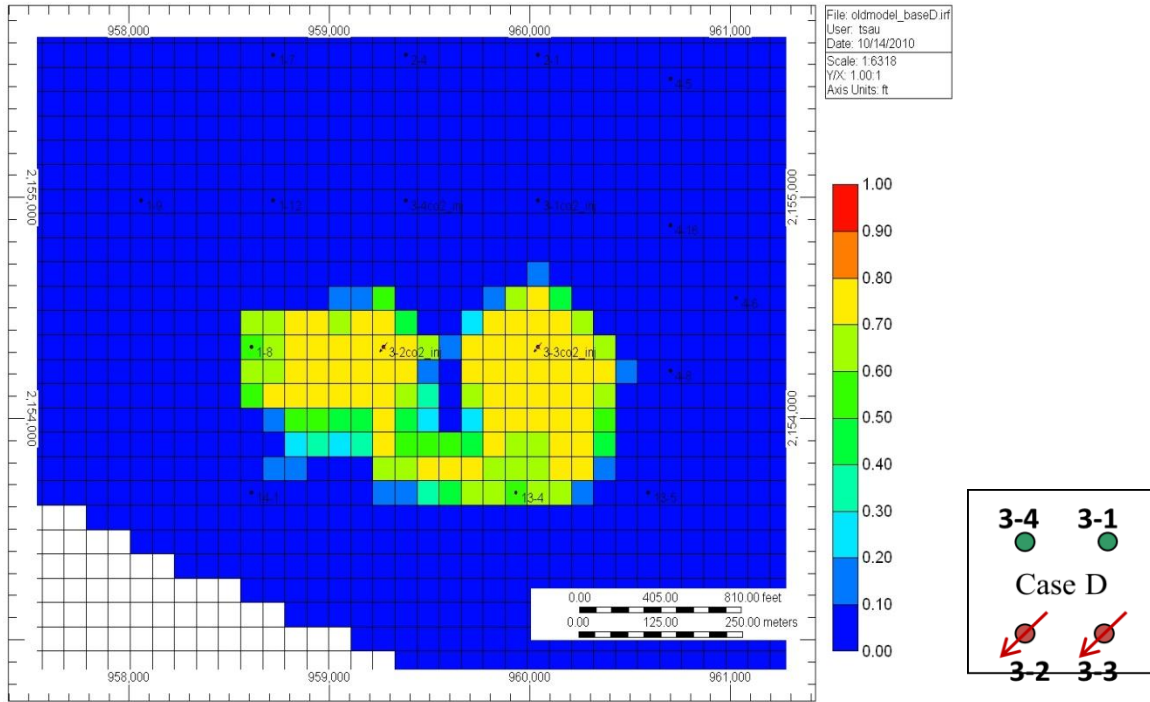


Figure 56 CO₂ distributions after 10 years of injection, Case D1.

Global Mole Fraction(CO2) 2019-02-01 K layer: 1

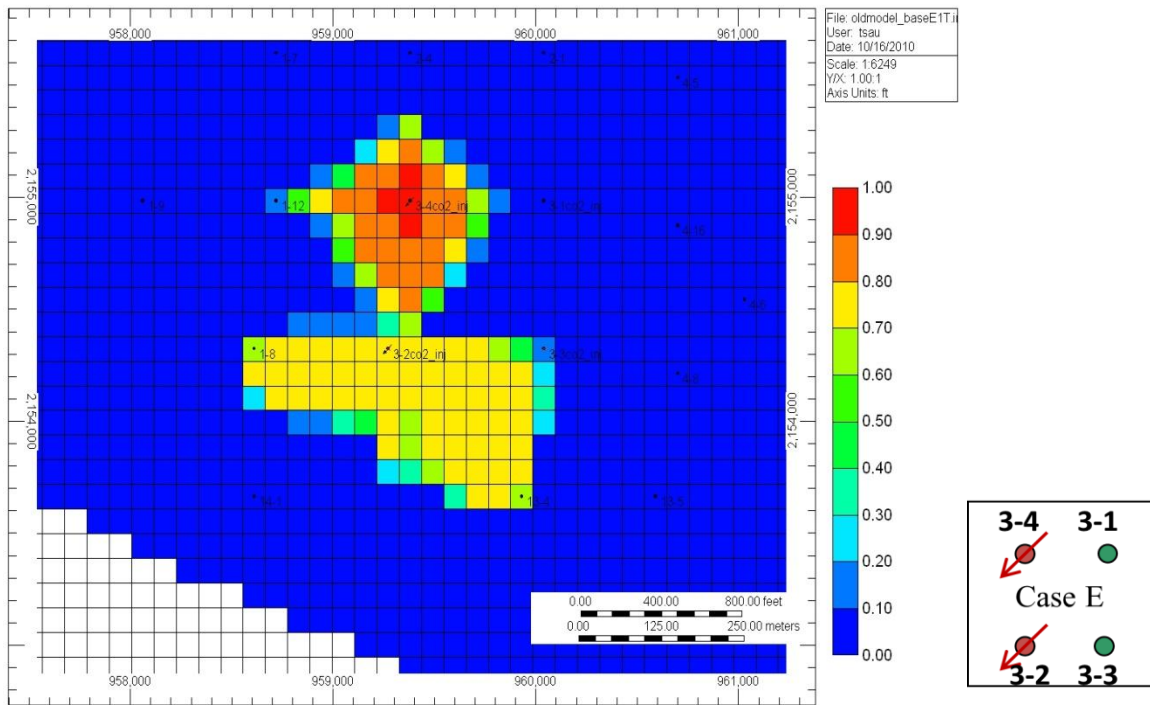


Figure 57 CO₂ distributions after 10 years of injection, Case E1.

Global Mole Fraction(CO2) 2019-02-01 K layer: 1

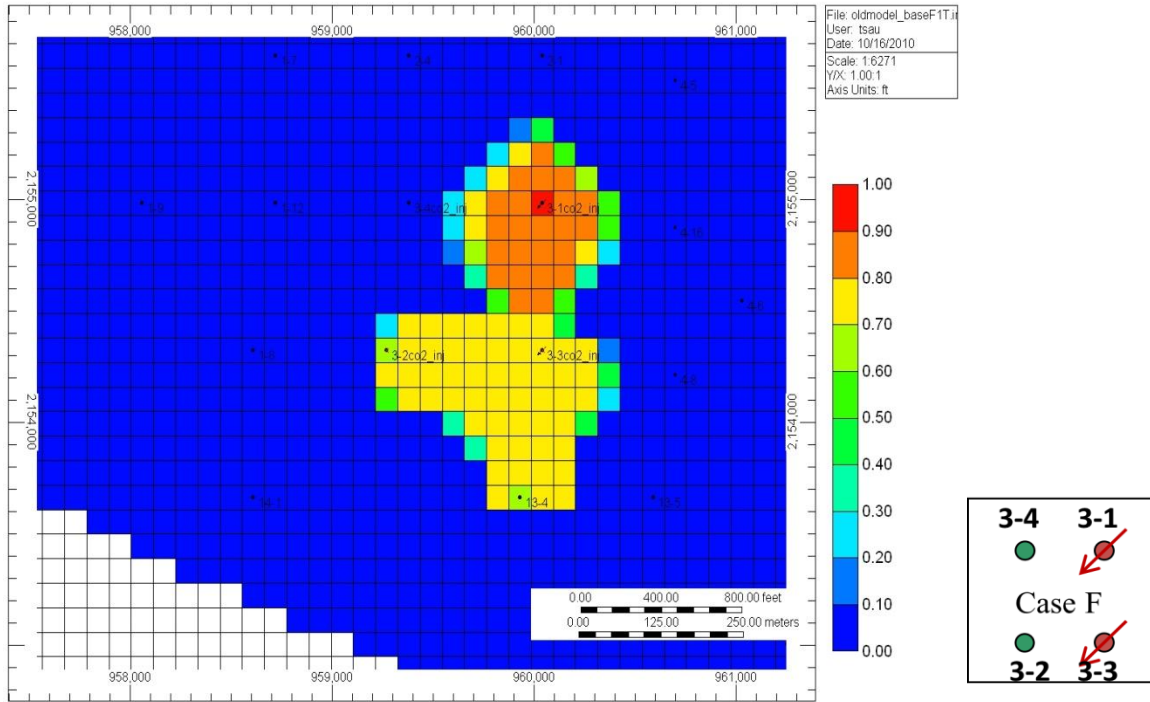


Figure 58 CO₂ distributions after 10 years of injection, Case F1.

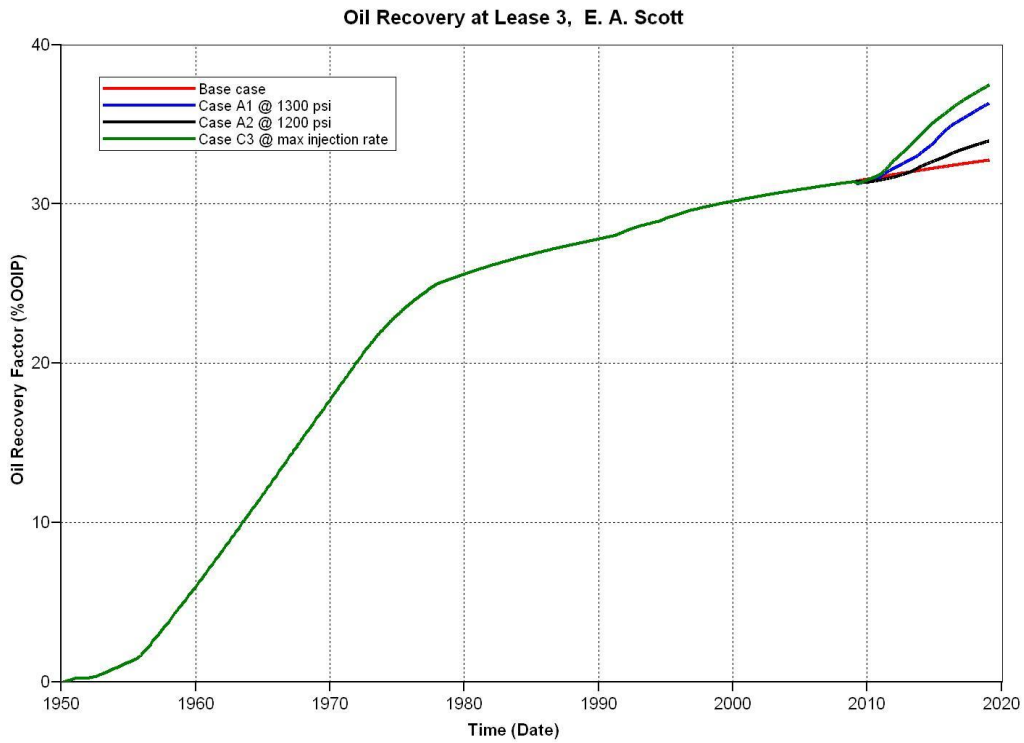


Figure 59 Comparison of oil recovery factors at Lease 3

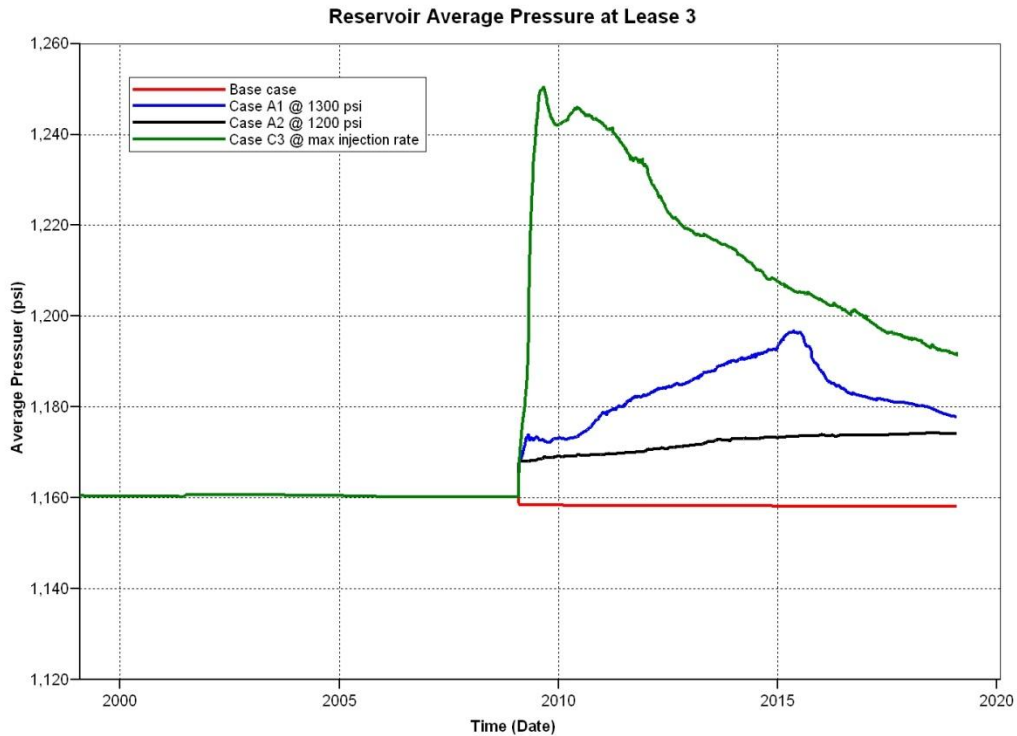


Figure 60 Average reservoir pressures at Lease 3 with/without CO₂ injection

The average reservoir pressure in the lease in all cases is below 1300 psi and above 1150 psi. Figure 60 shows the pressure history during CO₂ injection. When the BHP of injector is controlled at 1300 psi for well 3-3 and 3-4, the average reservoir increases slightly and never reaches the initial reservoir pressure of 1200 psi. When the maximum injection rate, 200 MSCF/day is maintained during the injection such as in Case C3, the average reservoir pressure rises above the initial reservoir pressure at the early stage of injection and declines to below that at the late stage of injection. When the BHP of injector is controlled at 1200 psi such as in the Case A2, the reservoir pressure only increases slightly. In all the cases, nevertheless, the reservoir pressure is maintained within the near miscible condition in which the recovery efficiency benefits from the improvement of relative mobility ratio of the CO₂ and oil and the efficacy of CO₂ extraction as demonstrated in the laboratory core flood study. However, the recovery efficiency is apparently affected by the reservoir heterogeneity which results in less improvement of oil production within the lease.

Detailed modeling results are summarized in Table 18 to Table 20. The CO₂ injected, produced and remained in the lease are listed in each table. The total incremental oil production resulting from the CO₂ injection is compared with the base case. The utilization of CO₂ and CO₂

retention percentage in each case are also calculated. The area sweep efficiency is affected by the reservoir heterogeneity. CO₂ injectors placed in well 3-4 and well 3-3 as in pattern case A performed better than the other patterns. A higher injection pressure of CO₂ also results in a better recovery performance. Depending on the injection pattern, the net utilization of CO₂ can be as low as 2 MSCF/STB and as high as 20 MSCF/STB. The effective CO₂ storage percentage in lease 3 can be as low as 3% and as high as 63% based on the theoretical storage capacity of 1.58 BSCF.

The theoretical CO₂ sequestration capacity is calculated based on the rock volume, porosity, initial oil saturation, and recovery factor. For reservoir underlain by an aquifer, the reservoir CO₂ sequestration capacity is reduced by the water influx from the aquifer but is augmented by the volume of water produced. The capacity for CO₂ sequestration in this case is given by equation:

$$V_{co2} = (A \times h) \times \phi \times RF \times S_{oi} - V_{flux} + V_{wp}$$

where V_{co2} : reservoir volume of CO₂ sequestered

A : area

h : thickness of formation

ϕ : porosity

RF : recovery factor

S_{oi} : initial oil saturation

V_{flux} : cumulative water influx

V_{wp} : cumulative water produced

Based on the reservoir model calculation, the pore volume of lease 3 is 3.64 MM bbl, average initial oil saturation is 0.472. The recovery factor of the primary production from 1951 to 2019 is 0.327 as shown in Figure 61. The cumulative water influx is 10.5 MM bbl and cumulative water production is 11.9 MM bbl. Therefore, the capacity of CO₂ sequestration is estimated as 1.86 MM bbl or 10.4 MMCF at reservoir condition (1200 psig and 110 °F) and 1.58 BSCF at standard condition.

Table 18 Result of case study with CO₂ injection at BHP of 1300 psi

	Base case	Case A1	Case B1	Case C1	Case D1	Case E1	Case F1
CO ₂ Injected (SCF)		1.23E9	9.89E8	7.58E8	1.45E9	1.15E9	9.36E8
CO ₂ Produced (SCF)		6.98E8	3.04E8	2.70E8	7.17E8	3.12E8	4.96E8
CO ₂ Remained (SCF)		5.34E8	6.84E8	4.88E8	7.29E8	8.35E8	4.40E8
Incremental oil from lease 3 (STB)	25473	60828	31443	54345	7292	26737	35394
Incremental oil from lease 13 (STB)	0	7620	11470	0	21700	12680	7380
Incremental oil from lease 4 (STB)	0	0	233	228	158	7	324
Incremental oil from lease 1 (STB)	0	153	9078	314	11533	10305	10
Incremental oil from lease 2 (STB)	0	7	9	19	0	11	9
Incremental oil Total (STB)	25473	68608	52233	54915	40683	49740	43117
Incremental oil relative to Base case		43135	26760	29442	15210	24267	17644
Water production (STB)	1.19E7	1.05E7	9.24E6	1.13E7	9.17E6	9.20E6	1.08E7
GU (MCF/STB)		18	19	14	36	23	22
NU (MCF/STB)		8	13	9	18	17	10
CO ₂ retention %		43	69	64	50	73	47
Effective storage %		34	43	31	46	53	28

Table 19 Result of case study with CO₂ injection at BHP of 1200 psi

	Base case	Case A2	Case B2	Case C2	Case D2	Case E2	Case F2
CO ₂ Injected (SCF)		5.20E8	6.60E8	4.09E7	7.23E8	6.50E8	4.92E8
CO ₂ Produced (SCF)		2.57E8	2.14E8	0	2.01E8	2.19E8	2.61E8
CO ₂ Remained (SCF)		2.64E8	4.46E8	4.09E7	5.22E8	4.31E8	2.31E8
Incremental oil from lease 3 (STB)	25473	34207	21251	18623	7177	24871	29811
Incremental oil from lease 13 (STB)	0	6200	7650	0	9740	8320	6190
Incremental oil from lease 4 (STB)	0	0	9	4	42	0	50
Incremental oil from lease 1 (STB)	0	0	7904	6	8575	7955	5
Incremental oil from lease 2 (STB)	0	0	0	0	0	1	1
Incremental oil Total (STB)	25473	40407	36814	18633	25534	41147	36057
Incremental oil relative to Base case		14934	11341	(6840)	61	15674	10584
Water production (STB)	1.19E7	1.05E7	9.28E6	1.07E7	8.90E6	9.23E6	1.09E7
GU (MCF/STB)		13	18	2	28	16	14
NU (MCF/STB)		7	12	2	20	10	6
CO ₂ retention %		51	68	100	72	66	47
Effective storage %		17	28	3	33	27	15

Table 20 Result of case study with CO₂ injection at 200 MSCF/day/well

	Base case	Case A3	Case B3	Case C3	Case D3	Case E3	Case F3
CO ₂ Injected (SCF)		1.45E9	1.45E9	1.45E9	1.45E9	1.45E9	1.45E9
CO ₂ Produced (SCF)		8.18E8	6.07E8	7.42E8	7.17E8	4.39E8	7.02E8
CO ₂ Remained (SCF)		6.27E8	8.38E8	7.03E8	7.29E8	1.01E9	7.44E8
Incremental oil from lease 3 (STB)	25473	65375	48399	75206	7292	29452	58510
Incremental oil from lease 13 (STB)	0	7830	12670	0	21700	14680	10580
Incremental oil from lease 4 (STB)	0	0	1051	1085	158	7	1450
Incremental oil from lease 1 (STB)	0	3374	10038	3920	11533	16766	11
Incremental oil from lease 2 (STB)	0	0	59	97	0	35	73
Incremental oil Total (STB)	25473	76579	72217	80308	40683	60940	70642
Incremental oil relative to Base case		51106	46744	54835	15210	35467	45151
Water production (STB)	1.19E7	1.05E7	9.15E6	1.07E7	8.90E6	9.20E6	1.07E7
GU (MSCF/STB)		19	20	18	36	24	20
NU (MSCF/STB)		8	12	9	18	17	11
CO ₂ retention %		43	58	49	50	70	51
Effective storage %		39	53	44	46	63	47

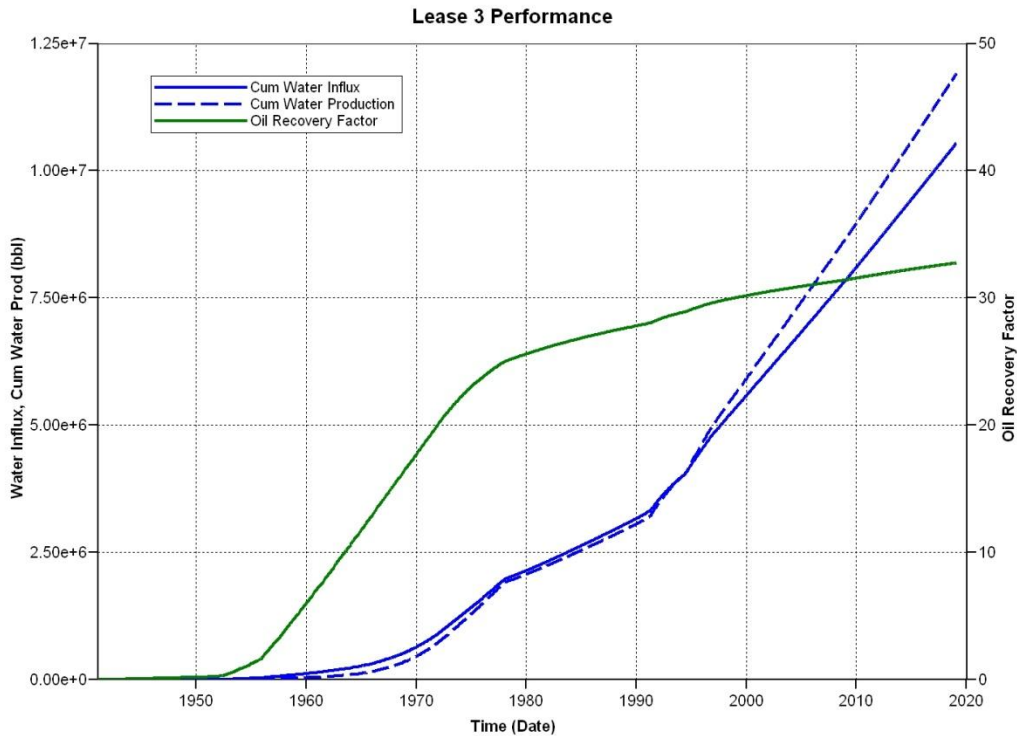


Figure 61 Lease 3 production performance without CO₂ injection

For the field application, the theoretical CO₂ storage capacity can be estimated with given information in the equation from the reservoir model or other resources such as reserve database and production history. Precise estimates of the effective CO₂ sequestration capacity during CO₂ IOR operations, however, requires numerical reservoir simulation as the calculation is affected by the nature of the displacement process and the reservoir heterogeneity,

The results presented in this section demonstrate the effect of pattern design and injection pressure and rate on the oil recovery efficiency and CO₂ sequestration. In general, it shows that improvement of oil recovery at near miscible condition is achievable under current reservoir operation pressure. The oil recovery efficiency and CO₂ sequestration capacity vary with the injection pattern which needs further investigation when the target area is extended to the whole oil field.

Because uncertainties exist in the current reservoir model where most of reservoir properties have not been verified by the history match process, the estimation of oil recovery and CO₂ storage capacity for the whole field has not been implemented. Plan to verify current reservoir model is underway by reviewing fourteen cored well data obtained lately. These wells are located at lease 1, 6, 7, 10 and 11 which are in the west, central east, and southeast part of the

field. Including these cored data with well logging interpretation will enhance the understanding and certainty about the current geological model and improve the model in prediction of reservoir performance. In addition, an evaluation plan devised to better understand this reservoir is proposed and will proceed in the near future. The proposed plan is to conduct tests to seek data that pertain to the pressure, residual oil saturation, reservoir properties and the nature of the flow from well to well in the reservoir. The tests will include single well transient pressure tests, multiple well interference tests, single well tracer tests and interwell tracer tests. With the current reviewing plan and future proposed tests, the current reservoir model is to be calibrated with a better reservoir description. The effect of reservoir heterogeneity on process performance will be reevaluated. The updated reservoir simulation results will be delivered when it is available.

Summary

1. The geological model was developed based on well-log interpretation and cross-plotting method. An in-house developed correlation between resistivity log and porosity log was successfully applied to calculate porosity based on microlog measurements.
2. The primary production history of a 47 acre lease (lease 3) containing four wells was reasonably matched. This lease was extensively examined for near miscible CO₂ injection process.
3. The simulation results indicate that near miscible displacement is achievable in lease 3 at current reservoir operation pressure. The incremental oil recovery generally increases with the injection pressure. The oil recovery efficiency was increased by 1.3 to 4.8% as a result of CO₂ injection.
4. The oil recovery efficiency and CO₂ sequestration capacity depend on the implementation of CO₂ injection which includes injection pressure, rate and pattern design.
5. The theoretical storage capacity of CO₂ in lease 3 was 1.58 BSCF. The net utilization of CO₂ in IOR process varied from 8 to 18 MSCF/STB when 1.45 BSCF CO₂ was injected in 10 years. The effective storage capacity of CO₂ varied from 39 to 63% at the end of CO₂ injection.

4. SUMMARY AND CONCLUSIONS

This project describes a research program to evaluate the application of CO₂ displacement at near miscible pressure for improved oil recovery and carbon sequestration. The research results are discussed in the experimental and computational study. The experimental study comprises fundamental studies of phase behavior for the CO₂/crude oil system and the displacement process at near miscible condition. The computational study discusses the methodologies of developing geological model and assessment of oil recovery as well as CO₂ sequestration at near miscible conditions by reservoir simulations. Some of the conclusions drawn from this research are summarized as follows:

1. Properties of Ogallah unit oil produced from an Arbuckle reservoir in Kansas were determined at reservoir temperature from a series of phase behavior and slim-tube experiments where CO₂ was dissolved in or used to displace the oil. The MMP at 110 °F was 1350 psig. The MMP increased to 1650 psig when the temperature increased to 125 °F.
2. At near miscible condition (pressure greater than 1100 psig), the oil viscosity was reduced by a factor of five due to the dissolution of carbon dioxide.
3. Phase behavior data were used to develop an equation of state that correlated properties of carbon dioxide saturated crude oil as a function of pressure at reservoir temperature.
4. Recovery of more than 50% of the waterflood residual oil from Berea, Baker dolomite and Arbuckle reservoir rock was obtained when CO₂ was injected at the current average reservoir pressure of 1150 psig, substantially less than the MMP (1350 psig).
5. Good agreement was observed between simulated and measured oil recovery from slim-tube tests for CO₂ injection over pressures ranging from 1000 psig to 1500 psig.
6. Significant extraction of oil by CO₂ started at pressure of 1150 psig which indicated that extraction/vaporization is the primary mechanism for oil recovery in the near miscible region from 1100 psig to 1350 psig at 110 °F.
7. At near miscible conditions, relatively high recovery efficiency in the slim-tube experiment supports extraction/vaporization as a principle displacement mechanism.
8. The swelling of crude oil due to the dissolution of CO₂ was determined accurately in our in-house build apparatus using small sample size.

9. The MMP estimated by the swelling/extraction test graphically is close to what determined from the slim-tube experiment.
10. The geological model was developed based on well-log interpretation and cross-plotting method. An in-house developed correlation between resistivity log and porosity log was successfully applied to calculate porosity based on microlog measurements.
11. The primary production history of a 47 acre lease (lease 3) containing four wells was reasonably matched. This lease was extensively examined for near miscible CO₂ injection process.
12. The simulation results indicate that near miscible displacement is achievable in lease 3 at current reservoir operation pressure. The incremental oil recovery generally increases with the injection pressure. The oil recovery efficiency was increased by 1.3 to 4.8% as a result of CO₂ injection.
13. The oil recovery efficiency and CO₂ sequestration capacity depend on the implementation of CO₂ injection which includes injection pressure, rate and pattern design.
14. The theoretical storage capacity of CO₂ in lease 3 was 1.58 BSCF. The net utilization of CO₂ in IOR process varied from 8 to 18 MSCF/STB when 1.45 BSCF CO₂ was injected in 10 years. The effective storage capacity of CO₂ varied from 39 to 63% at the end of CO₂ injection.

ACKNOWLEDGEMENT

The research effort reported on here was the results of hard work by Ly Huong Bui who performed most of the experiments; Woan Jing Teh who constructed geological model and conducted reservoir simulations; Scott Ramskill who helped in the laboratory work; Paul G. Willhite, Don Green, and Jenn-Tai Liang who provided useful discussions throughout this project. I also thank John Doveton and Bill Guy for providing useful suggestions on reservoir characterization; Dwayne McCune and Mark Ballard for assisting in analysis of the field operation; Dana Wreath for providing field data for reservoir simulation. I am grateful to Carmen Schmitt, Inc. for participation of this project and providing crude oil samples as well as field record. I am also indebted to Martha Cather for her active interest and encouragement. I appreciate the administrative assistance provided by Mayumi Crider, Barbara Sutterfield and Shelley Gerhke throughout this project. Finally, I thank the RPSEA and TORP for the support that made this work possible.

Funding for this project is provided by RPSEA through the “Ultra-Deepwater and Unconventional Natural Gas and Other Petroleum Resources” program authorized by the U.S. Energy Policy Act of 2005. RPSEA (www.rpsea.org) is a nonprofit corporation whose mission is to provide a stewardship role in ensuring the focused research, development and deployment of safe and environmentally responsible technology that can effectively deliver hydrocarbons from domestic resources to the citizens of the United States. RPSEA, operating as a consortium of premier U.S. energy research universities, industry, and independent research organizations, manages the program under a contract with the U.S. Department of Energy’s National Energy Technology Laboratory.

REFERENCES

- Byrnes, A. P., Franseen, E. K. and Steinhauhoff, D. M.: "Integrating plug to well-scale petrophysics with detailed sedimentology to quantify fracture, vug and matrix properties in carbonate reservoirs; an example from the Arbuckle Group, Kansas." University of Kansas, (pp.3) 1999.
- Bui, L.H., Tsau, J.S., and Willhite, G. P.: "Laboratory Investigations of CO₂ Near Miscible Application in Arbuckle Reservoir" paper SPE-129710 to be presented at 2010 SPE Improved Oil Recovery Symposium, Tulsa, April 24-28.
- Corey, A. T., "The Interrelations Between Gas and Oil Relative Permeabilities," Producers Monthly (Nov 1954), Vol. 19, p 38-41.
- Franseen, E. K., Byrnes, A. P., Cansel, J.R., Steinhauhoff, D. M., and Carr, T. R.: "The Geology of Kansas ARBUCKLE GROUP", *Current Research in Earth Sciences*, Bulletin 250, part 2.
- Franseen, E. K., Byrnes, A. P., Cansel, J.R., Steinhauhoff, D. M., and Carr, T. R., and Dubois, M.K.: "Geologic Controls on Variable Character of Arbuckle Reservoirs in Kansas-An Emerging Picture," Kansas Geological Survey, Open-file Report 2003-59
- Jennings, D.W. and R.C. Schucker: " Comparison of High-Pressure Vapor-Liquid Equilibria of Mixtures of CO₂ or Propane with Nonane and C₉ Alkylbenzenes," *Journal of Chemical & Engineering Data*, 1996. **41**(4): p. 831-838.
- Hand, J. L. and Plnczewshl, W. V.: "Interpretation of Swelling/Extraction Tests," *SPE* (November 1990) 595-600.
- Harmon, R. A. and Grigg, R. B.: "Vapor-Density Measurement for Estimating Minimum Miscibility Pressure," *SPE* (November 1988) 1215-1220.
- Holm, L.W. and Josendal, V.A.: "Effect of Oil Composition on Miscible-Type Displacement by Carbon Dioxide," *SPEJ* (February 1982) 87-98.
- Negahban, S. and V.J. Kremesec Jr.: " Development and Validation of Equation-of-State Fluid Descriptions for CO₂/Reservoir-Oil Systems, " *SPE*, 1992. **7**(3): p. 363-368.
- Nagarajan, N. and Robinson, R. L. J.: "Equilibrium Phase Compositions, Phase Densities, and Interfacial Tensions for CO₂ + Hydrocarbon Systems, 2. CO₂ + n-Decane," *J. Chem. Eng. Data*, 31, 168. 1986
- Negahban, S. and V.J. Kremesec Jr., *Development and Validation of Equation-of-State Fluid Descriptions for CO₂/Reservoir-Oil Systems. SPE*, 1992. **7**(3): p. 363-368.

Ren, Wei and Scurto, A.: "High –Pressure Phase Equilibria with Compressed Gases," Review of Scientific Instruments, 78, 125104, 2007.

Shelton, J.L.: "The Effects of Water Injection on Miscible Flooding Methods Using Hydrocarbons and Carbon Dioxide," 1975. **15**(3): p. 217-226.

Tsau, J. S.: "Near Miscible CO₂ Application to Improve Oil Recovery for Small Producers," RPSEA Technical Report 07123-03.01, 2010.

Whitson C. H. and Brule M. R.: "Phase Behavior", SPE Henry L. Doherty Series, Monograph Volume 20, Society of Petroleum Engineers, Inc. 2000.

Wylie, P. and Mohanty, K. K.: "Effect of Wettability on Oil Recovery by Near-miscible Gas Injection," paper SPE 39620 presented at the Improved Oil Recovery Symposium, Tulsa, OK. April 19-22, 1998.